

UNIVERSIDADE FEDERAL DE SANTA MARIA
CENTRO DE TECNOLOGIA
PROGRAMA DE PÓS-GRADUAÇÃO EM ENGENHARIA QUÍMICA

Maria Amélia Zazycki

**PREPARAÇÃO DE *BIOCHAR* A PARTIR DE MATÉRIAS-PRIMAS
ALTERNATIVAS E SUA APLICAÇÃO NA ADSORÇÃO DE
CORANTES**

Santa Maria, RS
2019

Maria Amélia Zazycki

**PREPARAÇÃO DE *BIOCHAR* A PARTIR DE MATÉRIAS-PRIMAS
ALTERNATIVAS E SUA APLICAÇÃO NA ADSORÇÃO DE
CORANTES**

Tese de doutorado apresentada ao Programa de Pós-Graduação em Engenharia Química da Universidade Federal de Santa Maria (UFSM), como requisito parcial para a obtenção do título de **Doutora em Engenharia Química**.

Orientador: Prof. Guilherme Luiz Dotto
Coorientadora: Prof^ª. Gabriela Carvalho Collazzo

Santa Maria, RS
2019

ZAZYCKI , MARIA AMÉLIA
PREPARAÇÃO DE BIOCHAR A PARTIR DE MATÉRIAS-PRIMAS
ALTERNATIVAS E SUA APLICAÇÃO NA ADSORÇÃO DE CORANTES /
MARIA AMÉLIA ZAZYCKI .- 2019.
115 p.; 30 cm

Orientadora: Guilherme Luiz Dotto
Coorientadora: Gabriela Carvalho Collazzo
Tese (doutorado) - Universidade Federal de Santa
Maria, Centro de Tecnologia, Programa de Pós-Graduação em
Engenharia Química, RS, 2019

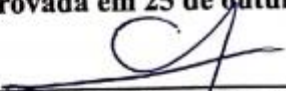
1. Adsorventes alternativos 2. Área de superfície 3.
Efluentes coloridos 4. Pirólise 5. Resíduos I. Dotto,
Guilherme Luiz II. Carvalho Collazzo, Gabriela III.
Título.

Maria Amélia Zazycki

**PREPARAÇÃO DE *BIOCHAR* A PARTIR DE MATÉRIAS-PRIMAS
ALTERNATIVAS E SUA APLICAÇÃO NA ADSORÇÃO DE
CORANTES**

Tese de doutorado apresentada ao Programa de Pós-Graduação em Engenharia Química da Universidade Federal de Santa Maria (UFSM), como requisito parcial para a obtenção do título de **Doutora em Engenharia Química**.


Aprovada em 25 de outubro de 2019.




Guilherme Luiz Dotto, Dr. (UFSM)
(Presidente, Orientador).



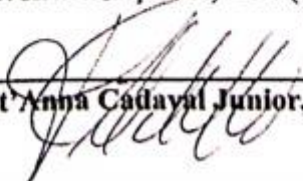
Adriano Cancelier, Dr. (UFSM)



Fernanda de Castilhos, Dr^a. (UFSM)



Janaina Oliveira Gonçalves, Dr^a. (UFSM)



Tito Roberto Sant'Anna Cadaval Junior, Dr. (FURG)

Santa Maria, RS
2019

DEDICATÓRIA

Dedico essa tese a minha mãe Zilei Teresinha Zazycki, com todo meu amor e admiração. Por estar sempre do meu lado me apoiando. Por acreditar em mim, quando eu mesma não acredito. Pelas orações e por toda “torcida”. Isso só me fortalece e me faz tentar, não ser a melhor, mas fazer o melhor de mim. Obrigada pelo amor incondicional!

AGRADECIMENTOS

A **Deus** pela vida, por me iluminar e abençoar meu caminho.

A minha família, minha mãe **Zilei Terezinha Zazycki** e meus irmãos **Marcos Vinícius Zazycki** e **Eduardo Augusto Zazycki**, um simples obrigado não seria o suficiente para agradecer por tudo o que fizeram e fazem por mim, sem vocês não teria chegado até aqui. Muito obrigada pelo incentivo, paciência, ensinamentos, confiança, amor, carinho e dedicação.

Agradeço em especial, ao meu orientador, professor **Dr. Guilherme Luiz Dotto**. Obrigada por me acolher, por acreditar em mim, pelas palavras de incentivo, puxões de orelha, paciência e ensinamentos, essenciais para ter chegado até aqui. Admiro-te muito como pessoa e profissional.

A minha coorientadora, professora **Dra. Gabriela Carvalho Collazzo**, pelos ensinamentos, incentivo, competência, dedicação e ajuda.

Aos professores **Dr. Marcelo Godinho** e **Dra. Daniele Perondi** do Laboratório de Energia e Bioprocessos (LEBio) da Universidade de Caxias do Sul (UCS) pela parceria e auxílio na preparação e caracterização das minhas amostras.

Às minhas IC's, **Priscila Azambuja Borba** e **Rafaela Nogueira Fontoura da Silva**, por me acompanharem nas longas horas de trabalho em laboratório. Obrigada por toda ajuda e dedicação na minha pesquisa.

Aos amigos, **Rana Louise Andrade da Paixão** e **Régis Maximiliano Roos de Carvalho**, por estarem sempre ao meu lado, por vibrarem comigo a cada conquista. Agradeço pelo apoio, palavras de estímulo e ajuda.

Aos demais amigos, que mesmo de longe nunca estiveram ausentes, agradeço a amizade e o carinho.

Aos demais professores, funcionários e colegas por toda a aprendizagem, amizade e apoio.

À Universidade Federal de Santa Maria e ao Programa de Pós-Graduação em Engenharia Química pela oportunidade e por terem me recebido de braços abertos.

Agradeço de coração a todos

RESUMO

PREPARAÇÃO DE *BIOCHAR* A PARTIR DE MATÉRIAS-PRIMAS ALTERNATIVAS E SUA APLICAÇÃO NA ADSORÇÃO DE CORANTES

AUTORA: Maria Amélia Zazycki
ORIENTADOR: Guilherme Luiz Dotto

A contaminação das águas naturais tem sido um dos grandes problemas da sociedade. Os setores têxtil e alimentício apresentam especial destaque, devido às grandes quantidades de efluentes lançados nos corpos hídricos. Desse modo é preciso desenvolver e aprimorar tecnologias que promovam o tratamento eficiente de efluentes e que sejam viáveis. Neste estudo, foram produzidos *biochars* a partir de materiais residuais alternativos, os quais foram aplicados no tratamento de efluentes coloridos. Os materiais precursores foram resíduos de cascas de noz-pecan, quitina e chapas de MDF. Os resíduos foram obtidos, caracterizados e pirolisados, transformando-os em *biochars*. Os *biochars* e seus precursores foram caracterizados utilizando técnicas de microscopia eletrônica de varredura (MEV), espectroscopia de infravermelho com transformada de Fourier (FTIR), difração de raios-x (DRX) e análise da área superficial (BET e BJH). Por fim foi estudada a adsorção de corantes do ponto de vista cinético, de equilíbrio e termodinâmico. As análises de caracterização indicaram que os *biochars* apresentaram características adequadas para adsorção, incluindo estruturas microporosas e mesoporosas e suficiente área de superfície. O *biochar* derivado de resíduos de cascas de noz-pecan apresentou uma área de superfície de $93 \text{ m}^2 \text{ g}^{-1}$. A capacidade máxima de adsorção foi de cerca de 130 mg g^{-1} para o corante RR141 e a cinética de adsorção seguiu o modelo de PSO. O *biochar* derivado da quitina apresentou uma área de superfície de $275 \text{ m}^2 \text{ g}^{-1}$. A cinética de adsorção foi bem representada pelo modelo PSO e a capacidade máxima de adsorção, estimada pelo modelo de Liu, foi de $1120,8 \text{ mg g}^{-1}$ para o corante MV. O *biochar* derivado de resíduos de chapas de MDF apresentou área de superfície de $218,8 \text{ m}^2 \text{ g}^{-1}$. Os modelos PSO e Freundlich foram os melhores modelos para representar, respectivamente a cinética e as isotermas de adsorção. A capacidade máxima de adsorção foi de 210 mg g^{-1} para o corante FR17. Os resultados demonstraram que os *biochars* podem ser preparados a partir de resíduos, usando um processo simples na sua preparação, sendo uma alternativa viável para adsorção de corantes em soluções aquosas.

Palavras-chave: Adsorventes alternativos. Área de superfície. Efluentes coloridos. Pirólise. Resíduos.

ABSTRACT

BIOCHAR FROM ALTERNATE RAW MATERIALS FOR APPLICATION IN DYES ADSORPTION

AUTHOR: Maria Amélia Zazycki

ADVISOR: Guilherme Luiz Dotto

Contamination of natural waters has been one of the great problems of modern society. The textile and food sectors stands out especially due to the large amounts of effluents discharged into the water bodies. Thus, it is necessary the development and improvement of technologies that promote the efficient effluent treatment and are viable. In this study, biochars were produced from alternative raw materials and applied in the treatment of colored effluents. The precursor materials were pecan nutshells wastes, chitin and MDF sheets. The residues were obtained, characterized and pyrolysed, being then converted into biochars. The biochars and their precursors were characterized using scanning electron microscopy (SEM), Fourier transform infrared spectroscopy (FTIR), x-ray diffraction (XRD) and surface area analysis (BET and BJH) techniques. Finally, the adsorption of different dyes was analyzed from the kinetic, equilibrium and thermodynamic viewpoints. Characterization analyzes indicated that the biochars presented adequate characteristics for adsorption, including microporous and mesoporous structures and interesting surface area. The biochar derived from pecan nutshell residues presented a surface area of $93 \text{ m}^2 \text{ g}^{-1}$. The maximum adsorption capacity was about 130 mg g^{-1} for RR141 dye and the adsorption kinetics followed the PSO model. The chitin-derived biochar presented a surface area of $275 \text{ m}^2 \text{ g}^{-1}$. Adsorption kinetics was well represented by the PSO model and the maximum adsorption capacity estimated by the Liu model was 1120.8 mg g^{-1} for the MV dye. The biochar derived from MDF sheet residues had a surface area of $218.8 \text{ m}^2 \text{ g}^{-1}$. The PSO and Freundlich models were the best to represent the adsorption kinetics and isotherms, respectively. The maximum adsorption capacity was 210 mg g^{-1} for the FR17 dye. The results showed that promising biochars can be prepared from alternative wastes using a simple process in their preparation, being a viable alternative for dye adsorption from aqueous solutions.

Keywords: Alternative adsorbents. Surface area. Colored Effluents.. Pyrolysis. Waste.

LISTA DE ILUSTRAÇÕES

REVISÃO BIBLIOGRÁFICA

| | |
|---|----|
| Figura 1 – Estrutura química do corante reativo vermelho 141..... | 16 |
| Figura 2 – Estrutura química do corante metil violeta..... | 16 |
| Figura 3 – Estrutura química do corante vermelho nº 40..... | 17 |
| Figura 4 – Formas típicas de isotermas..... | 22 |
| Figura 5 – Fruto e cascas de noz-pecan..... | 27 |
| Figura 6 – Quitina em pó..... | 27 |
| Figura 7 – Placa de Fibra de Média Densidade (MDF)..... | 28 |

ARTIGO 1

| | |
|---|----|
| Figure 1 – Scheme for the biochar preparation..... | 34 |
| Figure 2 – Chemical structure of reactive red 141..... | 35 |
| Figure 3 – (a) XRD spectrum; (b) nitrogen adsorption–desorption isotherms and the Barrett–Joyner–Halenda desorption pore size distribution (inset); (c) and (d) FTIR spectra of Pecan nutshell and biochar..... | 39 |
| Figure 4 – SEM images of the biochar showing (a) and (b) the particle and (c) and (d) the cavities of the material..... | 42 |
| Figure 5– Influence of pH on the reactive red 141 removal percentage using pecan nutshell and biochar as adsorbents..... | 43 |
| Figure 6 – Effect of the contact time on the adsorption capacity of reactive red 141 on the biochar at different initial concentrations (pH = 3.0 and 298 K)..... | 44 |
| Figure 7 – Equilibrium curves for adsorption of reactive red 141 onto the biochar..... | 46 |

ARTIGO 2

| | |
|---|----|
| Figure 1 – Scheme of pyrolysis process and materials characterization..... | 58 |
| Figure 2 – FT–IR vibrational spectra of chitin and chitin derived biochar..... | 62 |
| Figure 3 – X–ray diffraction patterns of chitin and chitin derived biochar..... | 64 |
| Figure 4 – SEM images of chitin (a) and chitin derived biochar (b)..... | 64 |
| Figure 5 – N ₂ adsorption–desorption isotherms and pore size distribution curves of the chitin derived biochar..... | 66 |
| Figure 6 – Pareto charts for the responses adsorption capacity (a) and removal percentage (b)..... | 68 |
| Figure 7 – Response surfaces for adsorption capacity (a) and removal percentage (b)..... | 70 |
| Figure 8 – Kinetic curves for the MV adsorption on chitin derived biochar under different initial dye concentrations (adsorbent dosage of 0.5 g L ⁻¹ and pH of 6.8)..... | 72 |
| Figure 9 – Equilibrium curves for the MV adsorption on chitin derived biochar under different temperatures (adsorbent dosage of 0.5 g L ⁻¹ and pH of 6.8)..... | 73 |
| Figure 10– Reusability of chitin derived biochar..... | 75 |
| Figure 11 – Visible spectra of the untreated and treated with chitin derived biochar effluent..... | 76 |

ARTIGO 3

| | |
|--|----|
| Figure 1– SEM images of the MDF biochar showing (a) and (b) the particle and (c) and (d) the cavities of the material..... | 88 |
| Figure 2 – FTIR vibrational spectra of MDF residues and MDF biochar..... | 90 |
| Figure 3 – Nitrogen adsorption–desorption isotherms and the Barrett–Joyner–Halenda desorption pore size distribution (inside)..... | 91 |
| Figure 4 – Effects of pH (a) and adsorbent dosage (b) on the adsorption of FR17 dye by MDF and MDF biochar..... | 92 |
| Figure 5 – Adsorption kinetic profiles for the system MDF biochar/FR17..... | 94 |

| | |
|--|-----|
| Figure 6 – Adsorption isotherm profiles for the system MDF biochar/FR17..... | 95 |
| Figure 7– Adsorption capacities found in the consecutive adsorption–desorption cycles for the system MDF biochar/FR17..... | 97 |
| Figure 1S – Chemical structure of Food Red 17 dye..... | 103 |

LISTA DE TABELAS

REVISÃO BIBLIOGRÁFICA

Tabela 1 – Características dos processos para diferentes tipos de pirólises.....18

ARTIGO 1

Table 1 – Kinetic parameters for the adsorption of reactive red 141 on the biochar.....44

Table 2 – Equilibrium parameters for the adsorption of reactive red 141 onto the biochar.....46

Table 3 – Comparison between the new biochar and other adsorbents used for the adsorption of reactive red 141.....46

Table 4 – Thermodynamic parameters for the adsorption of reactive red 141 onto the biochar.....48

ARTIGO 2

Table 1 – Kinetic, equilibrium and thermodynamic equations used to study the MV adsorption on chitin derived biochar.....59

Table 2 – The relevant bands from FT-IR spectra of chitin and chitin derived biochar.....62

Table 3 – Elemental analysis of chitin and chitin derived biochar.....63

Table 4– Experimental and predicted values of dye removal percentage (R, %) and equilibrium adsorption capacity (q_e , mg g^{-1}) for the MV adsorption on the chitin derived biochar according to the RSM.....66

Table 5 – Kinetic parameters for the MV adsorption on the chitin derived biochar.....72

Table 6 – Isotherm parameters for the MV adsorption on the chitin derived biochar.....74

ARTIGO 3

Table 1– Maximum adsorption capacities of different adsorbents for FR17 dye.....96

Table 1S – Kinetic parameters for FR17 adsorption onto the MDF biochar.....103

Table 2S – Equilibrium parameters for the adsorption of FR17 onto the MDF biochar.....104

Table 3S – Thermodynamic parameters for the FR17 adsorption onto the MDF biochar.....104

SUMÁRIO

| | |
|--|------------|
| 1 INTRODUÇÃO..... | 12 |
| 2 OBJETIVOS..... | 14 |
| 2.1 OBJETIVO GERAL..... | 14 |
| 2.2 OBJETIVOS ESPECÍFICOS..... | 14 |
| 3. REVISÃO BIBLIOGRÁFICA..... | 15 |
| 3.1 CORANTES..... | 15 |
| 3.2 PIRÓLISE..... | 17 |
| 3.3 ADSORÇÃO..... | 19 |
| 3.3.1 Cinética de adsorção..... | 20 |
| 3.3.2 Isotherma de adsorção..... | 21 |
| 3.3.3 Termodinâmica de adsorção..... | 23 |
| 3.4 UTILIZAÇÃO DE <i>BIOCHAR</i> COMO MATERIAL ADSORVENTE..... | 24 |
| 3.5 MATÉRIAS-PRIMAS ALTERNATIVAS PARA PRODUÇÃO DE <i>BIOCHARS</i> | 26 |
| 4 RESULTADOS..... | 29 |
| ARTIGO 1 – NEW BIOCHAR FROM PECAN NUTSHELLS AS AN ALTERNATIVE ADSORBENT FOR REMOVING REACTIVE RED 141 FROM AQUEOUS SOLUTIONS..... | 30 |
| 4.2 ARTIGO 2 – CHITIN DERIVED BIOCHAR AS AN ALTERNATIVE ADSORBENT TO TREAT COLORED EFFLUENTS CONTAINING METHYL VIOLET DYE..... | 55 |
| 4.3 ARTIGO 3 – CONVERSION OF MDF WASTES INTO A BIOCHAR WITH REMARKABLE POTENTIAL TO REMOVE FOOD RED 17 DYE FROM AQUEOUS EFFLUENTS..... | 83 |
| 5 DISCUSSÃO DOS RESULTADOS..... | 107 |
| 6 CONCLUSÕES..... | 109 |
| REFERÊNCIAS..... | 111 |

1 INTRODUÇÃO

A contaminação das águas naturais tem sido um dos grandes problemas da sociedade, sendo que, os setores têxtil e alimentício apresentam especial destaque, devido às grandes quantidades de efluentes lançadas nos corpos hídricos. Os efluentes caracterizam-se por serem altamente coloridos, devido à presença de corantes que não se fixam no produto durante o processo de tingimento. Estima-se que 60% dos corantes não-fixados são descartados no meio ambiente (ABBASIAN et al., 2017). Os corantes sintéticos são substâncias potencialmente tóxicas, cancerígenas e não biodegradáveis caracterizados pela presença de cromóforos azo (N=N) ou ftalocianina (contendo cobre, níquel ou outros metais) e aromáticos (VANAAMUDAN E SUDHAKAR, 2015). A remoção destes corantes das águas residuais é um grande desafio ambiental e há uma necessidade constante de ter um processo eficaz para tal fim.

A Resolução CONAMA nº 357, de 17 de março de 2005, estabelece que os efluentes de qualquer fonte poluidora somente poderão ser lançados, direta ou indiretamente, nos corpos de água, após o devido tratamento e desde que obedeçam as condições, padrões e exigências dispostos nesta Resolução e em outras normas aplicáveis. A partir disto, as empresas começaram a dar uma maior importância às consequências dos seus processos produtivos, aumentando a preocupação por tratamentos de efluentes eficazes e economicamente viáveis.

Alguns métodos de tratamento químicos, físicos e biológicos para remoção de corantes de águas residuais são a coagulação-floculação (SAITOH et al., 2014), filtração (KAJEKAR et al., 2015), adsorção (DOTTO et al., 2015; WEBER et al., 2014), processos avançados de oxidação (COLLAZZO et al., 2012; VAIANO et al., 2015), troca iônica (WU et al., 2008), tratamento biológico (RODRIGUES et al., 2014) e separação magnética (PANKAJ E PATTAYIL, 2009). Entre estes métodos, a adsorção é uma das operações mais eficientes (AHMED, 2016) em termos de baixo custo, facilidade de implementação e operação, alta eficiência de remoção e capacidade de regeneração. No entanto, o alto custo de preparação e regeneração do carvão ativado (o principal adsorvente usado) limita a aplicação desta técnica (GAUTAM et al., 2014).

Novas pesquisas vêm sendo desenvolvidas com foco nos adsorventes de baixo custo com elevadas capacidades de adsorção na remoção de contaminantes tóxicos. Adsorventes de baixo custo, geralmente são produzidos a partir de compostos residuais abundantes e sem valor econômico significativo. Estudos sobre a produção de *biochar* a partir de materiais

obtidos de fontes naturais como possíveis precursores sustentáveis/baratos para a produção de materiais ricos em carbono estão ganhando destaque na literatura com bom custo benefício para adsorção (LI et al., 2017; DING et al., 2016; LIU et al., 2016.; TITIRICI et al. 2015). O *biochar* visa melhorar as propriedades do adsorvente em comparação com a respectiva matéria-prima, e também, reduzir os custos em comparação com a produção de carvão ativado, removendo o passo de ativação do processo.

Resíduos de cascas de noz-pecan, quitina e chapas de MDF são abundantes no Rio Grande do Sul e são descartados sem nenhuma destinação adequada. Uma alternativa para o aproveitamento desses resíduos é a sua preparação e utilização como *biochar*, podendo ser aplicados para diversos fins, onde se destaca o tratamento de efluentes coloridos. Assim consegue-se sanar dois grandes problemas ambientais: a destinação incorreta de resíduos sólidos e remoção de contaminantes presentes em efluentes.

2 OBJETIVOS

2.1 OBJETIVO GERAL

O objetivo geral deste trabalho foi desenvolver *biochars* de baixo custo a partir de materiais residuais alternativos e aplicar na remoção de corantes.

2.2 OBJETIVOS ESPECÍFICOS

- Obter e caracterizar três tipos de materiais precursores (noz-pecan, quitina e MDF);
- Preparar o *biochar* a partir dos três precursores (noz-pecan, quitina e MDF);
- Caracterizar os *biochars* utilizando técnicas de microscopia eletrônica de varredura (MEV), espectroscopia de infravermelho com transformada de Fourier (FTIR), difração de raios-x (DRX) e análise da área superficial (BET e BJH);
- Estudar a cinética, isoterma e termodinâmica de adsorção no tratamento de efluentes coloridos contendo corantes utilizando os *biochars* produzidos.

3 REVISÃO BIBLIOGRÁFICA

3.1 CORANTES

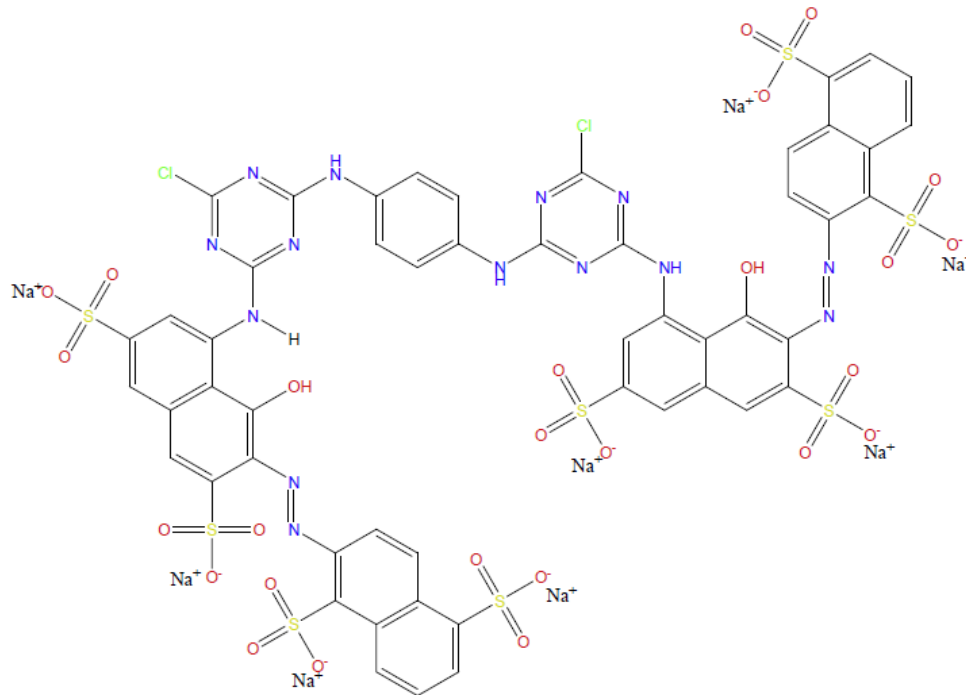
Diferentes tipos de corantes são usados em muitas indústrias, tais como, têxteis, de tintas, alimentícias, plásticas, de cosméticos, gráfica, fotográfica, como aditivos em derivados de petróleo, etc. Os corantes são definidos como sendo substâncias orgânicas que possuem a característica de serem coloridas ou fluorescentes, podendo ser de origem natural ou sintéticos, tendo a propriedade de alterar a cor de diversos materiais pela adsorção seletiva da luz (BORTOLUZZI, 2015).

Os corantes são, em geral, moléculas constituídas por dois componentes principais: os cromóforos, os quais são responsáveis por conferir a cor e, os auxocromos, responsáveis pela solubilidade e interação com o produto a ser colorido (SALLEH et al., 2011). Segundo Fernandes et al. (2010), os corantes podem ser classificados em relação a sua aplicação (ácidos, básicos, dispersos, diretos, reativos e solventes), solubilidade (solúveis e insolúveis), classe química (trifenilmetanos, azóicos, antraquinonas, nitro, xantenos e outras) e estrutura química (aniônicos, catiônicos e não iônicos) e devem possuir elevada estabilidade química e fotolítica, satisfazendo assim as propriedades de solidez exigidas.

Mais de 10 mil tipos de corantes são empregados anualmente pelas indústrias, equivalentes a cerca de 700.000 ton ano⁻¹. No Brasil, este número é equivalente a 26,5 mil ton ano⁻¹. Muitos destes são visíveis em meio aquoso em concentrações menores que 1 mg L⁻¹ e a maioria dos corantes sintéticos são altamente resistentes à degradação devido à sua estrutura química complexa (KHAN et al., 2013). Estudos recentes afirmam que dos 3000 tipos de corantes utilizados para o tingimento na indústria, estima-se que 70% são classificados como do tipo azo (N=N). Corantes dessa classe merecem maior destaque, pois, possuem alto potencial carcinogênico e mutagênico (AFTAB et al., 2011; MENDONÇA, 2011).

O vermelho reativo 141 é um corante azóico, extensivamente empregado na indústria têxtil no processo de tingimento de fibras, pois possui uma alta estabilidade da cor. Os corantes reativos representam cerca de 60% dos corantes utilizados no mundo (DÁVILA, 2016). A estrutura química do corante é ilustrada na Figura 1.

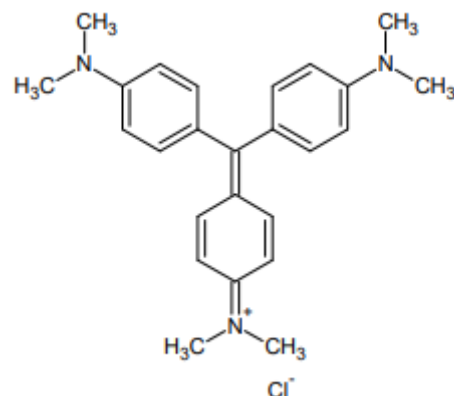
Figura 1 - Estrutura química do corante reativo vermelho 141.



Fonte: ZAZYCKI et al., 2018.

O corante têxtil metil violeta, pertence ao grupo dos triarilmetanos, sendo amplamente usado como corante roxo para têxteis tais como algodão e seda, e em tintas de impressão (BORTOLUZZI, 2015). A estrutura química do metil violeta é apresentada na Figura 2.

Figura 2 - Estrutura química do corante metil violeta.

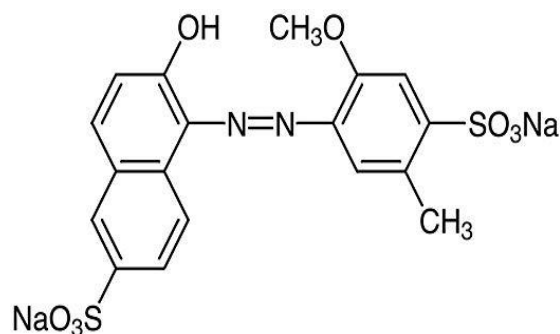


Fonte: KUMAR, 2011.

O corante alimentício vermelho nº 40, também conhecido como Food Blue 17, pertence à classe dos azocorantes, apresentando boa estabilidade à luz, calor e em ácido. É

muito utilizado em bebidas, devido sua estabilidade na presença do ácido ascórbico, um agente redutor (VIANNA et al., 2008). A estrutura química do corante é ilustrada na Figura 3.

Figura 3 - Estrutura química do corante vermelho nº 40.



Fonte: Vianna et al., 2008.

Conforme Abbasian et al. (2017), corantes são poluentes do meio ambiente que têm gerado grande preocupação, pois apresentam uma estrutura complexa e aromática fazendo com que sejam moléculas recalcitrantes e muito estáveis, dificultando sua degradação e remoção de efluentes. Devido seu grande potencial de poluição dos corpos d'água, os corantes sintéticos necessitam serem removidos, pois interferem na fotossíntese e alteram os processos biológicos da fauna e flora aquática (GUPTA; SUHAS, 2009).

O desenvolvimento de novas tecnologias para a remoção dos corantes é considerada um desafio ambiental, impulsionado pela grande diversidade e complexidade desses compostos (SALLEH et al, 2011). Um dos métodos mais eficientes para remoção de corantes sintéticos em efluentes líquidos é a técnica físico-química de adsorção. A adsorção tem se mostrado uma alternativa promissora no tratamento de efluentes coloridos comparada com outras técnicas principalmente em termos de eficiência na remoção de uma ampla gama de moléculas poluentes (TAN et al., 2007), baixo custo, facilidade de implementação e operação, alta eficiência de remoção e facilidade de regeneração (ALI et al., 2012).

3.2 PIRÓLISE

A pirólise é um processo de conversão termoquímica de um sólido orgânico por meio da quebra de ligações carbono-carbono que ocorre na ausência total ou parcial de oxigênio, resultando na formação de um grande número de compostos químicos com diversas aplicações (SHARUDDIN, et al. 2016). A pirólise transforma os diferentes tipos de biomassa

em três fases: uma sólida (*biochar*), outra gasosa, não condensável (biogás) e uma fase líquida composta por duas frações, uma aquosa e outra oleosa (bio-óleo) (KIM et al., 2012), e dependendo das condições no reator, um destes produtos pode ser maximizado (SANTOS, 2011).

Em função das condições de operação, os processos de pirólise são classificados em pirólise lenta (convencional), pirólise rápida e pirólise flash que fornecem diferentes porcentagens de rendimentos dos produtos sólidos, líquidos e gasosos (KIMURA, 2009). As características dos principais tipos de pirólise são destacadas na Tabela 1.

Tabela 1– Características dos processos para diferentes tipos de pirólises.

| | Temperatura (°C) | Taxa de Aquecimento | Tempo de Residência | Produtos Característicos |
|-----------------|------------------|---------------------|---------------------|--------------------------|
| Pirólise Lenta | 300 – 600 | Baixa | 5 a 30 min | <i>Biochar</i> |
| Pirólise Rápida | 400 – 650 | Alta | 0,5 a 5 s | Bio-óleo |
| Pirólise Flash | | | | |
| - Líquidos | 400 – 650 | Muito Alta | < 1 s | Bio-óleo |
| - Gases | > 400 | Muito Alta | < 1 s | Biogás |

Fonte: Adaptado de MOREIRA, 2015.

Conforme a Tabela 1, baixas temperaturas de processo e longos tempos de residência favorecem a produção de sólidos. Altas temperaturas e longos tempos de residência favorecem a conversão da biomassa em gás, sendo que temperaturas moderadas e curtos tempos de residência otimizam a produção de líquidos (BRIDGWATER, 2012).

A pirólise lenta é geralmente usada para a produção de *biochar*, /pois maximiza a quantidade de carvão produzido. Após pirólise lenta, a biomassa é convertida em *biochar*, enquanto o bio-óleo, o gás e o vapor são gerados como subprodutos (CHEN et al., 2014; UCHIMIYA et al., 2015). As características dos *biochars* dependem das variáveis de controle da pirólise, tais como, temperatura, taxa de aquecimento, tempo de residência, fluxo do gás de arraste, atmosfera (inerte) e matéria-prima (FIGUEIREDO et al., 2019; ZHAO et al., 2018; LIANG et al., 2016; LU et al., 2015).

De acordo com o estudo de Tang et al. (2013) o aumento na temperatura de pirólise pode conduzir ao aumento da área superficial do *biochar* facilitando o processo de adsorção. Após o processo de pirólise, cerca de 15 a 20% da matéria-prima é convertida em *biochar*,

devido à composição das biomassas em geral que apresentam em torno de 30% de matéria volátil (KIM et al., 2012).

3.3 ADSORÇÃO

Adsorção é uma operação unitária que envolve preferencialmente transferência de massa, na qual as moléculas contidas em um fluido (adsorbato) entram em contato com um sólido (adsorvente), a partir de força de atração entre o sólido e as moléculas do fluido causam sua adesão na superfície do sólido (GOMIDE, 1980). A adsorção é considerada um fenômeno complexo, na qual a intensidade das forças de atração depende da natureza e superfície do adsorvente, tipo de adsorbato, de suas interações e das condições da operação (temperatura, pH, agitação, relação adsorbato/adsorvente) (GOMIDE, 1980; HAGHSERESHT et al., 2002). A atração do sólido por certos tipos de moléculas é tão intensa que praticamente todas as moléculas incidentes ficam retidas até saturar os sítios ativos ou até que as condições da superfície (pH, forças iônicas) sejam alteradas de modo a reduzir as forças de atração (GOMIDE, 1980).

As moléculas e os átomos podem aderir à superfície de um adsorvente por meio de adsorção química ou adsorção física. Na adsorção química ou quimissorção ocorrem ligações químicas entre o adsorbato e o adsorvente, envolvendo o rearranjo de elétrons do fluido que interage com o sólido ocasionando, geralmente (mas não tão somente) as seguintes características: formação de uma única camada sobre a superfície sólida, irreversibilidade e liberação de uma quantidade considerável de energia (RUTHVEN, 1997). Na adsorção física, a interação molecular é causada geralmente por forças de Van der Waals e/ou interações eletrostáticas. As energias que são liberadas são baixas e atingem rapidamente o equilíbrio. Na fisissorção, normalmente ocorre a deposição de mais de uma camada de adsorbato sobre a superfície do adsorvente (RUTHVEN, 1997). Apesar destes aspectos gerais, a principal diferença entre a adsorção física e química é a troca ou não de elétrons entre o adsorvente e o adsorbato.

Dos métodos existentes para o tratamento de efluentes, a adsorção tem se mostrado promissora em termos de eficiência para remover uma ampla gama de moléculas contaminantes (TAN et al., 2007). É amplamente utilizada para fins de separação e purificação, tendo como uma importante aplicação à remoção de cor e contaminantes orgânicos de efluentes industriais (AL-QODAH, 2000). De acordo com Polaert et al. (2002) pode ser considerada uma técnica eficiente para remoção de contaminantes dos efluentes têxteis.

3.3.1 Cinética de adsorção

A cinética fornece parâmetros importantes como taxa de adsorção e velocidade em que acontecem (DOTTO; PINTO, 2011). Os estudos cinéticos são fundamentais para determinar as condições ideais para se alcançar a eficiência no sistema, o qual pode ser influenciado diretamente pelas características físico-químicas do adsorbato (natureza do adsorbato, massa molar, solubilidade, etc.), do adsorvente (natureza, estrutura de poros) bem como da solução (pH, temperatura e concentração) (SCHIMMEL, 2008).

Para um melhor estudo sobre o comportamento cinético de adsorção, as curvas experimentais geralmente são ajustadas a modelos da literatura, tais como, o de pseudoprimeira ordem (PPO), pseudossegunda ordem (PSO), ordem geral (OG) e Elovich.

O modelo cinético de pseudoprimeira ordem foi proposto inicialmente por Lagergren no ano de 1898, baseado na lei de resfriamento de Newton. O modelo assume que a adsorção ocorre como consequência de um gradiente de concentração entre a superfície do adsorvente e a solução, e pode ser expresso de acordo com a Equação 1 (QIU et al., 2009):

$$q_t = q_1(1 - \exp(-k_1 t)) \quad (1)$$

onde q_1 é o valor teórico da capacidade de adsorção (mg g^{-1}) e k_1 é a constante cinética de pseudoprimeira ordem (min^{-1}).

O modelo cinético de pseudossegunda ordem é geralmente adequado em processos de adsorção química (SKODRAS et al., 2008). Este modelo pode ser representado de acordo com a Equação 2 (QIU et al., 2009):

$$q_t = \frac{1}{(1/k_2 q_2^2) + (t/q_2)} \quad (2)$$

em que q_2 é o valor teórico da capacidade de adsorção (mg g^{-1}) e k_2 é a constante cinética do referido modelo ($\text{g mg}^{-1} \text{min}^{-1}$).

Uma alternativa para os modelos de pseudoprimeira ordem (PPO) e pseudossegunda ordem (PSO) é o modelo de ordem geral (OG). Para este modelo o processo de adsorção na superfície do adsorvente é assumido como sendo a etapa que controla a velocidade, representado pela Equação 3 (ALENCAR et al., 2012):

$$q_t = q_n - \frac{q_n}{[k_n(q_n)^{n-1}t(n-1) + 1]^{1/(n-1)}} \quad (3)$$

onde q_n é a capacidade teórica de adsorção (mg g^{-1}), k_n é a constante cinética ($\text{min}^{-1}(\text{g mg}^{-1})^{n-1}$) e n é a ordem de reação.

Quando os processos de adsorção envolvem quimissorção em superfície sólida, e a velocidade de adsorção decresce com o tempo devido à cobertura da camada superficial, o modelo de Elovich é um dos mais usados, e é representado na Equação 4 (WU et al., 2009):

$$q_t = \frac{1}{a} \ln(1 + abt) \quad (4)$$

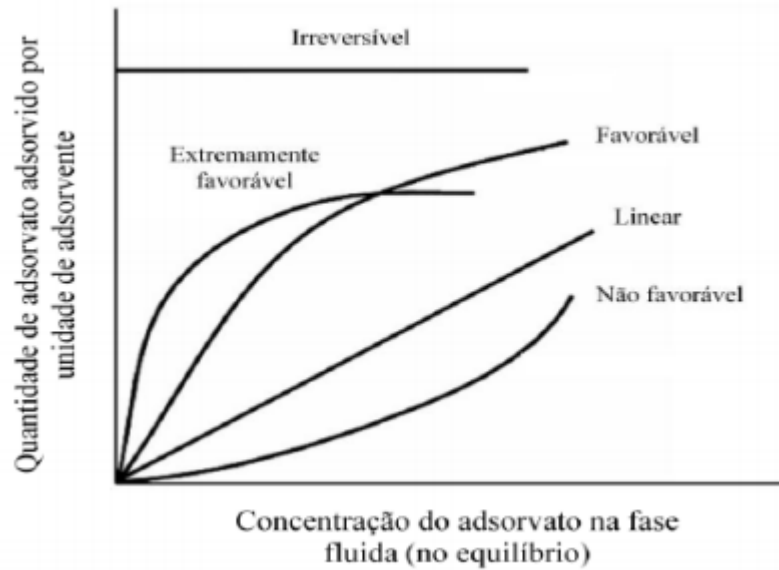
onde 'b' é a taxa inicial de adsorção devido $(dq/dt)=b$, quando $q_t=0$ ($\text{mg g}^{-1} \text{min}^{-1}$) e 'a' é a constante de dessorção do modelo de Elovich (g mg^{-1}), que indica a extensão da cobertura da superfície.

3.3.2 Isoterma de adsorção

As isotermas de adsorção indicam o mecanismo da adsorção, possibilitando descrever os estados de equilíbrio de um sistema. De acordo com Geankoplis (1993), a isoterma de adsorção é a relação do equilíbrio entre a concentração na fase fluida e a concentração nas partículas adsorventes a uma dada temperatura. Na adsorção, o pH, a temperatura e o tipo de material adsorvente influenciam e definem a forma da isoterma (GEANKOPLIS, 1993). A Figura 1 apresenta as formas mais comuns das isotermas de adsorção em fase líquida.

A isoterma linear considera que a quantidade de soluto adsorvido é proporcional à concentração no fluido. As isotermas convexas são consideradas favoráveis, uma vez que grandes quantidades de soluto podem ser obtidas a baixas concentrações no fluido. É irreversível quando a afinidade entre o adsorbato e o adsorvente é muito elevada e por isso há um aumento inicial rápido. As isotermas côncavas são consideradas não favoráveis, uma vez que quantidades relativamente baixas de soluto são adsorvidas e também são consideradas raras, mas auxiliam na compreensão do processo de dessorção (McCABE et al., 2005).

Figura 4– Formas típicas de isotermas.



Fonte: McCABE et al., 2005.

Diversos modelos foram propostos para descrever os dados de equilíbrio de adsorção, incluindo, Langmuir, Freundlich e multicamadas BET (WON et al., 2014).

O modelo de isoterma de Langmuir, conforme a Equação 5, considera uma adsorção em monocamada sobre superfície homogênea, onde os sítios de ligação possuem a mesma afinidade e energia (LANGMUIR, 1918).

$$q_e = \frac{q_m k_L C_e}{1 + k_L C_e} \quad (5)$$

em que q_m é a máxima capacidade de adsorção (mg g^{-1}), k_L é a constante de Langmuir (L mg^{-1}), q_e é a capacidade de adsorção (mg g^{-1}) e C_e é a concentração de equilíbrio (mg L^{-1}).

Um aspecto importante do modelo de Langmuir é o fator de equilíbrio, R_L (Equação 6). Os valores de R_L indicam a natureza da isoterma.

$$R_L = \frac{1}{1 + (k_L C_e)} \quad (6)$$

para $R_L = 1$, a isoterma é linear, $0 < R_L < 1$ indica um processo favorável e, $R_L = 0$ indica um processo irreversível.

A isoterma de Freundlich considera que a adsorção ocorre em superfície heterogênea e que a quantidade de adsorbato adsorvido aumenta infinitesimalmente com um aumento da concentração (FREUNDLICH, 1906) (Equação 7):

$$q_e = k_F C_e^{1/n} \quad (7)$$

em que k_F é a constante de Freundlich ($(\text{mg g}^{-1})(\text{L mg}^{-1})^{1/n}$) e $1/n$ é o fator de heterogeneidade.

O modelo de Sips é a combinação dos modelos de Langmuir e Freundlich e, pode ser expresso na forma da Equação 8 (SIPS, 1948):

$$q_e = \frac{q_m k_S C_e^{1/ns}}{1 + k_S C_e^{1/ns}} \quad (8)$$

onde k_S é a constante de equilíbrio de adsorção de Sips $(\text{mg L}^{-1})^{-1/ns}$, q_m é a capacidade máxima de adsorção (mg g^{-1}) e ns é o expoente de Sips.

A isoterma adotada para descrever a adsorção em multicamadas é a de BET (LIU, 2009) (Equação 9). Essa isoterma considera a formação de uma ou mais camadas de adsorção, sendo que a energia liberada na formação da primeira camada é típica de cada sistema e as energias liberadas na formação das demais camadas são iguais entre si.

$$q_e = \frac{q_{\text{BET}} k_1 C_e}{(1 - k_2 C_e)(1 - k_2 C_e + k_1 C_e)} \quad (9)$$

onde q_{BET} é a capacidade de adsorção em monocamada (mg g^{-1}) e k_2 e k_1 são constantes do BET (L mg^{-1}) .

3.3.3 Termodinâmica de adsorção

Os parâmetros termodinâmicos de adsorção, como, variação da energia livre de Gibbs padrão (ΔG°), variação da entalpia padrão (ΔH°) e variação da entropia padrão (ΔS°), são importantes para determinar se o processo é espontâneo, exotérmico ou endotérmico e se o adsorvente tem alta afinidade com o adsorbato. Com estes parâmetros também é possível obter informações relativas à heterogeneidade da superfície do adsorvente e se o processo envolve adsorção física ou química (MILONJIC et al., 2007; ZHANG et al., 2012).

A variação de energia livre de Gibbs pode ser estimada de acordo com a equação 10:

$$\Delta G^0 = -RT \ln(\rho_w k_D) \quad (10)$$

onde K_D é a constante de equilíbrio ($L g^{-1}$), ρ_w é a densidade da solução ($g L^{-1}$), T é a temperatura (K) e R é a constante universal dos gases ($8.314 J mol^{-1} K^{-1}$).

O conceito mais comum e conhecido sobre a termodinâmica é de que a energia livre de Gibbs corresponde à diferença entre a entalpia e a entropia a uma temperatura constante. Aplicando esse conceito a equação 10, os parâmetros termodinâmicos ΔH^0 e ΔS^0 podem ser determinados através do gráfico de Van't Hoff, ajustando os dados da Equação 11 (ZHANG et al., 2012):

$$\ln(\rho_w k_D) = \frac{\Delta S^0}{R} - \frac{\Delta H^0}{RT} \quad (11)$$

3.4 UTILIZAÇÃO DE *BIOCHAR* COMO MATERIAL ADSORVENTE

O carvão ativado é o adsorvente mais utilizado, por ser um sólido com alta porosidade e fácil de ser produzido a partir de diversos materiais carbonáceos, ou seja, que possuem alto teor de carbono, o carvão ativado tem uma grande aplicação como adsorvente com propriedades importantes se destacando como um adsorvente em potencial, diante da boa resistência mecânica para suportar o manuseio e utilização, e também mediante a sua natureza físico-química e seletividade (YANG; QIU, 2011).

Altenor et al. (2009) descrevem o carvão ativado como um importante material para adsorção de moléculas, porém sua desvantagem é seu alto custo. Como alternativa ao carvão ativado, materiais carbonizados não ativados como o *biochar* vêm ganhando destaque na literatura como material alternativo e com bom custo benefício para a adsorção. *Biochar* é o produto rico em carbono obtido da biomassa na presença de pouco ou nenhum oxigênio, ou seja, produzido por decomposição térmica da matéria orgânica sob condições limitadas de oxigênio (O_2) e a temperaturas relativamente baixas (<700 °C) (TAN et al., 2016; WOO et al., 2016).

O *biochar* pode ser usado no melhoramento dos solos, recuperação de áreas degradadas, remediação de áreas contaminadas, tratamento de águas e efluentes e na mitigação de gases de efeito estufa (GEE). Muitas pesquisas têm reportado o uso do *biochar* como adsorvente alternativo no tratamento de efluentes devido sua natureza porosa, grande

área superficial e abundantes grupos funcionais de superfície (TAN et al., 2015; MOHAN et al., 2014).

Sewu et al. (2017) produziram *biochar* a partir de repolho coreano (RC), palha de arroz (PA) e lascas de madeira (LM) e investigaram o uso como adsorvente alternativo ao carvão ativado (CA) no tratamento de águas residuais. O vermelho congo (VC) e o cristal violeta (CV) foram utilizados como modelos de corante aniônico e catiônico, respectivamente. O pH da solução inicial teve pouco efeito na adsorção de VC e CV. Os modelos isotérmicos e dados cinéticos mostraram que a adsorção de VC e CV em todos os *biochars* foram predominantemente por quimissorção. Todos os *biochars* apresentaram menor capacidade de adsorção para VC do que CA. RC apresentou maior capacidade de adsorção de Langmuir (1304 mg g^{-1}) do que CA (271.0 mg g^{-1}), PA (620.3 mg g^{-1}) e LP (195.6 mg g^{-1}) para CV. RC pode ser uma boa alternativa à CA convencional como adsorvente industrialmente viável para remoção de corantes catiônicos em águas residuais.

Lonappan et al. (2016) avaliaram micropartículas de *biochars* preparadas a partir de três tipos de *biochars* derivados de resíduos de madeira de pinheiro (BC-MP), estrume de porco (BC-EP) e papelão (BC-PA) sob várias condições de pirólise. A capacidade de adsorção de cada *biochar* foi determinada por testes de adsorção em azul de metileno e comparada com carvão ativado comercial. Os resultados experimentais mostraram que a adsorção do corante aumentou com a concentração inicial da dosagem de adsorvente. As micropartículas de *biochars* preparadas a partir de diferentes resíduos apresentaram melhora na capacidade de adsorção ($7,8 \pm 0,5 \text{ mg g}^{-1}$ a $25 \pm 1,3 \text{ mg g}^{-1}$) em comparação com o *biochar* bruto e o carvão ativado comercial. A capacidade de adsorção variou com o tipo de resíduo e o método de produção do *biochar*. A capacidade máxima de adsorção foi de 25 mg g^{-1} para micropartículas BC-EP a 25 °C para uma concentração de adsorvente de 500 mg L^{-1} em comparação com $48,30 \pm 3,6 \text{ mg g}^{-1}$ para o carvão ativado. Os dados de adsorção de equilíbrio foram melhores descritos pelo modelo de Langmuir para BC-EP e BC-PA e modelo de Freundlich para BC-MP.

Nautiyal et al. (2016) estudaram a utilização de biomassa residual (BR) de algas de *Spirulina platensis*, deixada após transesterificação in situ, para a preparação de *biochar*. O *biochar* (BC) foi examinado quanto a sua capacidade de adsorver o corante vermelho congo de soluções aquosas. Os resultados foram comparados com outros adsorventes utilizados no estudo, biomassa original de algas (BA) de *Spirulina platensis*, carvão ativado (CA) e BR. O BC mostrou um aumento no teor de carbono fixo e diminuição da matéria volátil em comparação com os outros adsorventes utilizados. Os adsorventes CA e BC mostraram

melhor desempenho na remoção de corante, 85,4% e 82,6% respectivamente, em comparação com BA (76,6%) e BR (78,1%). Os resultados dos estudos de adsorção mostraram que a absorção máxima para o BC foi observada em pH 2 com 0,2 g 100 ml⁻¹ de dosagem de adsorvente e 90 mg l⁻¹ de concentração inicial. A isoterma de Freundlich foi a que melhor se ajustou aos dados com valor de coeficiente de correlação de 99,12%. A alta capacidade de adsorção do *biochar* destaca sua utilização como adsorvente efetivo para a remoção de corantes de águas residuais.

Portanto, muitos pesquisadores têm se concentrado na produção de *biochar* a partir de diferentes precursores sustentáveis e de baixo custo, incluindo resíduos agrícolas (casca de arroz, palha de milho, bagaço, etc.) e resíduos sólidos (lodo, resíduos de alimentos, resíduos de jardim, etc.) (CHEN et al., 2011; YAHYA et al., 2015).

3.5 MATÉRIAS-PRIMAS ALTERNATIVAS PARA PRODUÇÃO DE *BIOCHARS*

No sul do Brasil, existem extensas áreas de plantação de árvore de Nogueira–pecan (*Carya illinoensis*), nativas da América do Norte. O estado do Rio Grande do Sul é o maior produtor do país, seguido pelos estados do Paraná e Santa Catarina (ORTIZ, 2000). A longevidade da Nogueira–pecan pode superar 200 anos. Ela é uma árvore que pode atingir grande porte, superando 40 metros de altura, 40 metros de diâmetro de copa e 20 metros de circunferência de tronco. O fruto é uma drupa, agrupando-se em cachos com normalmente três a sete unidades, com epicarpo que se separa do fruto na maturação, aproveitando-se aproximadamente 40 a 60% do fruto (ORTIZ, 2000). A semente de noz–pecan é amplamente consumida no Brasil (VAGHETTI et al., 2009), no entanto, a casca de noz é um subproduto marrom de difícil biodegradação. As cascas de noz–pecan representam 49% da noz e têm pouco ou nenhum valor econômico. A sua disposição é dispendiosa e pode causar problemas ambientais (BANSODE et al., 2003). Dessa forma estudos sobre aproveitamento deste resíduo são de extrema importância. A figura 5 apresenta o fruto e cascas de noz-pecan.

A quitina (Figura 6) é o segundo biopolímero mais abundante na natureza e é extraída de casca de crustáceos como camarões e caranguejos (WAN NGAH et al., 2011). É um biopolímero biodegradável e renovável, possui um baixo custo, o que facilita seu uso. Possui uma estrutura compacta contendo grupamentos hidroxilas e N–acetil (DOTTO et al., 2013; DOTTO et al., 2015). As cascas e cabeças de camarões representam cerca de 50% do peso total do camarão e são compostas por 15 a 40 % de quitina (KHOR, 2002). Seu uso como adsorvente para tratamento de efluentes apresenta um efeito positivo para a proteção ambiental, uma vez que a quitina é obtida a partir de resíduos.

Figura 5– Fruto e cascas de noz–pecan.



Fonte: A autora, 2019.

Figura 6– Quitina em pó.



Fonte: A autora, 2019.

Placa de fibra de média densidade (MDF) é uma madeira compensada fabricada a partir de lâminas de pinus (*Pinus elliottii*), por meio da aglutinação de fibras de madeira, resina sintética e aditivos, através da ação de pressão e calor (PIEKARSKI et al. 2017). O Brasil é o terceiro maior fabricante mundial de MDF (FAOSTAT, 2014). Segundo a MOVERGS (Associação das Indústrias de Móveis do Estado do Rio Grande do Sul) o faturamento no Brasil que era de 32,5 bilhões de reais no ano de 2011, cresceu para 35,74 bilhões no ano de 2015, o que implica invariavelmente no aumento do volume de resíduos gerados. O Rio Grande do Sul representa o segundo estado no país em faturamento na produção de móveis (ABIMÓVEL, 2012). Boa parte dos resíduos gerados no setor moveleiro são subutilizados ou, descartados de forma incorreta. A utilização de estratégias para reduzir e reutilizar os resíduos sólidos gerados nas indústrias moveleiras é pouco praticável, sendo geralmente destinados a aterros sanitários e olarias (RIUL e RIBEIRO, 2012). A figura 7 ilustra a placa de fibra de média densidade (MDF).

Figura 7– Placa de fibra de média densidade (MDF).



Fonte: A autora, 2019.

4 RESULTADOS

Os resultados obtidos neste estudo, juntamente com a discussão, serão apresentados na forma de três artigos científicos, dois já publicados e um submetido à publicação.

O ARTIGO 1 está publicado no *Journal of Cleaner Production* (ISSN: 0959–6526) com fator de impacto de 6.395; classificada com Qualis A1 na área Engenharias II. O ARTIGO 2 está publicado na *Advanced Powder Technology* (ISSN: 0921–8831) com fator de impacto de 3.250, classificada com Qualis A1 na área Engenharias II. O ARTIGO 3 está sob avaliação na revista *Chemosphere* (ISSN: 0045–6535) com fator de impacto de 5.108; classificada com Qualis A2 na área Engenharias II.

4.1 ARTIGO 1 – NEW BIOCHAR FROM PECAN NUTSHELLS AS AN ALTERNATIVE ADSORBENT FOR REMOVING REACTIVE RED 141 FROM AQUEOUS SOLUTIONS

Maria A. Zazycki^a, Marcelo Godinho^b, Daniele Perondi^b, Edson L. Foletto^a,
Gabriela C. Collazzo^a, Guilherme L. Dotto^{a,*}

^aChemical Engineering Department, Federal University of Santa Maria e UFSM, 1000,
Roraima Avenue, 97105e900 Santa Maria, RS, Brazil

^bPostgraduate Program in Engineering Processes and Technology, University of Caxias do
Sul eUCS, 1130, Francisco Getúlio Vargas Street, 95070e560,
Caxias do Sul, RS, Brazil

* Corresponding author.

E-mail address: guilherme_dotto@yahoo.com.br (G.L. Dotto).

ABSTRACT

A new biochar derived from pecan nutshell was prepared, characterized, and applied as an alternative and low-cost adsorbent for removing Reactive Red 141 (RR141) from aqueous solutions. The yield from raw pecan nutshell to biochar was approx. 30%. The biochar presented a micro/mesoporous structure with a surface area of $93 \text{ m}^2 \text{ g}^{-1}$, which is considered high for biomass derived materials. For both, raw pecan nutshell and its biochar, the RR141 adsorption was favored under acid conditions (pH of 2 and 3, respectively). The dye removal percentage was 85% using the biochar as an adsorbent, and was only 23% when raw pecan nutshell was used. The adsorption kinetics of RR141 on the biochar followed the pseudo-second order model. The equilibrium isotherms were well represented by the Freundlich model. The maximum adsorption capacity was approx. 130 mg g^{-1} . The adsorption was spontaneous, favorable, and exothermic ($\Delta H^0 = -56.42 \text{ kJ mol}^{-1}$). These findings indicated that the new biochar prepared in this work is an alternative, low-cost, and eco-friendly adsorbent that can be used to remove dyes from colored effluents.

Keywords: Adsorption. Biochar. Chemisorption. Mesoporous structure. Peanut shells. Surface area.

1 INTRODUCTION

Textile wastes dumped into the environment, especially the synthetic dyes, represents one of the main environmental problems currently, due to its great potential to pollute water bodies (ABBASIAN et al., 2017). Synthetic dyes are potentially toxic, carcinogenic, and non-biodegradable substances characterized by the presence of azo chromophores ($-\text{N}=\text{N}-$) or phthalocyanine chromophores (containing copper, nickel, or other metals) and aromatic rings (VANAAMUDAN AND SUDHAKAR, 2015). The removal of these dyes from wastewaters is a major environmental challenge and, for this purpose, there is a constant search for effective and economically viable processes (LEECHART et al., 2009).

Some chemical, physical, and biological treatment methods for dye removal from wastewaters include coagulation-flocculation (SAITOH et al., 2014), filtration (KAJEKAR et al., 2015), adsorption (AUSAVASUKHI et al., 2016), advanced oxidation processes

(COLLAZZO et al., 2012), ion-exchange (WU et al., 2008), biological treatment (RODRIGUES et al., 2014), and magnetic separation (PANKAJ AND JOY, 2009). Among these methods, adsorption has been found to be promising compared with other techniques in terms of efficiency (TANG et al., 2017), low cost, ease of implementation and operation, high removal efficiency, and regeneration capacity. However, the high cost of preparation and regeneration of activated carbon (the main used adsorbent) limits the application of this technique (ALI et al., 2012).

New research has been conducted focusing on low-cost adsorbents. A low-cost adsorbent should be abundant in nature or a by-product or waste material from any industry. Then, adsorbents obtained from agricultural wastes are low-cost alternatives to activated carbon. In the South Region of Brazil, there are extended plantation areas of pecan trees (*Carya illinoensis*), native from North America. The kernel of the pecan nut is largely consumed in Brazil (VAGHETTI et al., 2009). However, nutshell is a by-product with a complicated management. Pecan nutshells represent 49% of the pecan nut and have little or no economic value. Their disposal is costly and can cause environmental problems (BANSODE et al., 2003). In this way, the reutilization of this waste, which is generated on a large scale, can be an alternative to obtain a new adsorbent to remove water contaminants. In this context, it is important to consider that pecan nutshells are vegetal wastes and it is possible that they contain cationic compounds with a significant effect on dyes adsorption (AGUAYO-VILLARREAL et al., 2013). On the other hand, several characteristics, such as surface area, pore volume, and surface chemistry, can govern the adsorption capacity of an adsorbent (LENG et al., 2015). Li et al. (2017) reported the production of biochars by the pyrolysis of agricultural wastes for wastewater treatment. The biochar from pyrolysis aims to improve the properties of the adsorbent in comparison with the respective raw material as well as reduce the costs in comparison with the production of activated carbon, removing the activation step from the process. According to Aldana et al. (2015), the thermal pyrolysis of pecan nutshell occurs in two stages: The first stage is the hemicellulose decomposition and the second stage is the cellulose decomposition.

Some works reported the development of biochars from alternative materials, including sewage sludge (LENG et al., 2015), peanut shells (GEORGIN et al., 2016) and oil distillation residue (LI et al., 2017). These biochars were used for the removal of contaminants from aqueous media. Also, works reported the use of raw pecan nutshells as alternative adsorbents to remove metals (VAGHETTI et al., 2009) and dyes (AGUAYO-VILLARREAL et al., 2013) from aqueous media. From the best of our knowledge, there are

no studies regarding to the preparation of a biochar from pecan nutshells and its application as an alternative adsorbent for removing a large dye molecules such as Reactive Red 141 from aqueous media. The development of a biochar from pecan nutshells and its application as adsorbent has a synergistic effect from the cleaner production viewpoint, contributing for the solid wastes management and for the treatment of liquid effluents.

Aiming to find a new and inexpensive adsorbent for dye removal as well as diminish the large amount of pecan nutshells, a new biochar was prepared, characterized, and applied for the removal of RR141 dye from aqueous solutions. First, the biochar was developed and characterized in detail. Then, the potential of biochar to adsorb RR141 was compared with its precursor (pecan nutshells). The adsorption of RR141 on the biochar was finally studied from the kinetic, equilibrium, and thermodynamic viewpoints.

2 MATERIALS AND METHODS

2.1 OBTENTION AND PRETREATMENT OF PECAN NUTSHELL

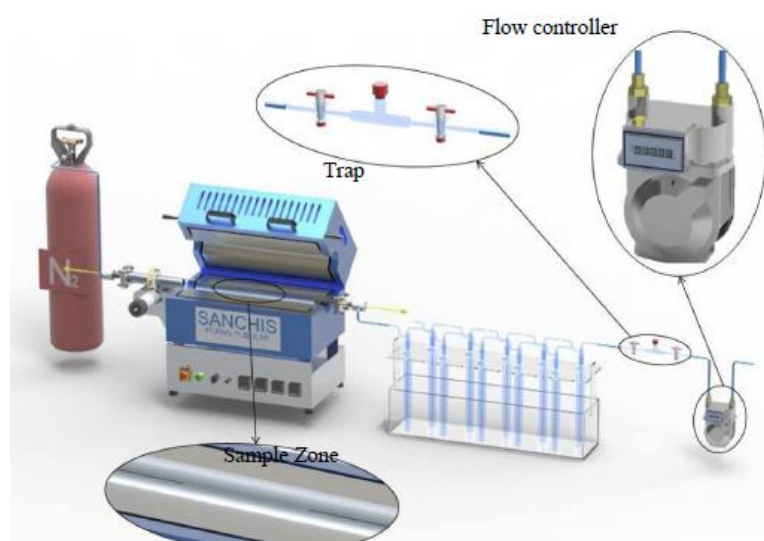
Pecan nutshell (*Carya Illinoensis*) samples were obtained from a pecan-producing region in the South Region of Brazil. The samples were washed several times with deionized water, oven dried at 60 °C for 8 h. Then, pecan nutshell samples were ground in a Wiley mill and subsequently sieved. The fraction with diameter of particles lower than 710 µm was stored in closed bottles to be used in the biochar preparation.

2.2 BIOCHAR PREPARATION

The biochar was prepared from pecan nutshell via pyrolysis process. The sample was pyrolyzed in a bench reactor that operates in a batch system (Figure 1). The system has an oven with a quartz reactor coupled internally. The reactor has the following dimensions: 981 mm length, 49 mm outside diameter, and 43 mm internal diameter. The useful length of the oven is 516 mm. The reactor is heated electrically by two resistors, each one with 1900 W. Two type K thermocouples are positioned inside the reactor. A cylindrical quartz reactor was charged with approximately 50 g of pecan nutshell (previously dried at 105 °C) and the system run under nitrogen gas (N₂) at 0.25 L min⁻¹. The heater temperature was increased at a rate of 10 °C min⁻¹ until 800 °C, being held at 800 °C for 60 min and allowed to cool still under N₂ flow to room temperature. The pyrolysis vapors condensation was conducted in accordance with CEN BT/TF 143 standard (CEN COMITÉ EUROPÉEN DE NORMALISATION, 2004), and ten bubblers were used. In each experiment, 100 mL of

isopropyl alcohol were added in each bubbler, except for the first and last (empty). All the bubblers were kept in a cold box (ice bath, salt, and isopropyl alcohol). The bio-oil and biochar were collected and their masses determined for yield computation. The biochars produced were treated with H_2SO_4 to remove ash, washed in distilled water and dried at 105 °C. Subsequently, the biochars were ground with a mortar and pestle, sieved and stored in plastic containers to be used for characterization and successive adsorption experiments. All the conditions used in the biochar preparation were determined by preliminary experiments.

Figure 1– Scheme for the biochar preparation.



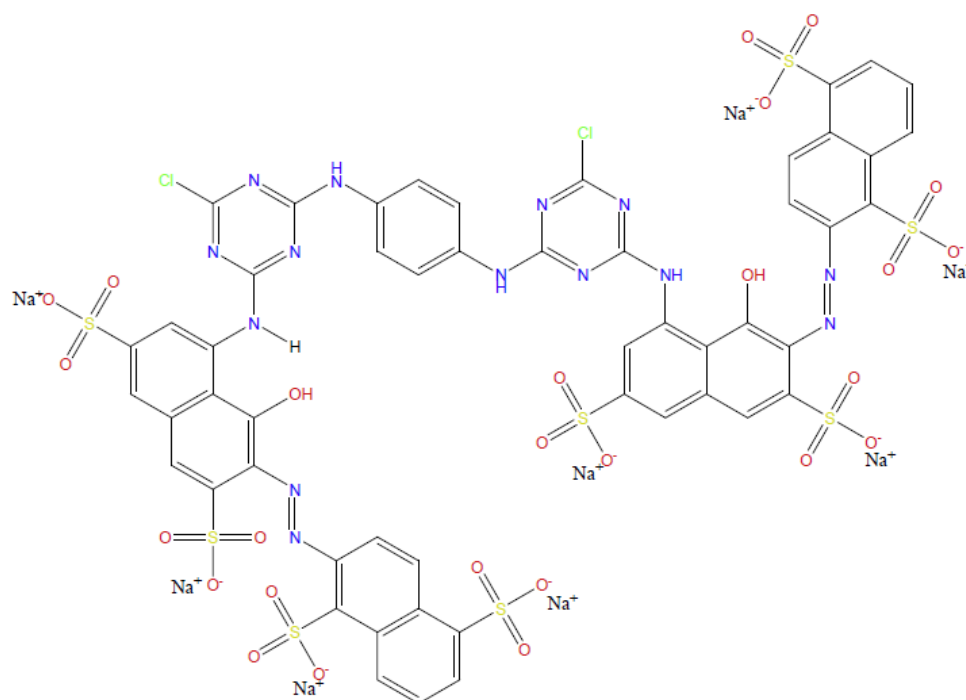
2.3 CHARACTERIZATION TECHNIQUES

The pecan nutshell and biochar characteristics were determined by scanning electron microscopy (SEM) (JEOL, JSM-6060, JAPAN) (GOLDSTEIN et al., 1992), Fourier transform infrared spectroscopy (FTIR) (SHIMADZU, PRESTIGE 21, JAPAN) (SILVERSTEIN et al., 2007) the FTIR analysis was performed by ATR (total attenuate reflectance) technique. The samples thicknesses were remained the same in order to compare the transmittance values. The thicknesses were obtained from 10 measurements taken at different locations on the sample by a digital micrometer (INSIZE, IP54, BRAZIL) with 0.0010 mm of resolution, X-ray diffraction (XRD) (RIGAKU, MINIFLEX 300, JAPAN) (BRINDLEY AND BROWN, 1980), and surface area analysis (QUANTACHROME INSTRUMENTS, NOVA 1200E, USA). The specific surface area was determined from the Brunauer, Emmett, and Teller (BET) multipoint method and the pore size distribution was obtained using Barret, Joyner, and Halenda (BJH) method (THOMMES et al., 2015).

2.4 BATCH ADSORPTION EXPERIMENTS

The dye used as a model compound was Reactive Red 141 (RR141) (CAS number 61931-52-0, chemical formula is $C_{52}H_{26}O_{26}S_8Cl_2N_{14}Na_8$, molecular weight = $1774.15 \text{ g mol}^{-1}$), extensively used in the textile industry. The optimized chemical structure of the dye is shown in Figure. 2.

Figure 2– Chemical structure of reactive red 141.



Chemical Formula: $C_{52}H_{26}Cl_2N_{14}Na_8O_{26}S_8$

Molecular Weight: 1774.150

Elemental Analysis: C, 35.20; H, 1.48; Cl, 4.00; N, 11.05; Na, 10.37; O, 23.45; S, 14.46

The experiments were carried out in a thermostatted shaker (SOLAB, SL 222, BRAZIL) at 250 rpm. The pH effect on the dye removal was examined for raw pecan nutshell and its biochar. The studied pH was from 2.0 to 8.0, adjusted by the addition of HCl or NaOH. 0.05 g of adsorbent was added to 50 mL of dye aqueous solutions with initial concentration of 50 mg L^{-1} and stirred at $25 \text{ }^\circ\text{C}$ for 4 h. For the kinetic studies, 0.05 g of biochar was added to 50 mL of dye aqueous solutions at different initial concentrations (50, 100, 200, 300 and 500 mg L^{-1}). The contact time was from 0 to 240 min. For the equilibrium studies, 0.05 g of biochar was added to 50 mL of dye aqueous solutions with different initial

concentrations (50, 100, 200, 300, and 500 mg L⁻¹) and different temperatures (298–328 K), being stirred until the equilibrium.

After all of the experiments, the solid phase was separated by filtration using a filter paper (with negligible interaction with the dye) and, the dye concentration in liquid phase was determined by spectrophotometry at the maximum wavelength of absorption ($\lambda_{\text{max}} = 538$ nm) using a spectrophotometer (BIOSPECTRO, SP-22, BRAZIL). The experiments were carried out in triplicate and blanks were performed. The dye removal percentage (R, %), adsorption capacity at any time t (q_t , mg g⁻¹) and the equilibrium adsorption capacity (q_e , mg g⁻¹), were determined by Equations. (1)–(3), respectively:

$$R = \frac{(C_0 - C_f)}{C_0} 100 \quad (1)$$

$$q_t = \frac{V(C_0 - C_t)}{m} \quad (2)$$

$$q_e = \frac{V(C_0 - C_e)}{m} \quad (3)$$

where, C_0 is the initial dye concentration in liquid phase (mg L⁻¹), C_t is the dye concentration in liquid phase at any time (mg L⁻¹), C_e is the equilibrium dye concentration (mg L⁻¹), m is the amount of adsorbent (g) and V is the volume of solution (L).

2.5 KINETIC, EQUILIBRIUM, AND THERMODYNAMIC STUDIES

The kinetic aspects involved in the adsorption of RR141 onto biochar was studied using pseudo-first order (Equation (4)) (LAGERGREN, 1898), pseudo-second order (Equation (5)) (HO AND MCKAY, 1998) and Elovich (Equation (6)) (ZELDOWITSCH, 1934) models.

$$q_t = q_1(1 - \exp(-k_1 t)) \quad (4)$$

$$q_t = \frac{1}{(1/k_2 q_2^2) + (t/q_2)} \quad (5)$$

$$q_t = \frac{1}{a} \ln(1 + abt) \quad (6)$$

where, k_1 and k_2 are the rate constants of pseudo–first order and pseudo–second order models, respectively, in (min^{-1}) and ($\text{g mg}^{-1} \text{min}^{-1}$), q_1 and q_2 are the theoretical values for the adsorption capacity (mg g^{-1}), b is the initial velocity due to dq/dt with $q_t = 0$ ($\text{mg g}^{-1} \text{min}^{-1}$), b is the desorption constant of the Elovich model (g mg^{-1}) and t is the time (min).

The adsorption equilibrium isotherms were adjusted using the Freundlich (Equation (7)) (FREUNDLICH, 1906) and Langmuir (Equation (8)) (LANGMUIR, 1918) models.

$$q_e = k_F C_e^{1/n} \quad (7)$$

$$q_e = \frac{q_m k_L C_e}{1 + k_L C_e} \quad (8)$$

where q_m is the maximum adsorption capacity (mg g^{-1}), k_L is the Langmuir constant (L mg^{-1}), k_F is the Freundlich constant ($\text{mg g}^{-1}(\text{mg L}^{-1})^{-1/n}$) and $1/n$ is the heterogeneity factor.

Experimental data obtained for the adsorption of RR141 onto biochar were used to calculate the thermodynamic parameters. Standard Gibbs free energy change (ΔG^0) (kJ mol^{-1}), standard enthalpy change (ΔH^0) (kJ mol^{-1}), and standard entropy change (ΔS^0) ($\text{kJ mol}^{-1} \text{K}^{-1}$) were estimated, as follows (LIU, 2009):

$$\Delta G^0 = -RT \ln(\rho_w k_D) \quad (9)$$

$$\ln(\rho_w k_D) = \frac{\Delta S^0}{R} - \frac{\Delta H^0}{RT} \quad (10)$$

where, k_D is the equilibrium constant (L g^{-1}), ρ_w is the solution density (g L^{-1}), T is the temperature (K), and R is the universal gas constant ($8.314 \text{ J mol}^{-1} \text{K}^{-1}$). The k_D values were estimated from the isotherm model that provided the best fit (LIU, 2009).

2.6 PARAMETERS ESTIMATION

The kinetic, equilibrium, and thermodynamic parameters were determined by fitting the models with the experimental data, using nonlinear regression. The quasi–Newton estimation method was used and the calculations were performed using Statistica 9.1 software

(STATSOFT, USA). The determination coefficient (R^2), adjusted determination coefficient (R^2_{adj}), and average relative error (ARE) were used to evaluate the fit quality (EL-KHAIARY AND MALASH, 2011).

3 RESULTS AND DISCUSSION

3.1 CHARACTERIZATION OF PECAN NUTSHELL AND BIOCHAR

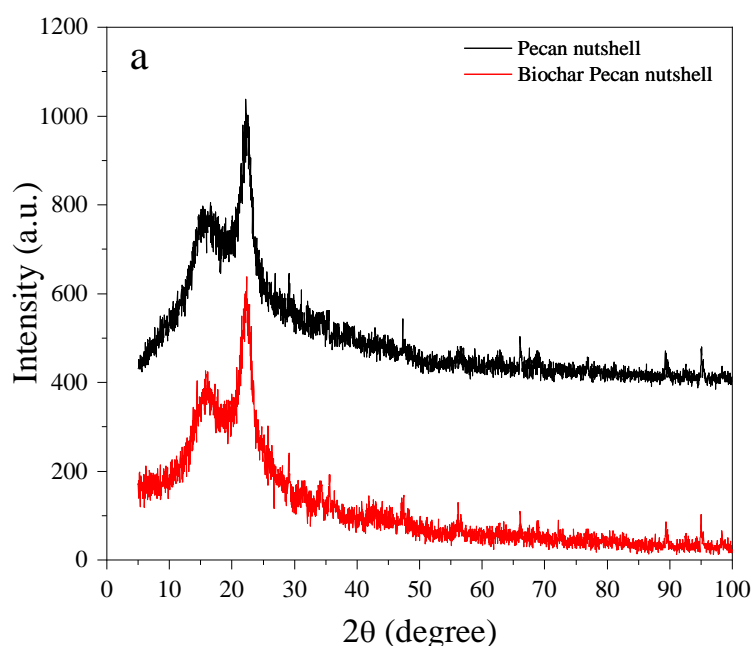
The physical and chemical properties of pecan nutshell and its biochar are shown in Figures. 3 and 4. The X-ray diffraction patterns were measured to investigate the crystal phase compositions of the pecan nutshell and its biochar. XRD diffraction patterns are shown in Figure 3a and not the crystalline phase was observed in both materials. Therefore, it can be stated that pecan nutshell and its biochar have an amorphous structure. The amorphous structure is in general adequate for dye adsorption purposes. An amorphous adsorbent have a more disorganized structure, with more empty spaces. This type of structure allows the accommodation of the large dye molecules into the adsorbent surface (CRINI AND BADOT, 2008).

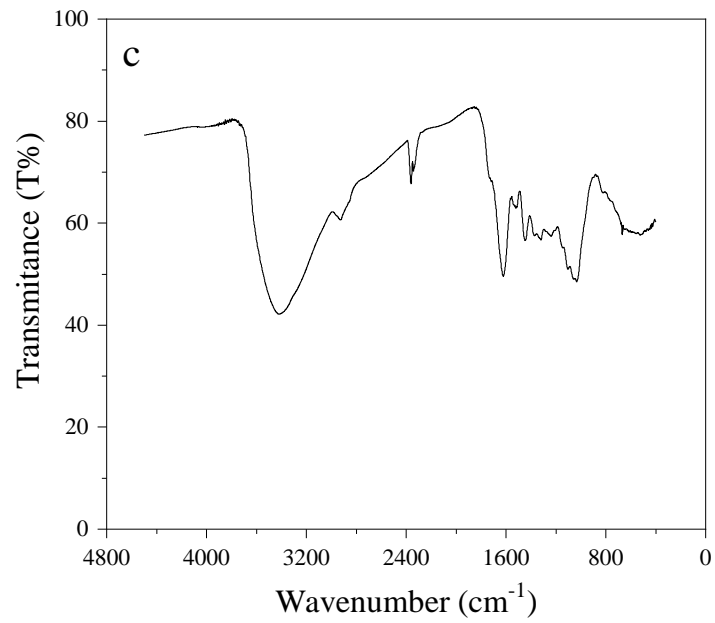
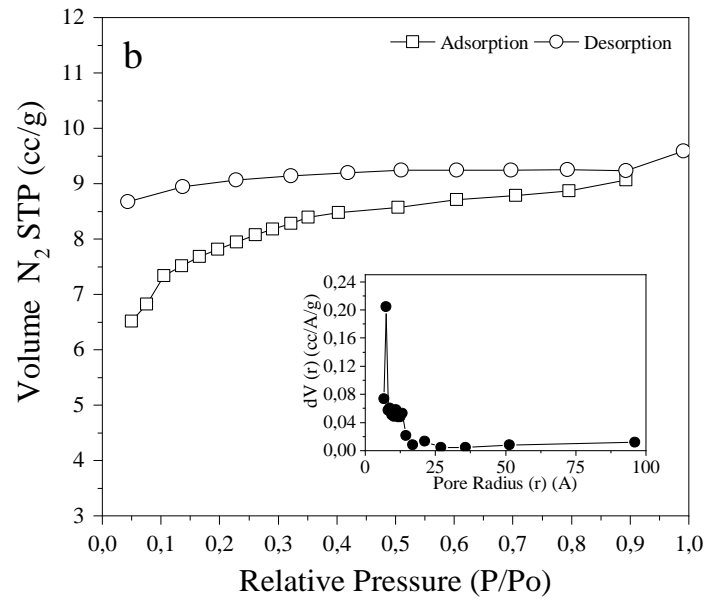
The biochar yield was around 30%, which is consistent with the ash and carbon content for the biochars from pecan nutshell, according to Aldana et al. (2015). Moreover, the biomasses generally have a volatile matter content of approx. 70%. The biochar yield shows that the pyrolysis of the raw sample was complete, eliminating all volatile matter. Therefore, producing a biochar composed of carbon and ash, with a high yield and probably high surface area. This result will be corroborated in the FTIR and surface area analysis.

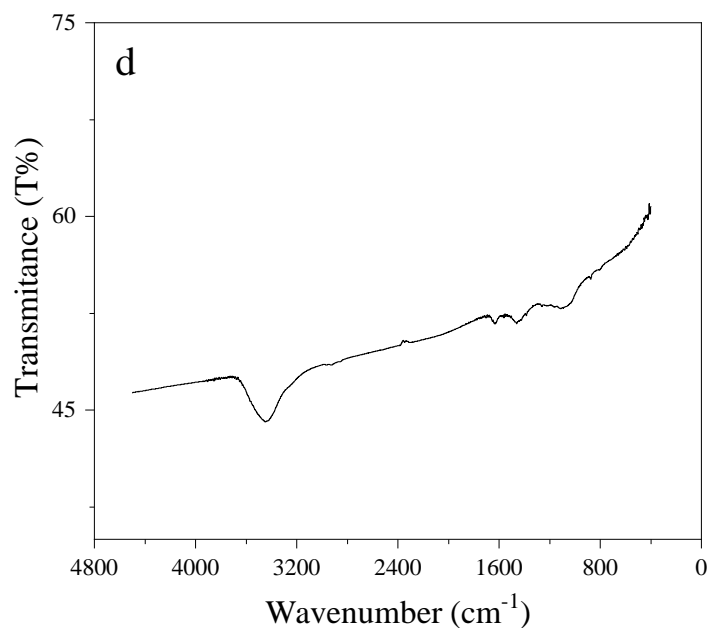
The FTIR vibrational spectra of raw pecan nutshell and its biochar are reported in Figure 3c and d, respectively. The main intense bands in Figure 3c were found at 3400 cm^{-1} , 2943 cm^{-1} , 1620 cm^{-1} , and 1030 cm^{-1} . Most of the bands are similar in relation to the FTIR spectrum of commercial cellulose (SUAREZ-GARCIA et al., 2002). The band at 3400 cm^{-1} can be assigned to the O-H stretching vibrations of carboxylic acids, phenols, alcohols, or water and the band at 2943 cm^{-1} was assigned to C-H bond presented in the pecan nutshell structure (TRAN et al., 2017). At 1620 cm^{-1} the C=C stretching of aromatic rings can be verified. Finally, at 1030 cm^{-1} might represent the C-O-C of an ether group (JACQUES et al., 2007). After the pyrolysis process (Figure 3d), the volatile matter was removed from the pecan nutshell and only the bands at 3400 , 1620 , and 1030 cm^{-1} remained, but at a lower intensity. This trend confirms that the volatile matter was removed, corroborating the biochar yield, and probably increasing the surface area.

As shown in Figure 3b, the N₂ adsorption isotherm is a Type I according to the IUPAC classification (THOMMES et al., 2015), which is a typical characteristic of microporous materials. Furthermore, a wide knee (hysteresis loop not well defined) is present in the adsorption/desorption isotherms, characterizing the presence of mesopores. From the pore size distribution data, the presence of micropores and mesopores with dimensions below 25 Å as observed. Finally, the biochar presented a high BET surface area (93 m² g⁻¹), high total pore volume (0.055 cm³ g⁻¹), and an average pore size of 12 Å. Usually, pyrolytic chars prepared from waste at temperatures from 450 to 1000 °C exhibit specific surface areas in the range of 78–90 m² g⁻¹ (LI et al., 2005). Furthermore, the biochar presented surface area 40 times higher than its precursor (pecan nutshell, surface area 2.1 m² g⁻¹).

Figure 3– (a) XRD spectrum; (b) nitrogen adsorption–desorption isotherms and the Barrett–Joyner–Halenda desorption pore size distribution (inset); (c) and (d) FTIR spectra of Pecan nutshell and biochar.



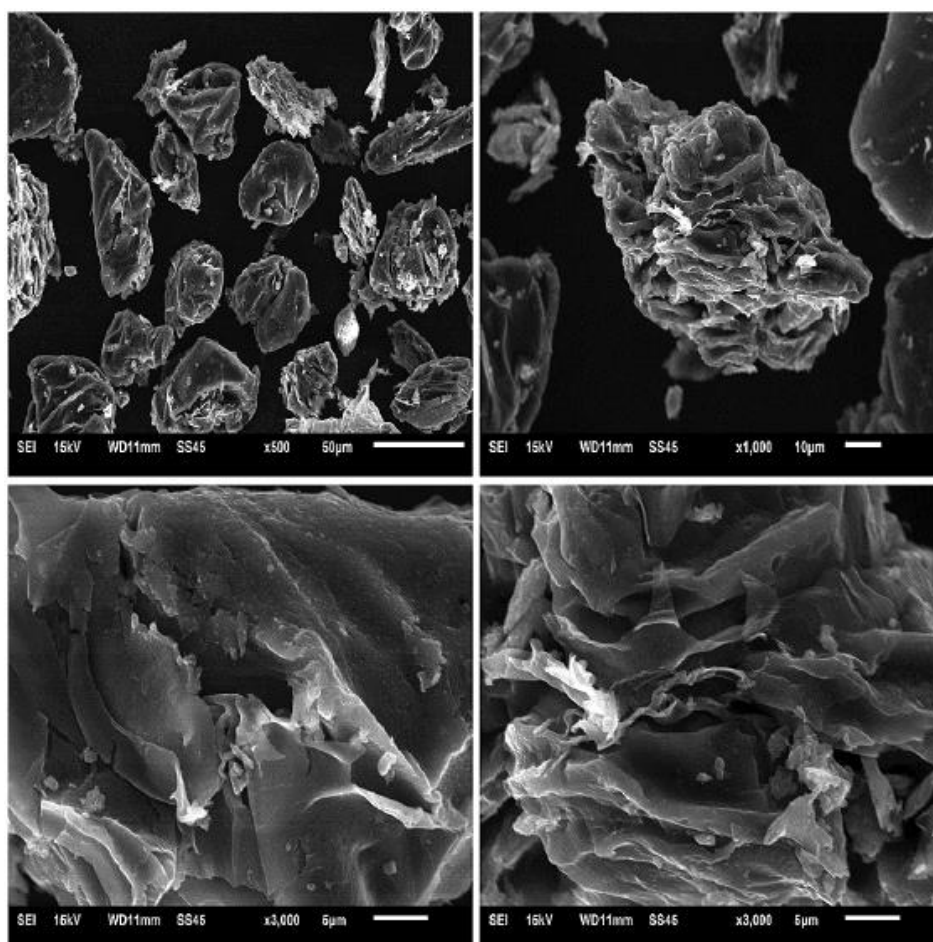




The biochar SEM images are shown in Figure 4. Cavities and some visible pores were observed. These SEM images confirm that the pyrolysis process provided important modifications in the pecan nutshell surface as well as the results of the other characterization techniques. Protuberances, cavities, and grooves are favorable for adsorption purposes, since they allow the penetration of the dyes into the adsorbent structure (SOLTANI et al., 2015). The biochar prepared in this study can be compared with researches from Vagheti et al. (2009). They showed that pecan nutshell presented a compact surface with some fissures in its structure, mainly in the cross section. In addition, Figure 4 illustrates that the biochar presented an irregular and heterogeneous surface. The biochar particle diameter and the mean size of the surface cavities were measured on the image and were approx. 60 and 5 mm, respectively. These cavities are large, allowing for the penetration of dye molecules into the lignocellulosic structure and then interaction with the surfasse groups (BRITO et al., 2010).

In general lines, Figures. 3 and 4 revealed that the biochar prepared from pecan nutshell presented improvements in the physicochemical characteristics in relation to the raw pecan nutshell. Characteristics such as, surface area, pore volume, and average pore radius were increased and important modifications on the adsorbent surface were visualized.

Figure 4– SEM images of the biochar showing (a) and (b) the particle and (c) and (d) the cavities of the material.



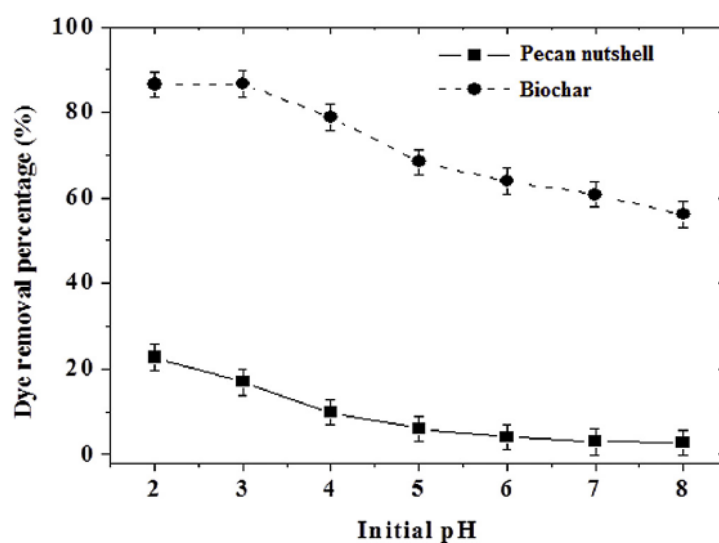
3.2 pH EFFECT

The adsorption of RR141 on raw pecan nutshell and its biochar was examined from pH 2.0 to 8.0. The results are depicted in Figure 5. For both adsorbents, it was observed that the dye removal percentage increased with the pH decrease, being the best results obtained at pH 2–3. This occurred because under acid conditions (pH 2 or 3) the adsorbents are positively charged. In parallel, the RR141 anionic dye (Figure 2) has several sulfonated groups (the pK_a of these groups are negative), which are negatively charged. Therefore, the negatively charged dye molecules are attracted by the positively charged groups on the adsorbents surfaces, increasing the dye removal percentage. In general, this behavior is common for anionic dyes, as presented by Gomes et al. (2016) in the adsorption of tannery dyes (optimum pH was 2.3) and Subramani and Thinakaran (2017) in the adsorption of RR198 (best pH was 4.0).

Figure 5 shows that the dye removal percentage was 85% using the biochar as an adsorbent, and was only 23% when raw pecan nutshell was used. This confirms that the

biochar preparation is an excellent alternative to improve the adsorption characteristics of the pecan nutshell biomass. This result can be explained on the basis of the changes of the pecan nutshell physicochemical characteristics, which occurred as a result of the biochar preparation. For example, the volatile matter was removed, pores and cavities were formed, and the surface area increased from unities ($2.1 \text{ m}^2 \text{ g}^{-1}$) to $93 \text{ m}^2 \text{ g}^{-1}$.

Figure 5– Influence of pH on the reactive red 141 removal percentage using pecan nutshell and biochar as adsorbents.



From the above results, it was demonstrated that the biochar was more efficient than raw pecan nutshell at adsorbing RR141, and the more adequate pH was 2.0–3.0. In this way, kinetic, equilibrium, and thermodynamic studies (next sections) were performed at pH 3.0 using only the biochar.

3.3 ADSORPTION KINETICS

The adsorption kinetic curves of RR141 onto the biochar were constructed at pH 3.0 and initial dye concentrations of 50, 100, 200, 300, and 500 mg L^{-1} . The results are shown in Figure 6.

Typical kinetic curves were obtained, where, an initial fast step was observed until 10 min. The adsorption rate gradually decreased until 50 min. For all initial dye concentrations, the equilibrium was attained within 80 min. Moreover, it was found that the increase in initial dye concentration provided an increase from 40 to 130 mg g^{-1} in the adsorption capacity. These results are interesting from the practical viewpoint, since more than 80% of saturation was reached within 10 min.

To better understand the kinetic profile, pseudo–first order (Equation (4)), pseudo–second order (Equation (5)), and Elovich (Equation (6)) models were fitted with the experimental data. The kinetic parameters for the reactive red 141 adsorption onto biochar are shown in Table 1.

The higher values of R^2 ($R^2 > 0.994$) and R^2_{adj} ($R^2_{adj} > 0.993$) and the lower values of ARE (ARE < 2.00%) shown in Table 1 revealed that the pseudo–second order model was the more suitable to represent the adsorption kinetics. This model was also adequate to represent the adsorption kinetics of anionic dyes on chitosan/polyamide nanofibers (DOTTO et al., 2017). As expected, the q_2 parameter increased with the initial dye concentration, indicating that the adsorption capacity was higher at 500 mg L⁻¹. Similar trend was found for the h_0 parameter (Table 1), indicating that at the initial stages, the adsorption was faster at 500 mg L⁻¹. Furthermore, it was verified that, for all initial concentrations, q_2 closed very well with the experimental value (q_e (exp)) (Table 1). This confirms the good fit of the pseudo–second order model.

Figure 6– Effect of the contact time on the adsorption capacity of reactive red 141 on the biochar at different initial concentrations (pH = 3.0 and 298 K).

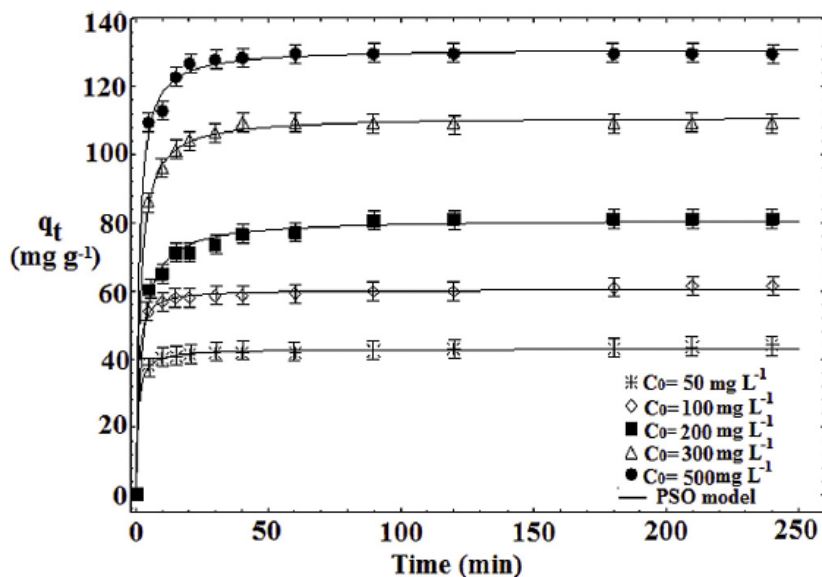


Table 1– Kinetic parameters for the adsorption of reactive red 141 on the biochar.

| Kinetic model | Biochar sample | | | | |
|-----------------------------|----------------|--------|--------|--------|--------|
| | 50 | 100 | 200 | 300 | 500 |
| Pseudo–first order | | | | | |
| q_1 (mg g ⁻¹) | 42.18 | 59.37 | 77.63 | 107.77 | 127.80 |
| k_1 (min ⁻¹) | 0.4651 | 0.4697 | 0.2499 | 0.2890 | 0.3436 |
| ARE (%) | 1.95 | 1.62 | 4.71 | 2.36 | 2.08 |

Table 1– Kinetic parameters for the adsorption of reactive red 141 on the biochar.

(Continuation)

| Kinetic model | Biochar sample | | | | |
|---|----------------|------------|----------|----------|--------------|
| | 50 | 100 | 200 | 300 | 500 |
| R^2 | 0.9919 | 0.9945 | 0.9659 | 0.9900 | 0.9885 |
| R^2_{adj} | 0.9912 | 0.9940 | 0.9628 | 0.9890 | 0.9875 |
| Pseudo–second order | | | | | |
| q_2 (mg g ⁻¹) | 42.98 | 60.38 | 81.08 | 111.19 | 131.15 |
| $k_2 \times 10^3$ (g mg ⁻¹ min ⁻¹) | 0.0343 | 0.0268 | 0.0060 | 0.0061 | 0.0069 |
| h_0 (mg g ⁻¹ min ⁻¹) | 63.36 | 97.70 | 39.69 | 76.47 | 119.50 |
| ARE (%) | 0.99 | 0.85 | 1.86 | 0.62 | 0.99 |
| R^2 | 0.9981 | 0.9985 | 0.9943 | 0.9990 | 0.9973 |
| R^2_{adj} | 0.9979 | 0.9984 | 0.9938 | 0.9989 | 0.9971 |
| Elovich | | | | | |
| a (mg g ⁻¹ min ⁻¹) | 0.6347 | 0.4440 | 0.1904 | 0.2013 | 0.1791 |
| b (g mg ⁻¹) | 1.11E+10 | 1.0612E+10 | 1.83E+05 | 1.62E+08 | 6.676906E+08 |
| ab (min ⁻¹) | 7.07E+09 | 4.71E+09 | 3.48E+04 | 3.27E+07 | 1.20E+08 |
| ARE (%) | 1.12 | 1.45 | 2.07 | 2.78 | 2.65 |
| R^2 | 0.9977 | 0.9959 | 0.9932 | 0.9853 | 0.9881 |
| R^2_{adj} | 0.9975 | 0.9955 | 0.9926 | 0.9840 | 0.9870 |
| q_e (exp) (mg g ⁻¹) | 43.95 | 61.48 | 81.22 | 109.49 | 129.68 |

3.4 ADSORPTION ISOTHERMS

The adsorption isotherms were obtained at 298, 308, 318, and 328 K. The curves are shown in Figure 7. It was found that the isotherms presented a curved portion at lower C_e values and after, the adsorption capacity tends to increase progressively. The curved portion was more pronounced at 298 K. This is a typical L1 type isotherm (GILES et al., 1960) and suggests that all the adsorption sites were not completely occupied. In addition, it was verified that the adsorption was favored by the temperature decrease, being the maximum values reached at 298 K. This behavior can be related with the RR141 solubility, which is higher at higher temperatures. As a consequence, at higher temperatures, the RR141 has a greater attraction for the water molecules, decreasing the adsorption capacity. A similar trend was found by Dotto et al. (2016) in the adsorption of amaranth and methylene blue dyes using chitosan hybrid films as adsorbent.

Freundlich and Langmuir models were used to interpret the adsorption equilibrium. The equilibrium parameters for the adsorption of reactive red 141 onto the biochar are presented in Table 2. From the statistical indicators (R^2 , R^2_{adj} , ARE), it was verified that for the temperatures of 308, 318, and 328 K, both models were suitable to represent the isotherms. However, it is clear that at 298, only the Freundlich model can represent the experimental data. Therefore, the Freundlich model was selected as the more adequate to

represent the adsorption of reactive red 141 on the biochar. The k_F constant (Table 2) increased with the temperature decrease, confirming that the adsorption was favored at 298 K. Otherwise, the heterogeneity factor ($1/n$) increased with the temperature (Table 2).

Figure 7– Equilibrium curves for adsorption of reactive red 141 onto the biochar.

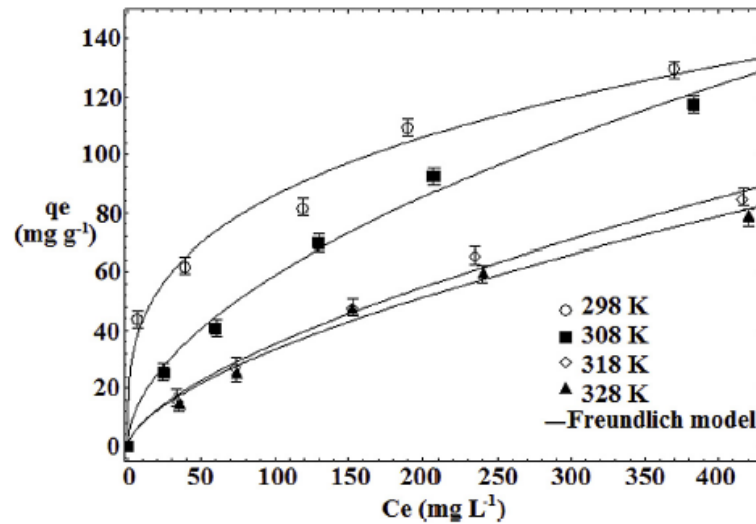


Table 2– Equilibrium parameters for the adsorption of reactive red 141 onto the biochar.

| Isotherm model | Temperature (K) | | | |
|---|-----------------|--------|--------|--------|
| | 298 | 308 | 318 | 328 |
| Freundlich model | | | | |
| k_F (mg g^{-1}) (mg L^{-1}) ^{-1/n_F} | 21.49 | 4.95 | 1.89 | 1.93 |
| $1/n_F$ | 0.3012 | 0.5376 | 0.6356 | 0.6191 |
| R^2 | 0.9838 | 0.9928 | 0.9915 | 0.9899 |
| R^2_{adj} | 0.9798 | 0.9910 | 0.9894 | 0.9874 |
| ARE (%) | 6.44 | 5.03 | 2.69 | 7.85 |
| Langmuir model | | | | |
| q_m (mg g^{-1}) | 129.47 | 173.00 | 151.76 | 135.48 |
| k_L (L mg^{-1}) | 0.0269 | 0.0055 | 0.0031 | 0.0033 |
| R^2 | 0.8958 | 0.9966 | 0.9990 | 0.9985 |
| R^2_{adj} | 0.8698 | 0.9958 | 0.9988 | 0.9981 |
| ARE (%) | 16.28 | 4.62 | 1.98 | 2.09 |

Table 3– Comparison between the new biochar and other adsorbents used for the adsorption of reactive red 141.

| Adsorbent | pH | T (°C) | q_{max} (mg g^{-1}) ^a | Reference |
|-----------------------------|-----|--------|--|------------------------|
| Biochar | 3.0 | 35 | 130.0 | This work |
| Chitosan | 5.0 | — | 442.6 | VANAAMUDAN (2015) |
| nano clay composite | — | — | — | — |
| Wood-shaving | — | 30 | 24.3 | LEECHART et al. (2009) |
| bottom ash/H ₂ O | — | — | — | — |
| Activated carbon | — | 30 | 41.5 | LEECHART et al. (2009) |

Table 3– Comparison between the new biochar and other adsorbents used for the adsorption of reactive red 141.

(Continuation)

| Adsorbent | pH | T (°C) | q_{\max} (mg g ⁻¹) ^a | Reference |
|---|---------|--------|---|-------------------------|
| Wood–shaving bottom ash/H ₂ SO ₄ | — | 30 | 29.9 | LEECHART et al. (2009) |
| Hydrotalcite | 2.0 | — | 320.5 | VANAAMUDAN (2015) |
| Modified chitin | 11.0 | 30 | 124.0 | DOLPHEN et al. (2007) |
| Chitin | 11.0 | 30 | 133.0 | DOLPHEN et al. (2007) |
| Peanut shell | 2.5 | 25 | 284.5 | GEORGIN et al. (2016) |
| [C8MIM]–Fe ₃ O ₄ particles | 2.5 | — | 71.4 | KAMRAN et al. (2014) |
| Ecological adsorbent | 5.0 | 25 | 78.74 | VASQUES et al. (2009) |
| Metal hydroxide sludge | 8.0–9.0 | 30 | 56.18 | NETPRADIt et al. (2003) |
| Papaya seeds | 2.5 | 25 | 73.26 | FOLETTTO et al. (2013) |
| Treated palm shell | 2.0–9.0 | 50 | 13.95 | SREELATHA et al. (2011) |
| Chitosan | 4.0 | 50 | 22.48 | SREELATHA et al. (2011) |
| Banana peel | — | — | 0.76 | SREELATHA et al. (2012) |
| Treated banana peel | — | — | 0.95 | SREELATHA et al. (2012) |
| Sawdust | — | — | 2.12 | SREELATHA et al. (2012) |
| Sonicated sawdust | — | — | 2.39 | SREELATHA et al. (2012) |
| Orange peel | — | — | 5.12 | SREELATHA et al. (2012) |
| Treated orange peel | — | — | 5.40 | SREELATHA et al. (2012) |
| TiO ₂ | — | — | 5.14 | SREELATHA et al. (2012) |
| Sonicated TiO ₂ | — | — | 5.46 | SREELATHA et al. (2012) |

^a Maximum adsorption capacity.

In order to verify the suitability of the new biochar as adsorbent, a comparison with other adsorbents was performed. The results are presented in Table 3. Among the 24 adsorbents used to remove RR141 (Table 3), the new biochar produced in this work presented the fifth maximum adsorption capacity. Furthermore, the new biochar was superior in relation to the activated carbon (the most common used adsorbent). This indicates the biochar from pecan nutshell is a promising adsorbent that can be used to remove RR141 from aqueous media. In addition, this adsorbent presents the following advantages: low–cost, since it is derived from a zero cost waste material by a simple processing; eco–friendly, since its preparation helps the management of pecan nutshell wastes; efficiency, since the removal percentage was approx. 85% and fast kinetics, since more than 80% of saturation was reached within 10 min.

3.5 ADSORPTION THERMODYNAMICS

The adsorption thermodynamics was evaluated according to the values of standard Gibbs free energy change (ΔG^0), standard enthalpy change (ΔH^0), and standard entropy change (ΔS^0). These values are shown in Table 4.

Table 4– Thermodynamic parameters for the adsorption of reactive red 141 onto the biochar.

| Temperature (K) | ΔG^0 (kJ mol ⁻¹) ^a | ΔH^0 (kJ mol ⁻¹) ^a | ΔS^0 (kJ mol ⁻¹ K ⁻¹) ^a |
|-----------------|---|---|---|
| 298 | -20.18±0.05 | | |
| 308 | -17.52±0.12 | | |
| 318 | -16.21±0.03 | -56.42±0.10 | -0.12±0.01 |
| 328 | -16.62±0.01 | | |

^a mean±standard error (n=3).

The negative ΔG^0 values indicated that the RR141 adsorption onto the biochar was a spontaneous and favorable process. The ΔG^0 values were more negative at 298 K, confirming that the adsorption was favored by the temperature decrease. The negative ΔS^0 values indicated that the disorder in solid/liquid interface decreased after the adsorption process. The negative ΔH^0 corroborated the RR141 adsorption onto the biochar was exothermic in nature. From the magnitude of ΔH^0 is possible to infer about the adsorbent/adsorbate interactions. Bonding forces lower than 40 kJ mol⁻¹ refer to physisorption while forces higher than 40 kJ mol⁻¹ refer to chemisorption. In this sense, we can infer that chemisorption occurred in the RR141 adsorption onto the biochar. To support this statement, desorption tests were made with NaOH and HCL (from 0.1 to 10 mol L⁻¹), NaCl, and acetone. No desorption was observed independent of the used eluent, confirming the strong interaction between the dye and the biochar.

4 CONCLUSION

In this research, a new biochar was produced from pecan nutshells and used as alternative adsorbent to remove RR141 dye from aqueous solutions. The biochar yield was approx. 30% and its characteristics were superior in relation to the precursor (pecan nutshells). The biochar presented an amorphous and micro/mesoporous structure, with surface area of 93 m² g⁻¹, total pore volume of 0.055 cm³ g⁻¹ and particle diameter around 60 nm. Cavities and protuberances were observed on the surface. The adsorption was favored at pH of 3.0. A comparison between the biochar and its precursor revealed that the dye removal percentage was 85% using the biochar, and was only 23% when raw pecan nutshell was used.

The adsorption kinetics followed the pseudo-second order model and 80% of saturation was attained within 10 min. The Freundlich model was the best to represent the adsorption equilibrium. The maximum adsorption capacity was around 130 mg g⁻¹. The adsorption of RR141 onto the biochar was a spontaneous, favorable, and exothermic process, being that chemical bonds occurred between the dye and the adsorbent. From the cleaner production viewpoint, the development of a biochar from pecan nutshells and its application as adsorbent, presented a synergistic effect: It was possible aggregate value to the pecan nutshells thought the biochar preparation, contributing to the solid wastes management; and, the biochar was an efficient, low-cost, and eco-friendly adsorbent to be used in the removal of RR141 from aqueous media, contributing with the treatment of liquid effluents.

ACKNOWLEDGEMENTS

The authors thank CAPES (Coordination for the Improvement of Higher Education Personnel), CNPq (National Council for Scientific and Technological Development), and FAPERGS for the financial support. The authors also thank CEME-SUL/FURG (Electron Microscopy Center of South/Federal University of Rio Grande/RS/Brazil) due to the microscopy images.

REFERENCES

- Abbasian, M., Jaymand, M., Niroomand, P., Farnoudian-Habibib, A., Ghasemi Karaj-Abad, S., 2017. Grafting of aniline derivatives onto chitosan and their applications for removal of reactive dyes from industrial effluents. *Int. J. Biol. Macromol.* 95, 393–403.
- Aguayo-Villarreal, I.A., Ramirez-Montoya, L.A., Hernandez-Montoya, V., Bonilla-Petriciolet, A., Montes-Moran, M.A., Ramirez-Lopez, E.M., 2013. Sorption mechanism of anionic dyes on pecan nut shells (*Carya illinoensis*) using batch and continuous systems. *Ind. Crop. Prod.* 48, 89–97.
- Aldana, H., Lozano, F.J., Acevedo, J., Mendoza, A., 2015. Thermogravimetric characterization and gasification of pecan nut shells. *Bioresour. Technol.* 198, 634–641.
- Ali, I., Asim, M., Khan, T.A., 2012. Low cost adsorbents for the removal of organic pollutants from wastewater. *J. Environ. Manag.* 113, 170–183.
- Ausavasukhi, A., Kamposoen, C., Kengnok, O., 2016. Adsorption characteristics of Congo red on carbonized leonardite. *J. Clean. Prod.* 134, 506–514.
- Bansode, R.R., Losso, J.N., Marshall, W.E., Rao, R.M., Portier, R.J., 2003. Adsorption of metal ions by pecan shell-based granular activated carbons. *Bioresour. Technol.* 89, 115–119.

Brindley, G.W., Brown, G., 1980. *Crystal Structures of Clay Minerals and Their X-ray Identification*. Mineralogical Society, London.

Brito, S.M.O., Andrade, H.M.C., Soares, L.F., Azevedo, R.P., 2010. Brazil nut shells as a new biosorbent to remove methylene blue and indigo carmine from aqueous solutions. *J. Hazard. Mater.* 174, 84–92.

CEN Comité Européen de Normalisation, 2004. BT/TF 143: Biomass Gasification: Tar and Particles in Product Gases Sampling and Analysis.

Collazzo, G.C., Paz, D.S., Jahn, S.L., Carreño, N.L.V., Foletto, E.L., 2012. Evaluation of niobium oxide doped with metals in photocatalytic degradation of leather dye. *Lat. Am. Appl. Res.* 42, 51–54.

Crini, G., Badot, P.M., 2008. Application of chitosan, a natural aminopolysaccharide, for dye removal from aqueous solutions by adsorption processes using batch studies: a review of recent literature. *Prog. Polym. Sci.* 33, 399–447.

Dolphen, R., Sakkayawong, N., Thiravetyan, P., Nakbanpote, W., 2007. Adsorption of Reactive Red 141 from wastewater onto modified chitin. *J. Hazard. Mater.* 145, 250–255.

Dotto, G.L., Rodrigues, F.K., Tanabe, E.H., Fröhlich, R., Bertuol, D.A., Martins, T.R., Foletto, E.L., 2016. Development of chitosan/bentonite hybrid composite to remove hazardous anionic and cationic dyes from colored effluents. *J. Environ. Chem. Eng.* 4, 3230–3239.

Dotto, G.L., Santos, J.M.N., Tanabe, E.H., Bertuol, D.A., Foletto, E.L., Lima, E.C., Pavan, F.A., 2017. Chitosan/polyamide nanofibers prepared by Forc spinning® technology: a new adsorbent to remove anionic dyes from aqueous solutions. *J. Clean. Prod.* 144, 120–129.

El-Khaiary, M.I., Malash, G.F., 2011. Common data analysis errors in batch adsorption studies. *Hydrometallurgy* 105, 314–320.

Foletto, E.L., Weber, C.T., Bertuol, D.A., Mazutti, M.A., 2013. Application of papaya seeds as a macro/mesoporous biosorbent for the removal of large pollutant molecule from aqueous solution: equilibrium, kinetic, and mechanism studies. *Sep. Sci. Technol.* 48, 2817–2824.

Freundlich, H., 1906. Over the adsorption in solution. *Z. Phys. Chem.* A57, 358–471.

Georgin, J., Dotto, G.L., Mazutti, M.A., Foletto, E.L., 2016. Preparation of activated carbon from peanut shell by conventional pyrolysis and microwave irradiation–pyrolysis to remove organic dyes from aqueous solutions. *J. Environ. Chem. Eng.* 4, 266–275.

Giles, C.H., MacEwan, T.H., Nakhwa, S.N., 1960. Studies in adsorption. Part XI. A system of classification of solution adsorption isotherms, and its use in diagnosis of adsorption mechanisms and in measurement of specific surface areas of solids. *J. Chem. Soc.* 786, 3973–3993.

Goldstein, J.I., Newbury, D.E., Echil, P., Joy, D.C., Romig Jr., A.D., Lyman, C.E., Fiori, C., Lifshin, E., 1992. *Scanning Electron Microscopy and X-ray Microanalysis*. Plenum Press, New York.

Gomes, C.S., Piccin, J.S., Gutterres, M., 2016. Optimizing adsorption parameters in tannery–dye–containing effluent treatment with leather shaving waste. *Proc. Saf. Environ. Prot.* 99, 98–106.

Ho, Y.S., McKay, G., 1998. Kinetic models for the sorption of dye from aqueous solution by wood. *Proc. Saf. Environ. Prot.* 76, 183–191.

Jacques, R.A., Lima, E.C., Dias, S.L.P., Mazzocato, A.C., Pavan, F.A., 2007. Yellow passion–fruit shell as biosorbent to remove Cr(III) and Pb(II) from aqueous solution. *Sep. Purif. Technol.* 57, 193–198.

Kajekar, A.J., Dodamani, B.M., Isloor, A.M., Karim, Z.A., Cheer, N.B., Ismail, A.F., Shilton, S.J., 2015. Preparation and characterization of novel PSf/PVP/PANI–nanofiber nanocomposite hollow fiber ultrafiltration membranes and their possible applications for hazardous dye rejection. *Desalination* 365, 117–125.

Kamran, S., Tavallali, H., Azad, A., 2014. Fast removal of reactive red 141 and reactive yellow 81 from aqueous solution by Fe₃O₄ magnetic nanoparticles modified with ionic liquid 1–Octyl–3–methylimidazolium bromide. *Iran. J. Anal. Chem.* 1, 78–86.

Lagergren, S., 1898. About the theory of so-called adsorption of soluble substances. *Kung. Sven. Vetensk.* 24, 1–39.

Langmuir, I., 1918. The adsorption of gases on plane surfaces of glass, mica and platinum. *J. Am. Chem. Soc.* 40, 1361–1403.

Leechart, P., Nakbanpote, W., Thiravetyan, P., 2009. Application of ‘waste’ wood–shaving bottom ash for adsorption of azo reactive dye. *J. Environ. Manag.* 90, 912–920.

Leng, L., Yuan, X., Huang, H., Shao, J., Wang, H., Chen, X., Zeng, G., 2015. Bio–char derived from sewage sludge by liquefaction: characterization and application for dye adsorption. *Appl. Surf. Sci.* 346, 223–231.

Li, H., Mahyoub, S.A.A., Liao, W., Xia, S., Zhao, H., Guo, M., Ma, P., 2017. Effect of pyrolysis temperature on characteristics and aromatic contaminants adsorption behavior of magnetic biochar derived from pyrolysis oil distillation residue. *Bioresour. Technol.* 223, 20–26.

Li, S.Q., Yao, Q., Wen, S.E., Chi, Y., Yan, J.H., 2005. Properties of pyrolytic chars and activated carbons derived from Pilot-Scale pyrolysis of used tires. *J. Air Waste Manag. Assoc.* 55, 1315–1326.

Liu, Y., 2009. Is the free energy change of adsorption correctly calculated? *J. Chem. Eng. Data* 54, 1981–1985.

Netpradit, S., Thiravetyan, P., Towprayoon, S., 2003. Application of 'waste' metal hydroxide sludge for adsorption of azo reactive dyes. *Water Res.* 37, 763–772.

Pankaj, T., Joy, P.A., 2009. Superparamagnetic nanocomposite of magnetite and activated carbon for removal of dyes from waste water. *Nanosci. Nanotechnol. Lett.* 1, 171–175.

Rodrigues, C.S.D., Madeira, L.M., Boaventura, R.A.R., 2014. Synthetic textile dyeing wastewater treatment by integration of advanced oxidation and biological processes e performance analysis with costs reduction. *J. Environ. Chem. Eng.* 2, 1027–1039.

Saitoh, T., Saitoh, M., Hattori, C., Hiraide, M., 2014. Rapid removal of cationic dyes from water by coprecipitation with aluminum hydroxide and sodium dodecyl sulfate. *J. Environ. Chem. Eng.* 2, 752–758.

Silverstein, R.M., Webster, F.X., Kiemle, D.J., 2007. *Spectrometric Identification of Organic Compounds*. John Wiley & Sons, New York.

Soltani, N., Bahrami, A., PecheCanul, M.I., Gonzalez, L.A., 2015. Review on the physicochemical treatments of rice husk for production of advanced materials. *Chem. Eng. J.* 264, 899–935.

Sreelatha, G., Ageetha, V., Parmar, J., Padmaja, P., 2011. Equilibrium and kinetic studies on reactive dye adsorption using palm shell powder (an Agrowaste) and chitosan. *J. Chem. Eng. Data* 56, 35–42.

Srivatasa, P., Tanwar, B., Goyal, S., Patnala, P.K., 2012. A comparative study of sonosorption of Reactive Red 141 dye on TiO₂, banana peel, orange peel and hardwood saw dust. *J. Appl. Chem.* 1, 505–511.

Suarez-Garcia, F., Martinez-Alonso, A., Tascon, J.M.D., 2002. A comparative study of the thermal decomposition of apple pulp in the absence and presence of phosphoric acid. *Polym. Degrad. Stabil.* 75, 375–383.

Subramani, S.E., Thinakaran, N., 2017. Isotherm, kinetic and thermodynamic studies on the adsorption behaviour of textile dyes onto chitosan. *Proc. Saf. Environ. Prot.* 106, 1–10.

Tang, J., Li, Y., Wang, X., Daroch, M., 2017. Effective adsorption of aqueous Pb^{2+} by dried biomass of *Landoltia punctata* and *Spirodela polyrhiza*. *J. Clean. Prod.* 145, 25–34.

Thommes, M., Kaneko, K., Neimark, A.V., Olivier, J.P., Rodriguez-Reinoso, F., Rouquerol, J., Sing, K.S.W., 2015. Physisorption of gases, with special reference to the evaluation of surface area and pore size distribution (IUPAC Technical Report). *Pure Appl. Chem.* 87, 1051–1069.

Tran, H.N., You, S., Chao, H., 2017. Fast and efficient adsorption of methylene green 5 on activated carbon prepared from new chemical activation method. *J. Environ. Manag.* 188, 322–336.

Vaghetti, J.C.P., Lima, E.C., Royer, B., Cunha, B.M., Cardoso, N.F., Brasil, J.L., Dias, S.L.P., 2009. Pecan nutshell as biosorbent to remove Cu(II), Mn(II) and Pb(II) from aqueous solutions. *J. Hazard. Mater.* 162, 270–280.

Vanaamudan, A., Sudhakar, P.P., 2015. Equilibrium, kinetics and thermodynamic study on adsorption of reactive blue 21 and reactive red 141 by chitosane organically modified nanoclay (Cloisite 30B) nano-bio composite. *J. Taiwan Inst. Chem. Eng.* 55, 145–151.

Vanaamudan, A., Chavada, B., Padmaja, P., 2016. Adsorption of reactive blue 21 and reactive red 141 from aqueous solutions onto hydrotalcite. *J. Environ. Chem. Eng.* 4, 2617–2627.

Vasques, A.R., Souza, S.M.G.U., Valle, J.A.B., Souza, A.A.U., 2009. Application of ecological adsorbent in the removal of reactive dyes from textile effluents. *J. Chem. Technol. Biotechnol.* 84, 1146–1155.

Wu, J.S., Liu, C.H., Chu, K.H., Suen, S.Y., 2008. Removal of cationic dye methyl violet 2B from water by cation exchange membranes. *J. Membr. Sci.* 309, 239–245.

Zeldowitsch, J., 1934. Über den mechanismus der katalytischen oxydation von CO an MnO_2 . *Acta physicochem. URSS* 1, 449–464.

4.2 ARTIGO 2 – CHITIN DERIVED BIOCHAR AS AN ALTERNATIVE ADSORBENT TO TREAT COLORED EFFLUENTS CONTAINING METHYL VIOLET DYE

Maria A. Zazycki^a, Priscila A. Borba^a, Rafaela N.F. Silva^a, Enrique C. Peres^a, Daniele Perondi^b, Gabriela C. Collazzo^a, Guilherme L. Dotto^{a,*}

^aChemical Engineering Department, Federal University of Santa Maria, UFSM, Roraima Avenue, 1000, 97105–900 Santa Maria, RS, Brazil

^bPostgraduate Program in Engineering Processes and Technology, University of Caxias do Sul – UCS, Caxias do Sul, RS, Brazil

Corresponding author.

E-mail address: guilherme.dotto@ufsm.br (G.L. Dotto).

ABSTRACT

Chitin was used to prepare an alternative, eco-friendly and low-cost adsorbent by a simple pyrolysis process. The adsorbent, named chitin derived biochar, was characterized and applied to treat colored effluents containing methyl violet dye (MV). Pyrolysis using N₂ flow rate of 0.25 L min⁻¹, heating rate of 10 °C min⁻¹ until 800 °C was suitable to prepare a chitin derived biochar with good characteristics. Chitin derived biochar presented surface area of 275.0 m² g⁻¹. The MV adsorption on the chitin derived biochar was favored in alkaline conditions and ambient temperature. The adsorption process presented fast kinetics and, the maximum adsorption capacity was higher than 1000 mg g⁻¹. Chitin derived biochar can be used for 7 consecutive adsorption/desorption cycles maintaining the same adsorption capacity. Also, the material was suitable to treat colored effluents, reaching color removal percentage of 95%. In brief, it was demonstrated that chitin derived biochar is a low-cost and efficient material to treat colored effluents.

Keywords: Adsorption. Biochar. Chitin. Dyes. Pyrolysis.

1 INTRODUCTION

The inadequate disposal of colored effluents is a well known environmental problem. These effluents contain dissolved organic dyes which can cause several damages to the aquatic biota [1]. Organic dyes are characterized by a complex structure, presenting aromatic rings, and for this reason, its degradation is difficult [2]. Specifically, methyl violet (MV) is a cationic dye of the triarylmethane class, widely utilized in the textile industry for coloring natural fibers [3]. The indiscriminate use of dyes has caused the generation of large volumes of colored effluents, which in turn, are an environmental concern [4]. Then, many physical, chemical, biological and hybrid techniques have been developed and extensively used to treat colored effluents [5]. Among these techniques, adsorption is normally highlighted, since is efficient, has low cost and is of easy operation [6].

In the field of dyes adsorption, activated carbon is the most common used adsorbent [7], but, its activation process and regeneration are costly [8]. Several alternative adsorbents are being tested in the last years to remove dyes from aqueous media [9–11]. “Biochars” are a class of alternative adsorbents, which are normally produced by heating crop wastes, wood or

other biomasses in oxygen-limited conditions [12]. “Biochars” are competitive adsorbents because possesses interesting textural characteristics and also functional groups, even without additional steps of activation in the preparation process [13]. In this context, several biochars have been produced from different precursors and applied for dye removal from aqueous solutions [14–18]. Until now, the potential of chitin as precursor for the biochar production and its application to treat colored effluents is little investigated.

Chitin is a natural and abundant material, which can be found as waste of fishery industries [19]. Considering the high amount of carbon and inherent functional groups, recently, some studies reported the use of chitin as precursor to produce carbon derived materials, including biochar [20–22]. The chitin pyrolysis was studied by Wanjun et al. [20] and the thermal degradation occurred from ambient temperature to 600 °C under N₂ atmosphere. Yuan et al. [21] developed an activated carbon sheet from chitin, which was an interesting material for electrocatalytic applications. Magnacca et al. [22] prepared biochar from chitin for energetic and environmental applications. They found biochars with surface area around 330 m² g⁻¹. Good efforts have been made in this context, as demonstrated in the cited literature [20–22]. In spite of the above mentioned investigations, studies regarding the preparation of chitin derived biochar and its application as adsorbent to treat colored effluents, taking into account, equilibrium, kinetic, thermodynamic and reusability are still scarce.

This work aimed to evaluate the potential of chitin to produce a biochar, using a simple pyrolysis process, and apply the chitin derived biochar to treat colored effluents containing methyl violet dye. Chitin derived biochar was produced and characterized by several techniques. For comparison, chitin was also characterized. The potential of chitin derived biochar as adsorbent to treat colored effluents containing methyl violet dye was extensively evaluated. For this purpose, the factors affecting adsorption of methyl violet on chitin derived biochar were evaluated by response surface methodology (RSM), kinetic, equilibrium and thermodynamic ways. The reusability of the adsorbent was tested using consecutive adsorption/desorption tests. Chitin derived biochar was also used to treat simulated dye house effluents.

2 MATERIAL AND METHODS

2.1 MATERIALS AND REAGENTS

Chitin with deacetylation degree of 45% was obtained from shrimp (*Penaeus brasiliensis*) wastes according previous work [23]. Samples were washed with deionized

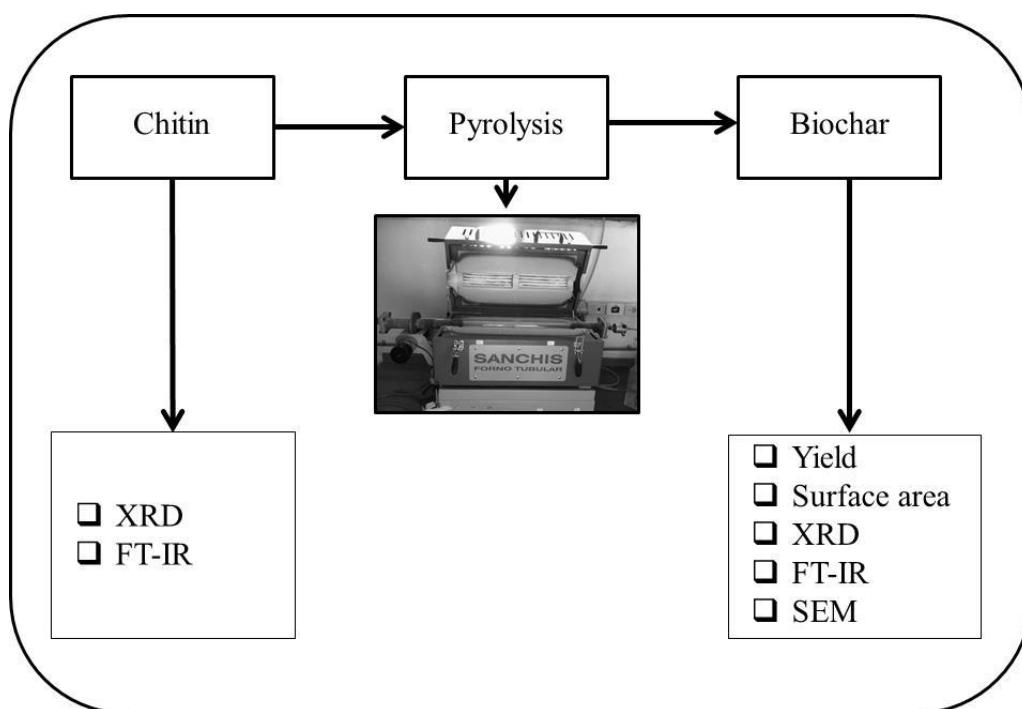
water, dried at 60 °C for 8 h, ground and sieved. Particles lower than 710 μm were used for the biochar preparation. N_2 was from White Martins. All inorganic salts, acids and alkalis were from VETEC (Brazil). The target dye molecule used in the adsorption experiments was methyl violet 10B (MV) (purity of 99%, color index 42555, molecular weight of 407.98 g mol^{-1} ; $\lambda_{\text{max}} = 590 \text{ nm}$) from INLAB (Brazil). A MV stock solution of 1.00 g L^{-1} was prepared and all the adsorption experiments were realized by diluting this solution. Distilled water was used for the adsorption experiments.

2.2 PREPARATION AND CHARACTERIZATION OF CHITIN DERIVED BIOCHAR

The shortened scheme for preparation and characterization of the materials is depicted in Figure 1. Chitin derived biochar was prepared from chitin via pyrolysis process. A quartz reactor was charged with approximately 50 g of chitin and the system was run under nitrogen gas (N_2) at 0.25 L min^{-1} . The heater temperature was increased at a rate of 10 $^\circ\text{C min}^{-1}$ until 800 $^\circ\text{C}$, being held at 800 $^\circ\text{C}$ for 60 min and allowed to cool still under N_2 flow until room temperature. The biochar was collected and its weight was determined to calculate the yield. The pyrolysis conditions were based in preliminary tests and literature [14, 15]. The complete pyrolysis apparatus is presented in our previous work [14].

Chitin and chitin derived biochar were characterized by several techniques. The structure and morphology was verified by scanning electron microscopy (Jeol, JSM-6610LV, Japan). The functional groups were verified by Fourier transform infrared spectroscopy (FT-IR) (Prestige, 21210045, Japan). X-ray diffraction (XRD) (Rigaku, Miniflex 300, Japan) was used to verify the materials structure. N_2 adsorption/desorption isotherms were performed to obtain the surface area, pore volume and pore diameter of the materials (QUANTACHROME INSTRUMENTS, NOVA 1200E, USA). The carbon, hydrogen, and nitrogen contents were determined using an elemental analyzer (ELEMENTAR, VARIO MACRO CUBE, GERMANY) [24]. Also, the point of zero charge of both materials was determined by the eleven point's experiment.

Figure 1– Scheme of pyrolysis process and materials characterization.



2.3 ADSORPTION TESTS

The potential of chitin derived biochar to adsorb MV dye was evaluated by adsorption tests, which were carried out in batch mode (MARCONI, MA 093, BRAZIL) at 260 rpm using 50 mL of dye solutions. These assays were performed in three steps: (I) the effects of pH (3.0, 6.0 and 9.0) and adsorbent dosage (0.50, 0.75 and 1.00 g L⁻¹) were first evaluated. Dye solutions (50 mg L⁻¹) were placed in Erlenmeyer flasks and the pH was adjusted to the desired conditions using NaOH or HCl. Pre-determined amounts of chitin derived biochar were put in the flasks, which were stirred at 298 K for 2 h; (II) kinetic curves were obtained using the best pH and adsorbent dosage above determined. In this case, the initial dye concentrations were 30, 50, 100, 200 and 300 mg L⁻¹. Solutions were agitated at 298 K and the contact time ranged from 0 to 120 min; (III) finally, equilibrium isotherms were constructed at 298, 308, 318 and 328 K with initial dye concentration range from 0 to 500 mg L⁻¹. Solutions were stirred until the equilibrium, which was considered after three equal measurements of dye concentration in liquid phase.

The quality of the experimental data was ensured by blank tests and triplicates. Also, all adequate procedures like storage and cleaning of the adsorbent, solutions and recipients were performed [25]. The measurements of MV concentration in liquid phase were carried out in a spectrophotometer at 590 nm (SHIMADZU, UV MINI 1240, JAPAN). The

adsorption of MV on chitin derived biochar was evaluated in terms of dye removal percentage (R , %), equilibrium adsorption capacity (q_e , mg g^{-1}) and adsorption capacity at any time (q_t , mg g^{-1}). These values were obtained by simple global mass balance [26].

2.4 OPTIMIZATION BY RESPONSE SURFACE METHODOLOGY

A 3^2 factorial design was performed to optimize the MV adsorption. The independent variables were pH (3.0, 6.0 and 9.0) and adsorbent dosage (0.50, 0.75 and 1.00 g L^{-1}). The response variables were dye removal percentage (R , %) and equilibrium adsorption capacity (q_e , mg g^{-1}). The response variables were represented according to a quadratic model. The quality of this model was evaluated by analysis of variance (ANOVA), F-test and coefficient of determination (R^2). The representation of the results was performed using Pareto charts and response surfaces [26].

2.5 KINETIC, EQUILIBRIUM AND THERMODYNAMIC EVALUATION

MV adsorption on chitin derived biochar was evaluated according to the kinetic, equilibrium and thermodynamic aspects. For this purpose, some conventional models presented in literature were employed, as presented in Table 1 [27–32]. The parameters in Table 1 were estimated through nonlinear regression, minimizing the least squares function. Statistic 9.1 software (Statsoft, USA) was used for the calculations. Coefficient of determination (R^2) and average relative error (ARE) were used to verify the fit quality [33].

Table 1– Kinetic, equilibrium and thermodynamic equations used to study the MV adsorption on chitin derived biochar.

| | Equation | Parameters* | Reference |
|---------------------|---|--|-----------|
| Kinetic | | | |
| Pseudo–first order | $q_t = q_1(1 - \exp(-k_1t))$ | k_1 (min^{-1}) q_1 (mg g^{-1}) | [26] |
| Pseudo–second order | $q_t = \frac{t}{(1/k_2q_2^2) + (t/q_2)}$ | k_2 ($\text{g mg}^{-1} \text{min}^{-1}$) q_2 (mg g^{-1}) | [27] |
| Isotherm | | | |
| Langmuir | $q_e = \frac{q_m k_L C_e}{1 + k_L C_e}$ | q_m (mg g^{-1}) k_L (L mg^{-1}) | [28] |
| Freundlich | $q_e = k_F C_e^{1/n}$ | k_F (mg g^{-1})(mg L^{-1}) $^{-1/nF}$ $1/n$ | [29] |
| Liu | $q_e = \frac{q_g (k_g C_e)^g}{1 + (k_g C_e)^g}$ | q_g (mg g^{-1}) k_g (L mg^{-1}) g | [30] |

Table 1– Kinetic, equilibrium and thermodynamic equations used to study the MV adsorption on chitin derived biochar.

| (Continuation) | | | |
|----------------|--|--|-----------|
| | Equation | Parameters* | Reference |
| Thermodynamic | | | |
| | $\Delta G^0 = -RT\ln(K_e)$ | | |
| | $\Delta G^0 = \Delta H^0 - T\Delta S^0$ | ΔG^0 (kJ mol ⁻¹) | [31] |
| | $K_e = \frac{k_g M_w \gamma^{MV}}{\gamma}$ | ΔH^0 (kJ mol ⁻¹) | |
| | | ΔS^0 (kJ mol ⁻¹ K ⁻¹) | |

* q_1, q_2 =theoretical adsorption capacities. k_1, k_2 =rate constants. q_m, q_g =maximum adsorption capacities. k_L, k_F, k_g =isotherm constants. $g, 1/n$ =exponents. T =temperature (K). R =universal gas constant (8.314×10^{-3} kJ mol⁻¹ K⁻¹). K_e =thermodynamic equilibrium constant. M_w =molecular weight of MV dye (mg mol⁻¹), γ^{MV} =activity coefficient of MV dye in solution (dimensionless) and γ the unitary activity coefficient of MV (1 mol L⁻¹). It was assumed that the solution is sufficiently diluted in order to consider $\gamma^{MV}=1$. $\Delta G^0, \Delta H^0$ and ΔS^0 =standard values of Gibbs free energy, enthalpy and entropy, respectively.

2.6 ADSORPTION/DESORPTION CYCLES

The reusability of chitin derived biochar was evaluated performing several adsorption/desorption cycles [25, 26]. Firstly, the more adequate eluent was selected as follows: the MV loaded adsorbent (from the best adsorption condition) was inserted in 50 mL of different eluents (CH₃COOH, H₂SO₄) at different concentrations (0.1, 0.5 and 1.0 mol L⁻¹). The mixture was stirred at 260 rpm for 30 min and the dye concentration in liquid phase was measured (SHIMADZU, UV MINI 1240, JAPAN). Secondly, using the best eluent in the more adequate concentration, this procedure of adsorption/desorption was carried out 10 times. The results were presented in terms of desorption percentage (D, %) and adsorption capacity (q, mg g⁻¹).

2.7 TREATMENT OF COLORED EFFLUENT

Chitin derived biochar was tested to treat a simulated colored effluent, containing some dyes and inorganic compounds. The effluent was synthesized in laboratory with the composition based on the literature as follows [34]: 100 mg L⁻¹ of MV dye, 50 mg L⁻¹ of methylene blue, 50 mg L⁻¹ of malachite green, 50 mg L⁻¹ of NaCl, 50 mg L⁻¹ of Na₂CO₃ and 20 mg L⁻¹ of NaHCO₃. Chitin derived biochar (5.0 g L⁻¹) was inserted in 100 mL of the simulated effluent and, the mixture was stirred for 2 h at 260 rpm and 298 K. Then, the solid/liquid separation was carried out by centrifugation for 5 min at 3000 rpm. The effluents before and after the treatment were submitted to spectrophotometric scanning in the visible light region (SHIMADZU, UV MINI 1240, JAPAN). The efficiency of the treatment (E, %)

was measured comparing the areas below to the spectrophotometric curves, before and after the treatment. The areas below to the curves were estimated by integration using the origin software (ORIGIN PRO 2016) [34].

3 RESULTS AND DISCUSSION

3.1 CHARACTERISTICS OF CHITIN AND CHITIN DERIVED BIOCHAR

Firstly, the yield of biochar from chitin was calculated and it was approximately 27.3%. Subsequently, the material produced was characterized by FT-IR, XRD, SEM and N₂ adsorption/desorption isotherms. A comparison between the precursor material (chitin) and the adsorbent produced (chitin derived biochar) was carried out to verify if the production process (pyrolysis) is adequate for the production of adsorbents from chitin.

Before the discussion it is important to explain why the process occurred at 800 °C. According the literature, the chitin thermal decomposition occurred in two steps [35, 36]. First weight loss was due to the evaporation of water from hydrophilic groups in chitin chains [37]. The second weight loss corresponds to the degradation of polymeric structure, between 350 and 400 °C, i.e., saccharide ring dehydration and deterioration of acetylated chitin units [38, 39]. Furthermore, according to Agrafioti et al. [40], biochar produced at low temperatures is suitable for agricultural uses, while higher temperatures can improve its porosity and thus enhance its effectiveness in adsorbing. Based in previous studies for adsorbent production from pyrolysis process [14, 15], it was selected a temperature of 800 °C for this study, aiming the production of a material with surface area and porosity competitive with other adsorbents.

The FT-IR vibrational spectra of chitin and chitin derived biochar were showed in Figure 2 and the relevant bands were presented in Table 2. The FT-IR spectrum of chitin before pyrolysis displays the narrow peaks assigned to the crystalline polysaccharide structure. The sample obtained after pyrolysis evidence the loss of all the main relevant bands associated to chitin functional groups. After pyrolysis process maintain the bands at 3439 cm⁻¹, 2843 cm⁻¹, 1667 cm⁻¹, 1032 cm⁻¹, which could be associated with the presence of O-H and N-H, C-H, C=O (acetamido moiety – amide I), C-O-C, respectively [41, 42]. This fact occurred because during the pyrolysis process, the volatile matter is removed and probably increases the surface area and the porosity of the material.

According to the literature [43], the degradation mechanism of chitin favored the formation of H₂O, CO₂, CO, and CH₃COOH. The elemental composition changes during the pyrolysis process were reported in Table 3. The carbon content increased from 41.05% to

81.30%. Looking at some previous studies, the N% value has been recorded as 6.24% for shrimp shell chitin, 6.45% for beetle [44], 6.20% for the purified crab chitin [45] and commercial chitin from Sigma Aldrich 6.13% [46]. In this study it was determined a similar value for chitin nitrogen content and, due to thermal degradation this value decreases after the pyrolysis as occurred with hydrogen and oxygen.

Figure 2– FT–IR vibrational spectra of chitin and chitin derived biochar.

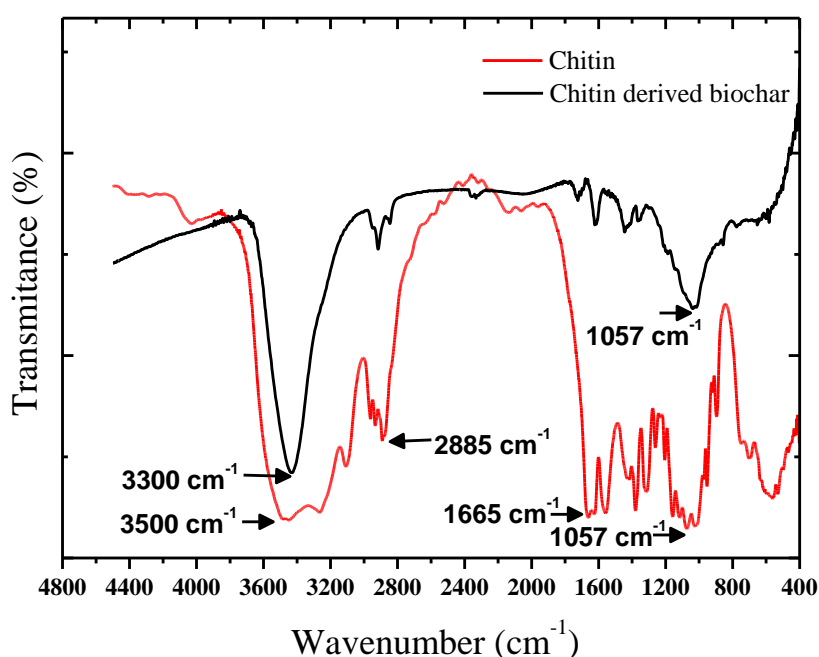


Table 2– The relevant bands from FT–IR spectra of chitin and chitin derived biochar.

| Functional group and vibration modes [41,42] | Classification | Chitin | Chitin derived biochar |
|--|-----------------------------|-----------|------------------------|
| O–H stretching | – | 3479 | 3439 |
| N–H stretchings | – | 3105–3260 | – |
| CH ₃ sym. stretch and CH ₂ asym. stretch | Aliphatic compounds | 2945 | 2940 |
| CH ₃ sym. Stretch | Aliphatic compound | 2886 | 2843 |
| C=O secondary amide stretch | Amide I | 1663 | 1743 |
| N–H bend, C–N stretch | Amide II | 1562 | 1627 |
| CH ₂ ending and CH ₃ deformation | – | 1426 | 1455 |
| CH bend, CH ₃ sym. Deformation | – | 1389 | 1365 |
| CH ₂ wagging | Amide components of protein | III, 1307 | – |

Table 2– The relevant bands from FT–IR spectra of chitin and chitin derived biochar.

| | | (Continuation) | | |
|--|------------------|----------------|------------------------|--|
| Functional group and vibration modes [41,42] | Classification | Chitin | Chitin derived biochar | |
| Asymmetric bridge oxygen stretching | – | 1161 | – | |
| Asymmetric in-phase ring stretching mode | – | 1115 | – | |
| C–O–C asym. stretch in phase ring | Saccharide rings | 1069 | 1032 | |
| C–O asym. stretch in phase ring | – | 1005 | – | |
| CH ₃ wagging | Along chain | 941 | – | |
| CH ring stretchings | Saccharide rings | 887 | 873 | |

Table 3– Elemental analysis of chitin and chitin derived biochar.

| Material | C (%) | H (%) | N (%) | O* (%) |
|------------------------|-------|-------|-------|--------|
| Chitin | 41.05 | 5.35 | 6.15 | 47.45 |
| Chitin derived biochar | 81.30 | 2.15 | 3.45 | 13.10 |

*By difference.

The XRD were measured to investigate the crystalline degree of the samples (see Figure 3). From the chitin diffractogram, it was possible to observe peaks at $2\theta = 9.6^\circ$, $2\theta = 19.15^\circ$ and $2\theta = 26^\circ$. Cardenas et al. [47] characterized chitin from different sources and they found similar peaks for shrimp chitin (9.22° , 19.18° , 26.18°) with plane (0 2 0), (1 1 0) and (0 1 3), respectively. In the chitin derived biochar diffractogram, these peaks were not observed, because during pyrolysis, occur the elimination of volatile compounds, due to the breakage of the weak bonds, which means that there were changes in the structure of the material.

The SEM images are shown in Figure 4. Chitin (Figure 4a), even at magnification of 5000 times, presented no visible cavities. According to Cardenas et al. [47], which studied the scanning electron microscopy of different parts of the exoskeleton, independent of the part of the shrimp exoskeleton, the isolated chitin retains its fiber character and in both cases (α -chitin and β -chitin) a rough surface without porosity is observed, which might be related to their high molecular packing, with inter or intramolecular hydrogen bonds. It can be noticed that chitin derived biochar (Figure 4b) presented a porous structure with cavities and protuberances evidencing an increase of surface area and porosity in the adsorbent material produced by pyrolysis. Then, from the SEM images, it is possible affirm that the pyrolysis process was an efficient method to change the structure of chitin giving suitable properties for application as an adsorbent.

Figure 3– X-ray diffraction patterns of chitin and chitin derived biochar.

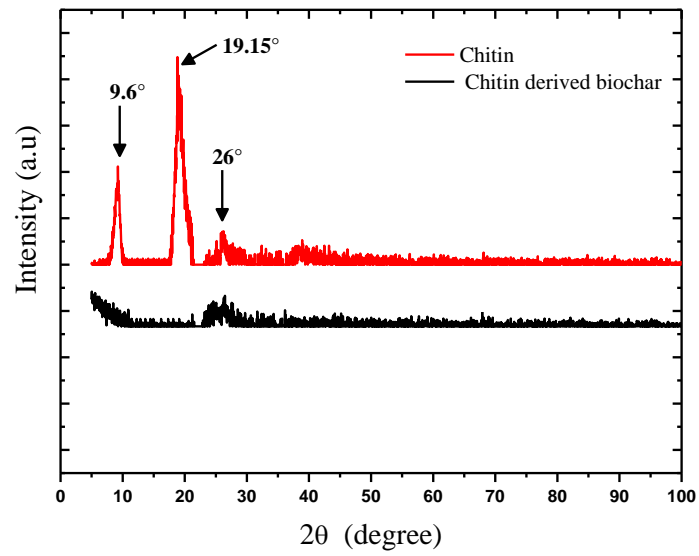
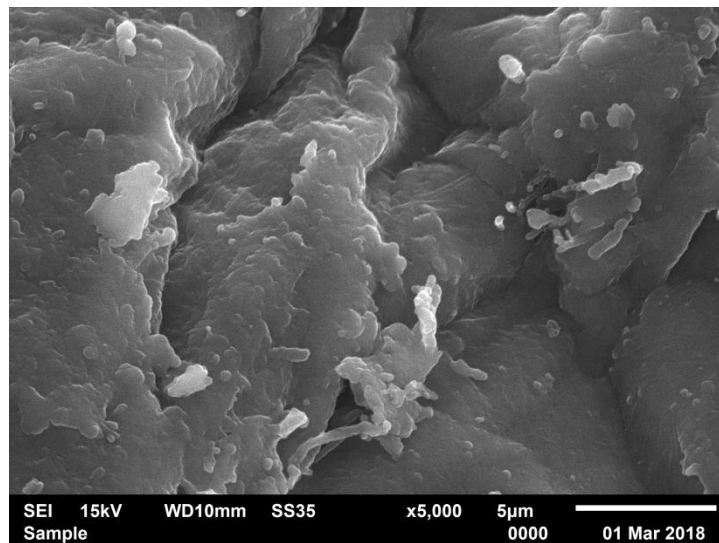
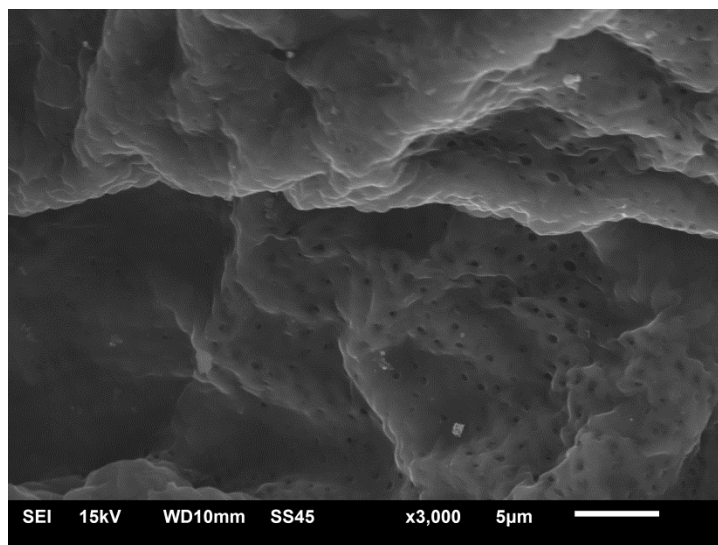


Figure 4– SEM images of chitin (a) and chitin derived biochar (b).



a)

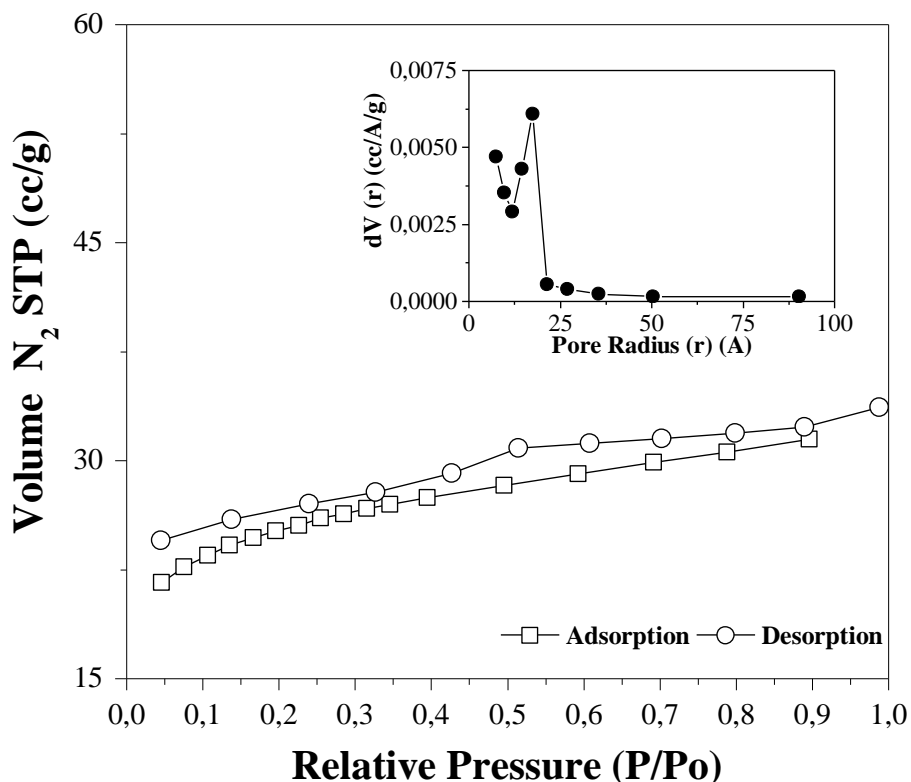


b)

In order to quantify the change in the structure of the material, the surface area is an important factor that controls the adsorption performance. Osada et al. [41] studied the physicochemical properties of different chitins (untreated, treated with supercritical water and mechanochemical grinded). For untreated chitin the BET surface areas were approximately $33 \text{ m}^2 \text{ g}^{-1}$. Therefore, there is a need to process a chitin because it has no surface area that is competitive. N_2 adsorption–desorption isotherms and pore size distribution curves of the chitin derived biochar are shown in Figure 5. According to the IUPAC, the N_2 adsorption isotherm showed a Type IV (a) with hysteresis H4 [48]. The hysteresis H4 is often found for micro–mesoporous materials. This fact is according with the pore size distribution (BJH method) that evidenced the presence of micropores and mesopores. Chitin derived biochar presented high BET surface area of ($275 \text{ m}^2 \text{ g}^{-1}$), total pore volume ($0.178 \text{ cm}^3 \text{ g}^{-1}$) and a mean pore size of 13 \AA . Zazycki et al. [14] reported a BET surface area ($93 \text{ m}^2 \text{ g}^{-1}$), total pore volume ($0.055 \text{ cm}^3 \text{ g}^{-1}$) and a mean pore size of 12 \AA for biochar derived from pecan nutshells using similar method.

It is then concluded that the pyrolysis process used in this study is suitable to promote changes in the chitin structure, providing developed porosity and surface area values suitable for use as an adsorbent.

Figure 5– N₂ adsorption–desorption isotherms and pore size distribution curves of the chitin derived biochar.



3.2 RSM RESULTS

RSM was used to verify the effects of pH (denoted as A) (3.0, 6.0 and 9.0) and adsorbent dosage (denoted as B) (0.50, 0.75 and 1.00 g L⁻¹) on the dye removal percentage (R, %) and equilibrium adsorption capacity (q_e, mg g⁻¹). The experimental and predicted values of R and q_e are provided in Table 4. The observed q_e values ranged between 45 and 97 mg g⁻¹ and the predicted values ranged between 46 and 96 mg g⁻¹, demonstrating good agreement. Removal percentage was 90–97% for predicted and observed values, presenting a high efficiency for all experiments.

Table 4– Experimental and predicted values of dye removal percentage (R, %) and equilibrium adsorption capacity (q_e, mg g⁻¹) for the MV adsorption on the chitin derived biochar according to the RSM.

| Runs | Coded Variables | | Dependent Variable | | | |
|------|-----------------|----|--------------------------------------|-----------|----------|-----------|
| | | | q _e (mg g ⁻¹) | | R (%) | |
| | A | B | Observed | Predicted | Observed | Predicted |
| 1 | -1 | -1 | 91.8 | 91.6 | 91.8 | 91.2 |
| 2 | 0 | -1 | 95.0 | 95.2 | 95.0 | 95.6 |
| 3 | 1 | -1 | 95.2 | 96.3 | 95.2 | 96.3 |

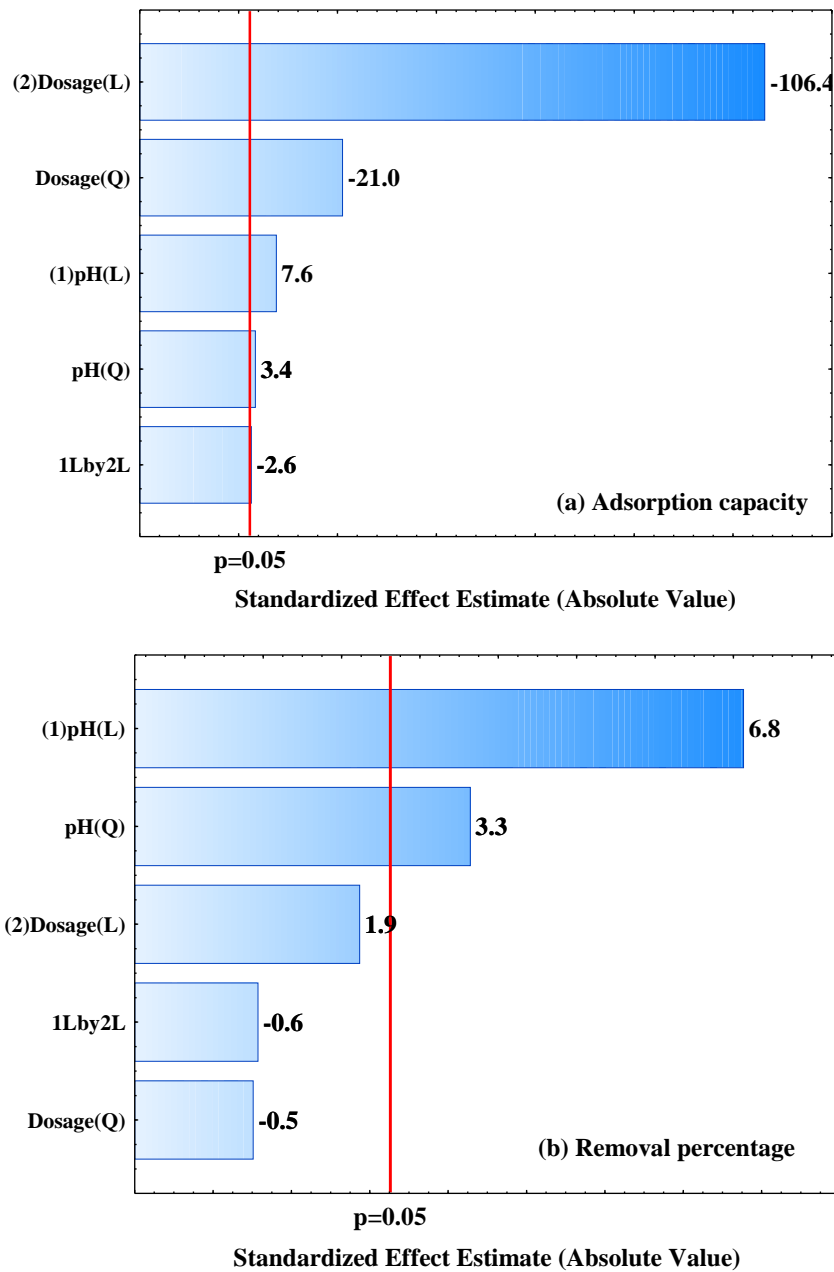
Table 4– Experimental and predicted values of dye removal percentage (R, %) and equilibrium adsorption capacity (q_e , mg g^{-1}) for the MV adsorption on the chitin derived biochar according to the RSM.

(Continuation)

| Runs | Coded Variables | | Dependent Variable | | | |
|------|-----------------|----|------------------------------|-----------|----------|-----------|
| | A | B | q_e (mg g^{-1}) | | R (%) | |
| | | | Observed | Predicted | Observed | Predicted |
| 40 | -1 | 0 | 61.2 | 61.0 | 91.8 | 91.8 |
| 5 | 0 | 0 | 64.4 | 64.0 | 96.6 | 96.0 |
| 6 | 1 | 0 | 64.1 | 64.4 | 96.2 | 96.3 |
| 7 | -1 | 1 | 45.6 | 46.4 | 91.2 | 93.0 |
| 8 | 0 | 1 | 48.3 | 48.7 | 96.6 | 96.9 |
| 9 | 1 | 1 | 48.1 | 48.4 | 96.3 | 97.1 |
| 10 | -1 | -1 | 91.7 | 91.6 | 91.7 | 91.2 |
| 11 | 0 | -1 | 95.3 | 95.2 | 95.3 | 95.6 |
| 12 | 1 | -1 | 97.3 | 96.3 | 97.3 | 96.3 |
| 13 | -1 | 0 | 60.3 | 61.0 | 90.4 | 91.8 |
| 14 | 0 | 0 | 63.9 | 64.0 | 95.9 | 96.0 |
| 15 | 1 | 0 | 64.9 | 64.4 | 97.4 | 96.3 |
| 16 | -1 | 1 | 47.5 | 46.4 | 95.0 | 93.0 |
| 17 | 0 | 1 | 48.9 | 48.7 | 97.8 | 96.9 |
| 18 | 1 | 1 | 48.5 | 48.4 | 97.0 | 97.1 |

The Pareto chart demonstrated in Figure 6a, for adsorption capacity (q_e), shows that all variables (linear, quadratic and interaction) were significant for the process ($p \leq 0.05$). The estimated values for the isolated effects show the strong linear influence of adsorbent dosage (2) in relation to the pH (1) linear influence. The negative signal of adsorbent dosage (L) represents that the increase of this factor caused a decrease in adsorption capacity. In relation to pH, the positive values of linear and quadratic effects indicated that at pH above 6, the adsorption of MV dye was favored. This occurred because at low values of pH there is a competition between the H^+ ions in solution with the MV cationic dye to occupy the adsorption sites (main adsorption sites are presented in Table 2). This strong dependence of adsorption in relation to the pH is an indicative that electrostatic interactions were involved in the mechanism. Considering the response removal percentage (Figure 6b), Pareto chart demonstrated that only the variable pH was significant ($p \leq 0.05$). The positive signal of pH (linear and quadratic) represent that MV is better adsorbed at higher pH values.

Figure 6– Pareto charts for the responses adsorption capacity (a) and removal percentage (b).



Considering only the significant variables, quadratic models were generated to represent equilibrium adsorption capacity (q_e , mg g^{-1}) and dye removal percentage (R , %). These models are presented, respectively, in Equations (1) and (2):

$$q_e = 63.98 + 1.67A - 1.28A^2 - 23.27B + 7.97B^2 - 0.68AB \quad (1)$$

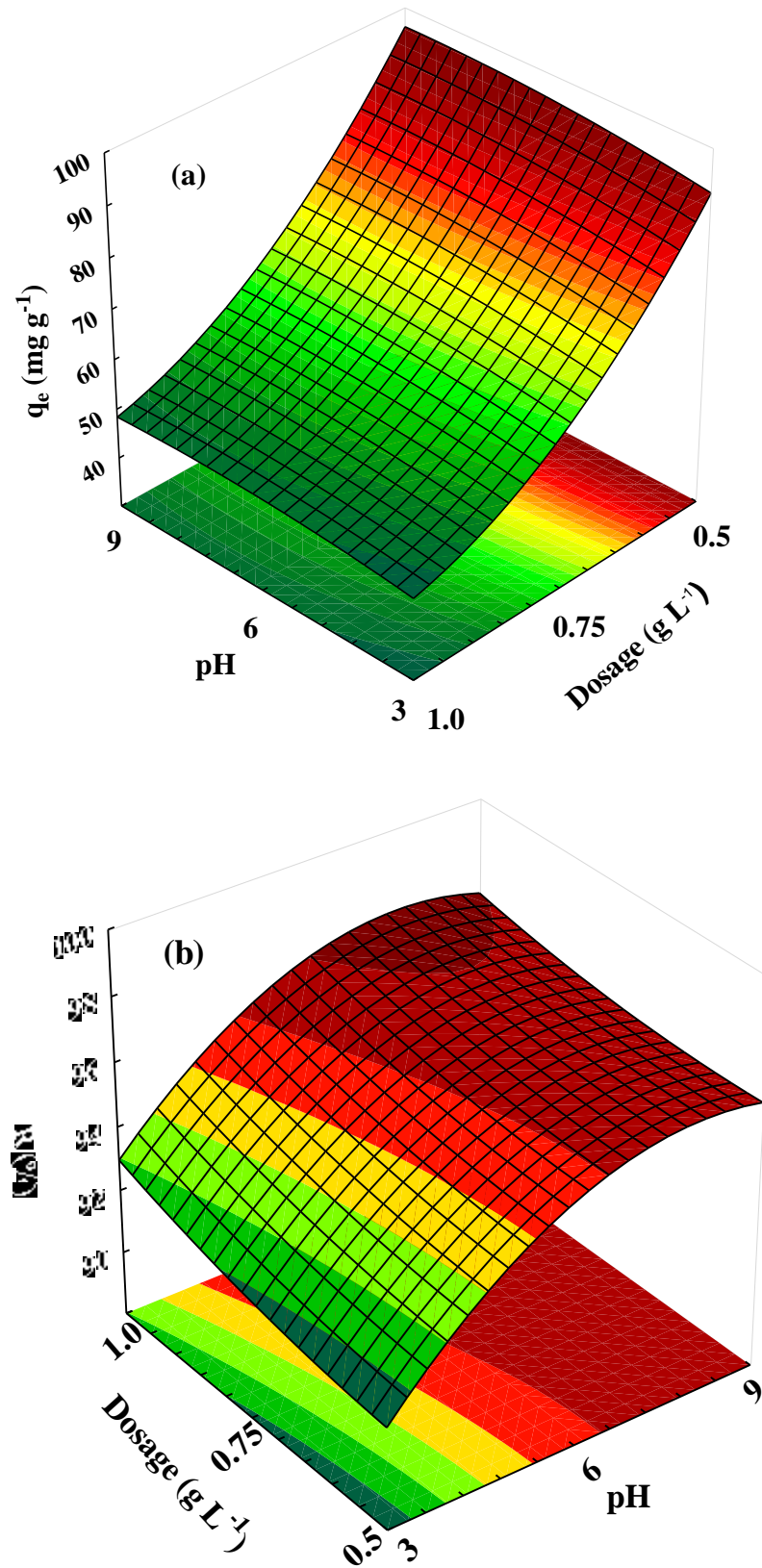
$$R = 96.18 + 2.29A + 1.92A^2 \quad (2)$$

In these equations, A and B are the coded values of pH and adsorbent dosage, respectively. To evaluate the potential of these models to predict the experimental values, ANOVA was performed (table not shown). The coefficient of determination (R^2) and the F value were also calculated. Regarding to the Equation (1), R^2 was 0.999 and F was 7260, while the standard F was 3.105. This shows that this model can be used to predict the adsorption capacity as a function of pH and adsorbent dosage. For the removal percentage (Equation (2)), R^2 was 0.789 and F was 25.28, while the standard F was 3.68. For Equation (2), R^2 was relatively low, since the non-significant terms were discarded. However, the F value for the model was around 7 times higher than the standard F, demonstrating that Equation (2) can be used to predict the MV removal percentage as a function of pH and adsorbent dosage.

Since the models (Equations (1) and (2)) were predictive, response surfaces were constructed to represent q_e and R as a function of independent variables. These response surfaces are depicted in Figure 7. It is clear in Figure 7a that the optimal values of adsorption capacity were found using 0.5 g L^{-1} of chitin derived biochar at pH higher than 6.0. In Figure 7b, it can be verified that the removal percentage was favored at pH values from 6.8 to 9.0 and, was independent of adsorbent dosage. Considering both responses, pH values from 6.8 to 9.0 presented no significant effect. So, pH of 6.8 was considered an optimal value for MV adsorption onto chitin derived biochar, since is near to the natural pH of the MV solution. This pH is within the range of textile effluents [49]. The good results in alkaline conditions can be explained by the cationic character of the MV dye. At higher pH values, the cationic dye MV has less competition with the H^+ ions for the available sites of chitin derived biochar.

In relation to the adsorbent dosage, lower values (0.5 g L^{-1}) provided higher adsorption capacities (Figure 7a) due to the more effective occupation of the adsorption sites. Furthermore, the removal percentage (Figure 7b) was not affected by this variable. In this sense it is reasonable the uses of 0.5 g L^{-1} as an optimal value. Finally, the optimal conditions for MV adsorption on chitin derived biochar were pH of 6.8 and adsorbent dosage of 0.5 g L^{-1} . These conditions furnished adsorption capacity of 95.74 mg g^{-1} and removal percentage of 96.90%. For comparison, MV adsorption was tested in these conditions, but using chitin. In this case, adsorption capacity was only 14.88 mg g^{-1} . These results justify the preparation of chitin derived biochar.

Figure 7– Response surfaces for adsorption capacity (a) and removal percentage (b).



3.3 ADSORPTION KINETIC RESULTS

Figure 8 shows the kinetic curves for the MV adsorption on chitin derived biochar under different initial dye concentrations. These curves were obtained using adsorbent dosage of 0.5 g L^{-1} and Ph of 6.8. It can be seen that the adsorption presented a very fast kinetics, being the equilibrium attained at around 10 min, independent of the initial concentration. This is interesting for wastewater treatment plants, considering that a high amount of dye is removed from the liquid in short time intervals.

To better interpret the kinetic curves, the adsorption reaction models of Pseudo-first order (PFO) and Pseudo-second order (PSO) were fitted to the experimental curves of Figure 8. Table 5 shows that both models were suitable to predict the kinetic curves, taking into account the R^2 values near to 1 and, the low values of average relative error (ARE). However, a detailed analysis of the R^2 and ARE values shows that PSO model is most suitable to represent the MV adsorption kinetic on the biochar derived from chitin. Based on the parameter q_2 (Table 5), it can be seen that the adsorption capacity was favored at higher initial dye concentrations. This occurred because at higher concentrations, more available sites were occupied with the MV molecule. Furthermore, the q_2 was very close with the experimental value (q_e (exp)) of equilibrium adsorption capacity, confirming the good prediction of the PSO model. Finally, concerning the rate parameter, it is reasonable the use of h_0 instead k_2 [25]. The initial adsorption rate is given by $h_0 = k_2 q_2^2$ [25]. It was found that this parameter increased with the initial concentration. This shows that, at the begin of the process, adsorption was faster at higher MV concentrations. This is due to a higher concentration gradient between the bulk solution and the adsorbent surface that exist using higher values of C_0 .

Figure 8– Kinetic curves for the MV adsorption on chitin derived biochar under different initial dye concentrations (adsorbent dosage of 0.5 g L^{-1} and pH of 6.8).

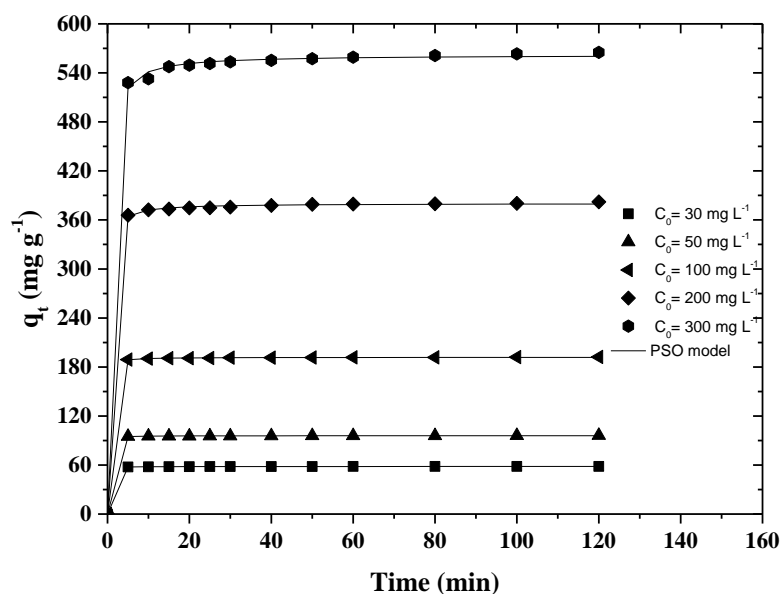


Table 5– Kinetic parameters for the MV adsorption on the chitin derived biochar.

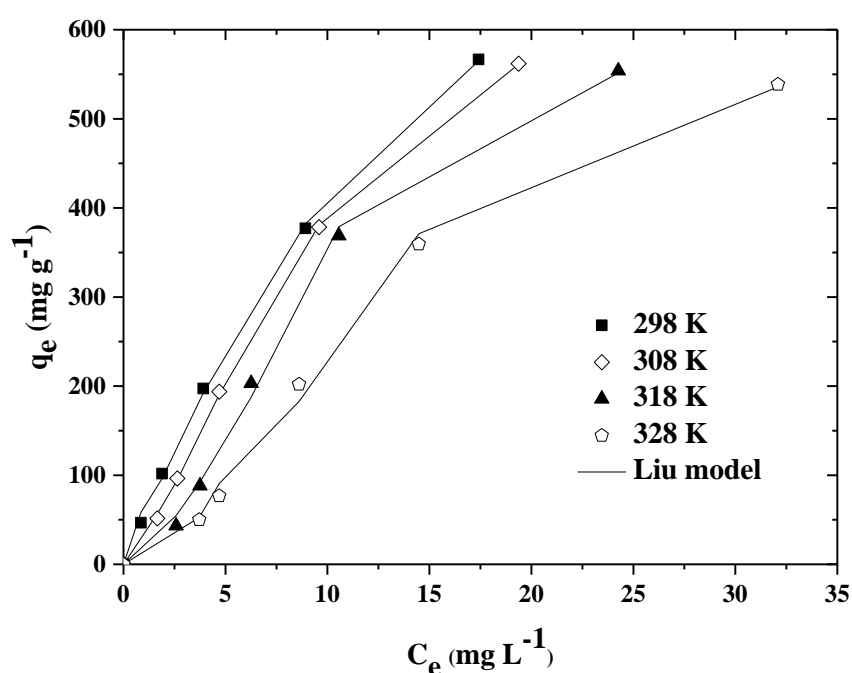
| Kinetic model | Initial dye concentration (mg L^{-1}) | | | | |
|---|--|--------|--------|--------|--------|
| | 30 | 50 | 100 | 200 | 300 |
| Pseudo–first order | | | | | |
| q_1 (mg g^{-1}) | 58.1 | 95.7 | 191.3 | 377.3 | 554.5 |
| k_1 (min^{-1}) | 0.960 | 1.000 | 0.890 | 0.691 | 0.592 |
| R^2 | 0.9999 | 0.9998 | 0.9998 | 0.9992 | 0.9972 |
| ARE (%) | 0.17 | 0.22 | 0.24 | 0.62 | 1.02 |
| Pseudo–second order | | | | | |
| q_2 (mg g^{-1}) | 58.3 | 95.9 | 191.9 | 380.2 | 562.0 |
| $k_2 \times 10^3$ ($\text{g mg}^{-1} \text{ min}^{-1}$) | 0.2898 | 0.1957 | 0.0637 | 0.0122 | 0.0046 |
| h_0 ($\text{mg g}^{-1} \text{ min}^{-1}$) | 983.6 | 1800.2 | 2345.9 | 1763.3 | 1453.1 |
| R^2 | 0.9999 | 0.9999 | 0.9999 | 0.9998 | 0.9994 |
| ARE (%) | 0.08 | 0.14 | 0.10 | 0.28 | 0.47 |
| $q_{e(\text{exp})}$ (mg g^{-1}) | 58.2 | 95.9 | 191.8 | 379.5 | 560.3 |

3.4 EQUILIBRIUM AND THERMODYNAMIC RESULTS

Figure 9 shows the isotherm curves for the MV adsorption on chitin derived biochar under different temperatures. These curves were obtained using adsorbent dosage of 0.5 g L^{-1} and pH of 6.8. The curves presented a favorable profile, where, the equilibrium adsorption capacity increases with the remaining concentration in liquid phase. This indicates that chitin derived biochar has several available sites to uptake the MV dye. Under the concentration

range used, a saturation plateau was not observed. This indicates that the adsorbent contains unoccupied sites and its potential is high. Concerning now the temperature effect, the MV adsorption was favored at 298 K. The temperature increase from 298 to 328 K, provoked a decrease in adsorption capacity. This can be related with the MV solubility, which is higher at higher temperatures. As consequence, at higher temperatures, MV has greater affinity with water molecules than with the adsorbent.

Figure 9– Equilibrium curves for the MV adsorption on chitin derived biochar under different temperatures (adsorbent dosage of 0.5 g L^{-1} and pH of 6.8).



Freundlich, Langmuir and Liu models were used to better interpret the equilibrium data. The fitting results are presented in Table 6. The Liu model was the most adequate to represent the adsorption isotherms, considering the lower values of ARE, and the higher values of R^2 and R^2_{adj} . The parameter related to the adsorption capacity of the Liu model (q_g) increased with the temperature decrease. The higher q_g value was 1120.8 mg g^{-1} , found at 298 K. This is a good value compared with several adsorbents presented in literature reviews [50, 51]. Thus, the biochar prepared in this work has excellent adsorption capacity. Other advantages are that the biochar is produced from a low cost and available material (chitin), by a simple process (pyrolysis).

Table 6– Isotherm parameters for the MV adsorption on the chitin derived biochar.

| Isotherm model | Temperature (K) | | | |
|---|-----------------|--------|--------|--------|
| | 298 | 308 | 318 | 328 |
| Freundlich | | | | |
| k_F (mg g ⁻¹) (mg L ⁻¹) ^{-1/n} | 72.0 | 55.8 | 45.3 | 33.6 |
| 1/n | 0.73 | 0.79 | 0.80 | 0.81 |
| R ² | 0.9945 | 0.9828 | 0.9536 | 0.9563 |
| R ² _{adj} | 0.9931 | 0.9785 | 0.9420 | 0.9454 |
| ARE (%) | 6.70 | 15.08 | 24.48 | 24.36 |
| Langmuir | | | | |
| q _m (mg g ⁻¹) | 1240.2 | 1469.4 | 1463.3 | 1497.1 |
| k _L (L mg ⁻¹) | 0.048 | 0.033 | 0.026 | 0.018 |
| R ² | 0.9989 | 0.992 | 0.9677 | 0.9692 |
| R ² _{adj} | 0.9986 | 0.9900 | 0.9596 | 0.9615 |
| ARE (%) | 4.80 | 11.55 | 22.81 | 22.99 |
| Liu | | | | |
| q _g (mg g ⁻¹) | 1120.8 | 761.6 | 618.8 | 614.4 |
| k _g (L mg ⁻¹) | 0.059 | 0.103 | 0.114 | 0.082 |
| g | 1.0 | 1.5 | 2.1 | 2.0 |
| R ² | 0.9999 | 0.9998 | 0.9977 | 0.9967 |
| R ² _{adj} | 0.9988 | 0.9998 | 0.9971 | 0.9959 |
| ARE (%) | 4.98 | 2.18 | 6.20 | 5.69 |

Standard Gibbs free energy change (ΔG_0), standard enthalpy change (ΔH_0), and standard entropy change (ΔS_0) were estimated aiming to verify the thermodynamic behavior of the adsorption process. The values of ΔG_0 ranged from -3.08 to -12 kJ mol⁻¹. The negative sign indicated that the MV adsorption onto the chitin derived biochar was a spontaneous and favorable process. The ΔS_0 value was -0.032 kJ mol⁻¹ K⁻¹. The negative sign indicated that the disorder in solid/liquid interface decreased after the adsorption process. The ΔH_0 value was -2.61 kJ mol⁻¹. The negative sign indicated the exothermic nature of the MV adsorption on the biochar. The magnitude of ΔH_0 indicated physical interactions between MV molecules and biochar, which are probably hydrogen bonds [52].

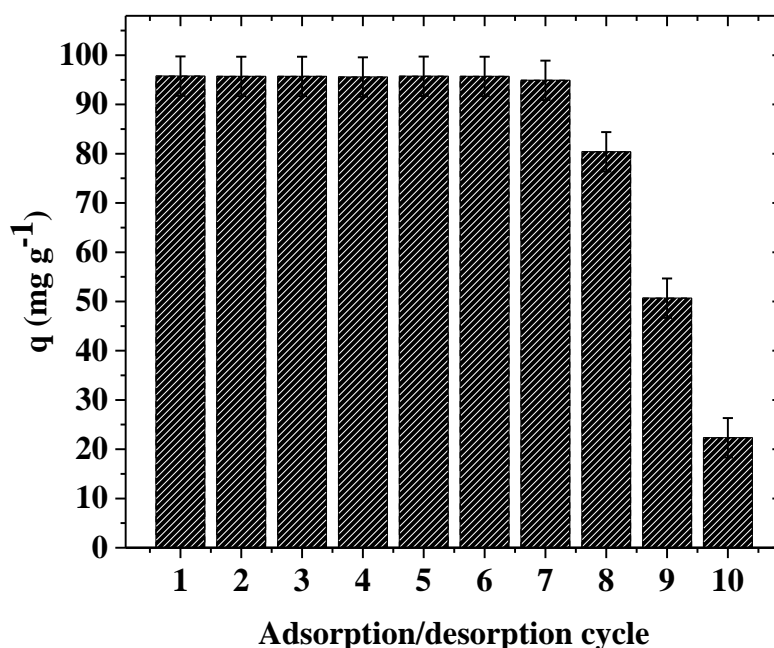
3.5 DESORPTION, MECHANISM AND REUSABILITY

Desorption was tested using CH₃COOH and H₂SO₄ as eluents, at concentrations of 0.1, 0.5 and 1.0 mol L⁻¹. Results revealed that CH₃COOH was a better eluent than H₂SO₄. This is an interesting result from the environmental viewpoint, since CH₃COOH is a weak organic acid, which causes less impact than H₂SO₄. It was found that 0.5 mol L⁻¹ of CH₃COOH was able to remove practically all dye from the biochar within 30 min (desorption percentage of 98.9%). In this sense, adsorption/desorption cycles were performed using this desorption

condition. Desorption in acid conditions is in agreement with the influence of pH (section RSM). This suggests that electrostatic forces are involved in the adsorption. In this sense, two main forces were involved in MV adsorption on the chitin derived biochar, hydrogen bonds (see thermodynamics) and electrostatic interactions.

The potential of reusability of chitin derived biochar was verified by performing 10 adsorption/desorption cycles. The results are presented in Figure 10. It can be verified that chitin derived biochar can be used 7 (seven) times without any loss of adsorption capacity. The adsorption capacity remained around 95 mg g^{-1} for seven consecutive cycles. After, adsorption capacity strongly decreased. These results show that chitin derived biochar has great potential to be used in several adsorption/desorption cycles, impacting directly in the operational costs.

Figure 10– Reusability of chitin derived biochar.

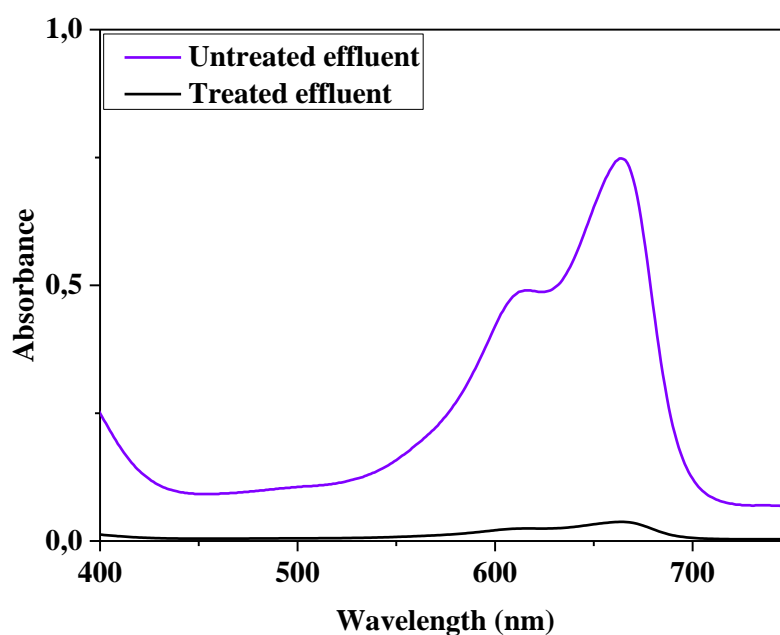


3.6. EFFICIENCY IN THE TREATMENT OF COLORED EFFLUENT

Chitin derived biochar was tested to treat a simulated colored effluent, containing some dyes and inorganic compounds. The visible spectra of the effluents before and after the treatment are presented in Figure 11. Comparing both spectra, it is clear that the spectrum of the effluent after the treatment was strongly amortized, demonstrating the excellent

performance of chitin derived biochar. The color removal percentage was 95.2%. These results shows that chitin derived biochar is an efficient adsorbent to be used in the treatment of colored effluents containing diferente kinds of dyes and also, inorganic compounds.

Figure 11– Visible spectra of the untreated and treated with chitin derived biochar effluents.



4 CONCLUSION

An alternative, eco-friendly and low-cost adsorbent was developed from chitin by a simple pyrolysis process, and the material was applied to treat colored effluents containing methyl violet dye (MV). Based on several characterization techniques, it was verified that chitin derived biochar presented suitable features for adsorption, including developed porosity and surface area. The optimal conditions for MV adsorption on chitin derived biochar were pH of 6.8 and adsorbent dosage of 0.5 g L^{-1} , providing adsorption capacity of 95.74 mg g^{-1} and removal percentage of 96.90%. Adsorption kinetics was fast, being the equilibrium attained at around 10 min and the curves were well represented by the PSO model. Equilibrium curves followed the Liu model, with maximum adsorption capacity of 1120.8 mg g^{-1} , attained at 298 K. Chitin derived biochar presented excellent reusability potential, being that, 7 consecutive adsorption/desorption cycles were possible maintaining the same adsorption capacity. Furthermore, chitin derived biochar was efficient to treat a colored effluent, with color removal percentage of 95%. The findings demonstrated that chitin derived

biochar can be prepared from an available and renewable biomass using a simple process, being a low– cost and eficiente adsorbent to treat colored effluents.

ACKNOWLEDGEMENTS

The authors would like to thank CAPES (Coordination for the Improvement of Higher Education Personnel) and CNPq (National Council for Scientific and Technological Development) for the financial support. Furthermore, the authors would like to thank CEME–SUL/FURG (Electron Microscopy Center of South/Federal University of Rio Grande/RS/Brazil) due to the scanning electron microscopy images.

REFERENCES

- [1] M.T. Yagub, T.K. Sen, S. Afroze, H.M. Ang, Dye and its removal from aqueous solution by adsorption: a review, *Adv. Colloid Interface Sci.* 209 (2014) 172–184.
- [2] P. Gregory, Classification of dyes by chemical structure, in: D.R. Waring, G. Hallas (Eds.), *Topics in Applied Chemistry*, Plenum Press, New York, 1990, pp. 17–47.
- [3] G.V. Brião, S.L. Jahn, E.L. Foletto, G.L. Dotto, Adsorption of crystal violet dye onto a mesoporous ZSM–5 zeolite synthetized using chitin as template, *J. Colloid Interface Sci.* 508 (2017) 313–322.
- [4] D.R. Lima, L. Klein, G.L. Dotto, Application of ultrasound modified corn straw as adsorbent for malachite green removal from synthetic and real effluents, *Environ. Sci. Pollut. Res. Int.* 26 (2017) 21484–21495.
- [5] V. Katheresan, J. Kansedo, S.Y. Lau, Efficiency of various recent wastewater dye removal methods: a review, *J. Environ. Chem. Eng.* 6 (2018) 4676–4697.
- [6] F. Rouquerol, J. Rouquerol, K.S.W. Sing, *Adsorption by Powders and Porous Solids: Principles, Methodology and Applications*, second ed., Elsevier, Amsterdam, 2014.
- [7] T.W. Leal, L.A. Lourenço, A.S. Scheibe, S.M.A.G.U. de Souza, A.A.U. de Souza, Textile wastewater treatment using low–cost adsorbent aiming the water reuse in dyeing process, *J. Environ Chem. Eng.* 6 (2018) 2705–2712.
- [8] D.M. Ruthven, *Principles of Adsorption and Adsorption Processes*, John Wiley & Sons, New York, 1984.
- [9] G.L. Dotto, S.K. Sharma, L.A.A. Pinto, Biosorption of organic dyes: research opportunities and challenges, in: Sanjay K . Sharma. (Org.) (Ed.), *Green Chemistry for Dyes Removal from Wastewater*, John Wiley & Sons, Inc., New York, 2015.

- [10] S. Shoukat, H.N. Bhatti, M. Iqbal, S. Noreen, Mango stone biocomposite preparation and application for crystal violet adsorption: a mechanistic study, *Micro. Meso. Mater.* 239 (2017) 180–189.
- [11] G.K. Sarma, S.S. Gupta, K.G. Bhattacharyya, Adsorption of Crystal violet on raw and acid-treated montmorillonite, K10, in aqueous suspension, *J. Environ. Manage.* 171 (2016) 1–10.
- [12] M.T. Moreira, I. Noya, G. Feijoo, The prospective use of biochar as adsorption matrix – a review from a lifecycle perspective, *Bioresour. Technol.* 246 (2017) 135–141.
- [13] S. Rangabhashiyam, P. Balasubramanian, The potential of lignocellulosic biomass precursors for biochar production: Performance, mechanism and wastewater application – a review, *Ind. Crop. Prod.* 128 (2019) 405–423.
- [14] M.A. Zazycki, M. Godinho, D. Perondi, E.L. Foletto, G.C. Collazzo, G.L. Dotto, New biochar from pecan nutshells as an alternative adsorbent for removing reactive red 141 from aqueous solutions, *J. Clean. Prod.* 171 (2018) 57–65.
- [15] M.A. Franciski, E.C. Peres, M. Godinho, D. Perondi, E.L. Foletto, G.C. Collazzo, G. L. Dotto, Development of CO₂ activated biochar from solid wastes of a beer industry and its application for methylene blue adsorption, *Waste Manage.* 78 (2018) 630–638.
- [16] A.F.M. Streit, L.N. Côrtes, S.P. Druzian, M. Godinho, G.C. Collazzo, D. Perondi, G. L. Dotto, Development of high quality activated carbon from biological sludge and its application for dyes removal from aqueous solutions In press *Sci. Total Environ.* (2018), <https://doi.org/10.1016/j.scitotenv.2019.01.027>.
- [17] Y. Chen, Y.C. Lin, S.H. Ho, Y. Zhou, N. Ren, Highly efficient adsorption of dyes by biochar derived from pigments extracted macroalgae pyrolyzed at diferente temperature, *Bioresour. Technol.* 259 (2018) 104–110.
- [18] D.D. Sewu, P. Boakye, S.H. Woo, Highly efficient adsorption of cationic dye by biochar produced with Korean cabbage waste, *Bioresour. Technol.* 224 (2017) 206–213.
- [19] G.L. Dotto, J.M.N. Santos, J.M. Moura, L.A.A. Pinto, Ultrasound-assisted treatment of chitin: evaluation of physicochemical characteristics and dye removal potential, *E-Polymers* 16 (2016) 49–56.
- [20] T. Wanjun, W. Cunxin, C. Donghua, Kinetic studies on the pyrolysis of chitin and chitosan, *Polym. Degrad. Stab.* 87 (2005) 389–394.
- [21] H. Yuan, L. Deng, X. Cai, S. Zhou, Y. Chen, Y. Yuan, Nitrogen-doped carbono sheets derived from chitin as non-metal bifunctional electrocatalysts for oxygen reduction and evolution, *RSC Adv.* 5 (2015) 56121.

- [22] G. Magnacca, F. Guerretta, A. Vizintin, P. Benzi, M.C. Valsania, R. Nisticò, Preparation, characterization and environmental/electrochemical energy storage testing of low-cost biochar from natural chitin obtained via pyrolysis at mild conditions, *Appl. Surf. Sci.* 427 (2018) 883–893.
- [23] J.M. Moura, B.S. Farias, D.A.S. Rodrigues, C.M. Moura, G.L. Dotto, L.A.A. Pinto, Preparation of chitosan with different characteristics and its application for biofilms production, *J. Polym. Environ.* 23 (2015) 470–477.
- [24] M.F.P.M. Latiff, I. Abustan, M.A. Ahmad, N.K.E.M. Yahaya, A.M. Khalid, Effect of preparation conditions of activated carbon prepared from corncob by CO₂ activation for removal of Cu (II) from aqueous solution, *AIP Conf. Proc.* 1774 (2016) 1–13.
- [25] N.F. Cardoso, E.C. Lima, B. Royer, M.V. Bach, G.L. Dotto, L.A.A. Pinto, T. Calvete, Comparison of *Spirulina platensis* microalgae and commercial activated carbon as adsorbents for the removal of Reactive Red 120 dye from aqueous effluents, *J. Hazard. Mater.* 241–242 (2012) 146–153.
- [26] T.V. Rêgo, T.R.S. Cadaval Jr., G.L. Dotto, L.A.A. Pinto, Statistical optimization, interaction analysis and desorption studies for the azo dyes adsorption onto chitosan films, *J. Colloid Interface Sci.* 411 (2013) 27–33.
- [27] S. Lagergren, About the theory of so-called adsorption of soluble substances, *K. Sven. Vetensk.* 24 (1898) 1–39.
- [28] Y.S. Ho, G. McKay, A comparison of chemisorption kinetic models applied to pollutant removal on various sorbents, *Trans. IChemE* 76 (1998) 332–340.
- [29] H. Freundlich, Over the adsorption in solution, *Z. Physic. Chem. A.* 57 (1906) 358–471.
- [30] I. Langmuir, The adsorption of gases on plane surfaces of glass, mica and platinum, *J. Amer. Chem. Soc.* 40 (1918) 1361–1403.
- [31] Y. Liu, H. Xu, J.H. Tay, Derivation of a general adsorption isotherm model, *J. Environ. Eng.* 131 (2005) 1466–1468.
- [32] E.C. Lima, A. Hosseini-Bandegharai, J.C. Moreno-piraján, I. Anastopoulos, A critical review of the estimation of the thermodynamic parameters on adsorption equilibria. Wrong use of equilibrium constant in the Van't Hoof equation for calculation of thermodynamic parameters of adsorption, *J. Mol. Liq.* 273 (2019) 425–434.
- [33] A.C. Fröhlich, C. Simoes, F.A. Pavan, E.C. Lima, E.L. Foletto, G.L. Dotto, Improvement of activated carbon characteristics by sonication and its application for pharmaceutical contaminant adsorption, *Environ. Sci. Pollut. Res.* 25 (2018) 24713–24725.

- [34] J. Georgin, F.C. Drumm, P. Grassi, D. Franco, D. Allasia, G.L. Dotto, Potential of *Araucaria angustifolia* bark as adsorbent to remove gentian violet dye from aqueous effluents, *Water Sci. Technol.* 78 (2018) 1693–1703.
- [35] M. Kaya, V. Baublys, I. Šatkauskienė, B. Akyuz, E. Bulut, V. Tubelyte, First chitin extraction from *Plumatella repens* (Bryozoa) with comparison to chitins of insect and fungal origin, *Int. J. Biol. Macromol.* 79 (2015) 126–132.
- [36] M.K. Jang, B.G. Kong, Y.I. Jeong, C.H. Lee, J.W. Nah, Physicochemical characterization of α -chitin, β -chitin, and γ -chitin separated from natural resources, *J. Polym. Sci. A Polym. Chem.* 42 (2004) 3423–3432.
- [37] M.K. Jang, B.G. Kong, Y.I. Jeong, C.H. Lee, J.W. Nah, Physicochemical characterization of α -chitin, β -chitin, and γ -chitin separated from natural resources, *J. Polym. Sci. Polym. Chem.* 42 (2004) 3423–3432.
- [38] A.T. Paulino, J.I. Simionato, J.C. Garcia, J. Nozaki, Characterization of chitosan and chitin produced from silkworm crysalides, *Carbohydr. Polym.* 64 (2006) 98–103.
- [39] Y. Wang, Y. Chang, L. Yu, C. Zhang, X. Xu, Y. Xue, Z. Li, C. Xue, Crystalline structure and thermal property characterization of chitin from Antarctic krill (*Euphausia superba*), *Carbohydr. Polym.* 92 (2013) 90–97.
- [40] E. Agrafioti, G. Bouras, D. Kalderis, E. Diamadopoulos, Biochar production by sewage sludge pyrolysis, *J. Anal. Appl. Pyrolysis* 101 (2013) 72–78.
- [41] M. Osada, C. Miura, Y.S. Nakagawa, M. Kaihara, M. Nikaido, K. Totani, Effects of supercritical water and mechanochemical grinding treatments on physicochemical properties of chitin, *Carbohydr. Polym.* 92 (2013) 1573–1578.
- [42] N. Liu, M. Zhu, H. Wang, H. Ma, Adsorption characteristics of Direct Red 23 from aqueous solution by biochar, *J. Mol. Liq.* 223 (2016) 335–342.
- [43] I. Corazzari, R. Nisticò, F. Turci, M.G. Faga, F. Franzoso, S. Tabasso, G. Magnacca, Advanced physico-chemical characterization of chitosan by means of TGA coupled on-line with FTIR and GCMS: thermal degradation and water adsorption capacity, *Polym. Degrad. Stab.* 112 (2015) 1–9.
- [44] S. Liu, J. Sun, L. Yu, C. Zhang, J. Bi, F. Zhu, Q. Yang, Extraction and characterization of chitin from the beetle *Holotrichia parallela* Motschulsky, *Molecules* 17 (2012) 4604–4611.
- [45] M.T. Yen, J.H. Yang, J.L. Mau, Physicochemical characterization of chitin and chitosan from crab shells, *Carbohydr. Polym.* 75 (2009) 15–21.

- [46] M. Kaya, T. Baran, M. Karaarslan, A new method for fast chitin extraction from shells of crab, crayfish and shrimp, *Nat. Prod. Res.* 29 (2015) 1477–1480.
- [47] G. Cardenas, G. Cabrera, E. Taboada, S.P. Miranda, Chitin characterization by SEM, FTIR, XRD, and C-13 cross polarization/mass angle spinning NMR, *J. Appl. Polym. Sci.* 93 (2004) 1876–1894.
- [48] M. Thommes, K. Kaneko, A.V. Neimark, J.P. Olivier, F. Rodriguez-Reinoso, J. Rouquerol, K.S.W. Sing, Physisorption of gases, with special reference to the evaluation of surface area and pore size distribution (IUPAC Technical Report), *Pure Appl. Chem.* 87 (2015) 1051–1069.
- [49] C. Hessel, C. Allegre, M. Maisseu, F. Charbit, P. Moulin, Guidelines and legislation for dye house effluents, *J. Environ. Manage.* 83 (2007) 171–180.
- [50] B. Mu, A. Wang, Adsorption of dyes onto palygorskite and its composites: a review, *J. Environ. Chem. Eng.* 4 (2016) 1274–1294.
- [51] A.M. Ghaedi, A. Vafaei, Applications of artificial neural networks for adsorption removal of dyes from aqueous solution: a review, *Adv. Colloid. Interface Sci.* 245 (2017) 20–39.
- [52] I. Anastopoulos, G.Z. Kyzas, Are the thermodynamic parameters correctly estimated in liquid-phase adsorption phenomena?, *J Mol. Liq.* 218 (2016) 174–185.

4.3 ARTIGO 3 – CONVERSION OF MDF WASTES INTO A BIOCHAR WITH REMARKABLE POTENTIAL TO REMOVE FOOD RED 17 DYE FROM AQUEOUS EFFLUENTS

M. A. Zazycki¹, D. Perondi², M. Godinho², M. L. S. Oliveira^{3,4}, G. C. Collazzo¹, G. L. Dotto^{1*}

¹Chemical Engineering Department, Federal University of Santa Maria, UFSM,
Roraima Avenue, 1000, 97105–900, Santa Maria, RS, Brazil.

²Postgraduate Program in Engineering Processes and Technology, University of
Caxias do Sul – UCS, Caxias do Sul, RS, Brazil.

³Department of Civil and Environmental, Universidad De La Costa, Calle 58 #55–66,
080002, Barranquilla, Atlántico, Colombia.

⁴Faculdade Meridional IMED, 304–Passo Fundo, RS, 99070–220, Brazil.

* Corresponding author: Chemical Engineering Department, Federal University of Santa Maria–UFSM, 1000, Roraima Avenue, 97105–900 Santa Maria, RS, Brazil. Email: guilherme_dotto@yahoo.com.br

ABSTRACT

Medium density fiberboard (MDF) wastes were converted into an efficient biochar able to uptake Food Red 17 dye (FR17) from colored effluents. The yield of the pyrolysis process, in terms of biochar, was 29%. The produced biochar presented micro and mesoporous, with surface area of $218.8 \text{ m}^2 \text{ g}^{-1}$ and total pore volume of $0.122 \text{ cm}^3 \text{ g}^{-1}$. Regarding to the FR17 adsorption, removal percentages of 90% were found at pH 2 and using 0.5 g L^{-1} of biochar. Pseudo-first and pseudo-second order models were adequate to represent the adsorption kinetic profile, being the equilibrium reached within 20 min. Freundlich model was selected to represent the equilibrium data. The maximum adsorption capacity was 210 mg g^{-1} . The adsorption of FR17 on the biochar was endothermic and physical in nature. The biochar was efficient for 8 adsorption-desorption cycles, maintaining the same adsorption capacity. In brief, this work demonstrated a useful practice in terms of cleaner production. It was possible add value to MDF wastes, generating an efficient and reusable adsorbent to treat colored effluents containing FR 17 dye.

Keywords: Adsorption. Biochar. MDF. Pyrolysis. Reusable adsorbent.

1 INTRODUCTION

Medium density fiberboard (MDF) is a lignocellulosic material composed by fresh wood, which is employed mainly in the furniture industry (GARCIA AND FREIRE, 2014). The worldwide production of MDF was 93.18 Mm^3 only in 2017. The largest MDF producers are Europa, accounting for 46.5% and Asia, responsible for 39%. Brazil is the third largest MDF producer (FAOSTAT, 2017). During the furniture processing MDF wastes are generated. For example, in Rio Grande do Sul state (BRAZIL), 5160 m^3 of MDF are produced by month, generating 332 tons of MDF wastes (FERREIRA et al., 2015). These MDF wastes are frequently discarded in landfills, burned in potteries, used in aviaries, or, incinerated for energy generation (MAYER et al., 2018). Alternatively, a sustainable way to add value for the MDF wastes is the thermochemical conversion by pyrolysis, generating a biochar (FERREIRA et al., 2015).

Pyrolysis is a thermochemical process where the volatile matter of a determined precursor is eliminated, generating a rich carbon product named biochar (ISAHAK et al.,

2012). Normally, this thermochemical conversion is performed at relatively low temperatures (WOO et al., 2016) and under a limited O₂ atmosphere (TAN et al., 2016). In this scenario, some studies reported the pyrolysis of MDF wastes. Ferreira et al. (2015) studied the pyrolysis of MDF in a screw reactor, under different conditions of temperature and time. They found biochar yields from 17.3 and 39.7%, and a surface area in the order of 500 m² g⁻¹. The pyrolysis of MDF wastes was also evaluated by Han et al. (2015). They have found char yield around 22%. In the study of Haeldermans and co-workers (2019), it was evaluated the conventional and microwave assisted pyrolysis of MDF. They concluded that both techniques were viable options to convert MDF in biochars. Aslan et al. (2018) evaluated the thermokinetic profile and the products during the pyrolysis of MDF. They concluded pyrolysis can prevent the environmental problems caused by the MDF disposal. The above referenced works presented significant contributions in the MDF pyrolysis, concerning the process and product characteristics. However, no data were presented in relation the application of the biochar. Here, MDF wastes were converted into an efficient biochar, which in turn, can be applied for the treatment of colored effluents.

The treatment of colored effluents is a global challenge. These effluents are generated mainly by the textile, paints and food sectors. If incorrectly treated, colored effluents can be environmentally dangerous (HASSAN AND CARR, 2018). In this context, the literature shows a series of treatment technologies (KATHERESAN et al., 2018), being that, adsorption stands out due its efficiency, ease of operation and possibility to use several adsorbent materials (ZHOU et al., 2019). Adsorption for environmental applications is preferred mainly when low cost materials derived from wastes are used as adsorbents (TRAN et al., 2019). The biochar from MDF wastes fits very well in this context, being possible add value to a largely available waste, and, at the same time, treat a colored effluent.

In order to simultaneously add value for medium density fiberboard (MDF) and produce an alternative adsorbent, MDF was pyrolyzed using N₂ to obtain a biochar able to treat colored effluents containing FR17 dye. The precursor MDF and the generated biochar were characterized by different techniques in order to verify the modifications caused by the thermochemical conversion. Both, MDF and biochar were used to treat synthetic solutions containing the FR17 dye, being investigated several factors affecting the batch adsorption. Standard studies of adsorption kinetics, isotherms and thermodynamics were performed. The recyclability of the biochar was also analyzed.

2 MATERIALS AND METHODS

2.1 MDF SAMPLES AND DYE AND REAGENTS

The MDF wastes were collected at a laser cutting company, localized in Santa Maria–RS, Brazil. The samples were washed with deionized water, oven dried at 60 °C for 8 h, ground in a Wiley mill and subsequently sieved. Particles with diameter lower than 710 μm were used for the study.

The industrial grade Food Red 17 dye (FR17) (color index 16035, molecular weight of 496.38 g mol^{-1}) (Figure 1S, Supplementary file) was used to prepare the colored effluents. This dye is commonly used in pharmaceutical and food industries (PICCIN et al., 2011). The synthetic effluents were prepared with FR17 and distilled water considering the dye purity of 85%. The pH of each solution was adjusted with NaOH and HCl. For all tests, blanks and triplicates were performed.

2.2 CONVERSION OF MDF WASTES INTO A BIOCHAR

The conversion of MDF into a biochar was performed by pyrolysis. The pyrolysis apparatus and conditions were based in preliminary tests and literature (FRANCISKI et al., 2018; ZAZYCKI et al., 2018). In the preliminary tests, the effects of temperature, heating rate and isotherm time were evaluated. A MDF sample of approximately 50 g was put in a tubular quartz reactor, which in turn was inserted in a furnace. The system was then heated at 10 °C min^{-1} until 800 °C under N_2 flux of 250 mL min^{-1} . The system remained at 800 °C under N_2 flux of 250 mL min^{-1} for 60 min. Subsequently, the system was cooled to room temperature (the nitrogen flow was maintained). The biochar produced was treated with H_2SO_4 to remove ashes, washed using distilled water and dried at 105 °C. The solid product was collected and the yield was computed.

2.3 CHARACTERIZATION OF MDF WASTES AND BIOCHAR

MDF wastes and biochar were characterized by SEM, FTIR, BET, BJH and pH_{zpc} techniques. Images of the biochar were acquired in a Jeol JSM–6010LV scanning electron microscope. FTIR vibrational spectra were obtained in a Shimadzu Prestige 21 infrared spectrophotometer. N_2 adsorption/desorption isotherms were obtained in a Micromeritics, ASAP 2020 equipment. Brunauer, Emmet and Teller (BET) method was used to calculate the surface area. Pore size distribution was obtained by the BJH (Barret, Joyner and Halenda) method (THOMMES et al., 2015). pH_{zpc} was determined according to Drumm et al. (2019).

2.4 POTENTIAL OF MDF BIOCHAR FOR FR17 ADSORPTION

The potential of MDF biochar to uptake the FR17 dye from synthetic aqueous effluents was evaluated by batch tests. These experiments were divided in four groups: evaluation of the pH effect; analysis of the adsorbent dosage effect; construction of the kinetic curves and construction of the equilibrium isotherms. All these tests were carried out in triplicate, using a Solab SL 222 thermostated shaker at 250 rpm. After the assays, the solid/liquid separation was performed by centrifugation and, the FR17 concentration in liquid phase was determined in a Shimadzu UV–mini spectrophotometer at 500 nm.

To evaluate the pH effect on the FR17 adsorption, several solutions of this dye, with volume of 50 mL and initial concentration of 50 mg L⁻¹ were prepared. The pH of these solutions was adjusted from 1.0 to 10.0. Then, 0.025 g of MDF or MDF biochar was put in contact with these solutions. The mixtures were agitated at 298 K for 2 h.

To analyze the adsorbent dosage effect on the FR17 adsorption, several solutions of this dye, with volume of 50 mL and initial concentration of 50 mg L⁻¹ were prepared. The pH of these solutions was set to 2.0. Then, different dosages of the MDF biochar (0.50, 0.75, 1.00, 1.20 and 1.50 g L⁻¹) were put in contact with these solutions. The mixtures were agitated at 298 K for 2 h.

The kinetic curves were constructed using pH of 2.0, adsorbent dosage of 0.50 g L⁻¹ and temperature of 298 K. The MDF biochar was contacted with the dye solutions, and the samples were collected at different time intervals, from 0 to 120 min. Five curves were constructed, varying the initial FR17 concentration (30, 50, 100, 200 and 300 mg L⁻¹).

The isotherm curves were constructed using pH of 2.0 and adsorbent dosage of 0.50 g L⁻¹. The MDF biochar was contacted with the dye solutions, and the mixture was stirred until the equilibrium. Isotherms were obtained at 298, 308, 318 and 328 K, in a FR17 concentration range from 0 to 300 mg L⁻¹.

The adsorption of FR17 on the MDF biochar was quantified according to the FR17 removal percentage (R_{FR17} , %) (Equation 1), equilibrium adsorption capacity (q_e , mg_{FR17} g⁻¹) (Equation 2) and adsorption capacity at any time (q_t , mg_{FR17} g⁻¹) (Equation 3).

$$R_{FR17} = \frac{(C_{0FR17} - C_{fFR17})}{C_{0FR17}} 100 \quad (1)$$

$$q_e = \frac{(C_{0FR17} - C_{eFR17})V}{m} \quad (2)$$

$$q_t = \frac{(C_{0FR17} - C_{tFR17})V}{m} \quad (3)$$

where, m (g) is the adsorbent mass, V (L) is the volume of the mixture, C_{0FR17} , C_{iFR17} , C_{eFR17} and C_{tFR17} (mg L^{-1}) denote the FR17 concentrations in liquid phase at the initial, final (2 h), equilibrium and any time stages, respectively.

2.5 MATHEMATICAL ANALYSIS OF THE FR17 ADSORPTION ON THE MDF BIOCHAR

FR17 adsorption on MDF biochar was evaluated as a unit operation using mathematical approaches to represent the kinetic and equilibrium profiles. Also, thermodynamic parameters were estimated. Kinetic evaluation was based on Lagergren (1898) and Ho and McKay (1998) models. Isotherms were analyzed according to Freundlich (1906), Langmuir (1918) and Sips (1948) equations. Thermodynamic parameters were obtained as suggested by Lima et al. (2019). The parameters estimation and fit quality were evaluated according to Dotto et al. (2013). All details are depicted in supplementary material.

2.6 ADSORPTION/DESORPTION TESTS IN THE SYSTEM MDF BIOCHAR/FR17

To evaluate the potential reuse of the MDF biochar, consecutive adsorption/desorption cycles were carried out. Adsorption was performed in the following conditions: temperature of 298 K, volume of solution of 1 L, pH of 2.0, stirring rate of 250 rpm, initial FR17 concentration of 300 mg L^{-1} , adsorbent dosage of 0.50 g L^{-1} . After adsorption, the solid was dried for 1h at $60 \text{ }^\circ\text{C}$ and used in desorption tests. Desorption tests were performed with NaOH (0.1, 0.3, 0.5, 0.7 or 1.0 mol L^{-1}) as eluent. 0.50 g L^{-1} of the FR17 loaded adsorbent was put in the eluent solution, which in turn was stirred for 1 h. The FR17 concentration in liquid phase was then measured by spectrophotometry. This cycles of adsorption/desorption were repeated 10 times.

3 RESULTS AND DISCUSSION

3.1 PYROLYSIS EVALUATION

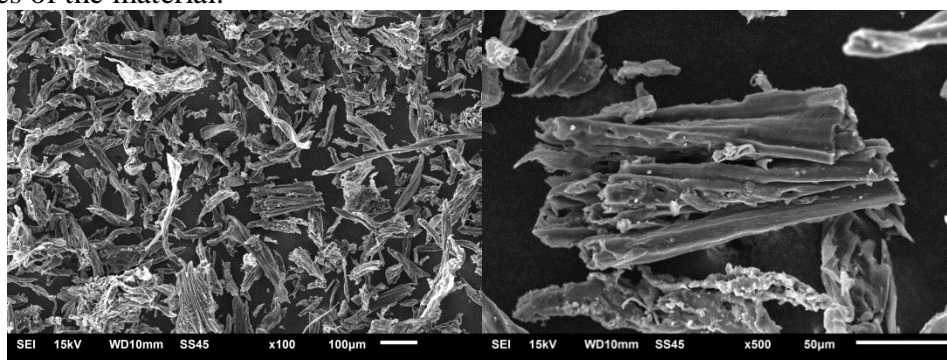
After the pyrolysis process, the biochar yield was calculated and the value was around 29 %. Haeldermans et al. (2019) found a MDF biochar yield of 28.4 and 27.0% with pyrolysis temperatures of 350 °C and 450 °C, respectively. Ferreira et al. (2015) observed that with increasing biomass residence time increased MDF biochar yield from 24.9 to 39.7% at the pyrolysis temperature of 450 °C. At 600 °C, the opposite was true, with the increase in the biomass residence time, the biochar yield decreased from 25.5% to 17.3%. According to Haeldermans et al. (2019) the lower yield at higher temperatures is due to the higher amount of volatiles produced. Biomass generally has a volatile matter content of approximately 70% (ZAZYCKI et al., 2018), which is confirmed by biochar yield.

3.2 CHARACTERISTICS OF MDF AND MDF BIOCHAR

The techniques of SEM, FTIR, BET/BHJ and point of zero charge (pH_{ZPC}) were used to characterize the MDF residues and its biochar.

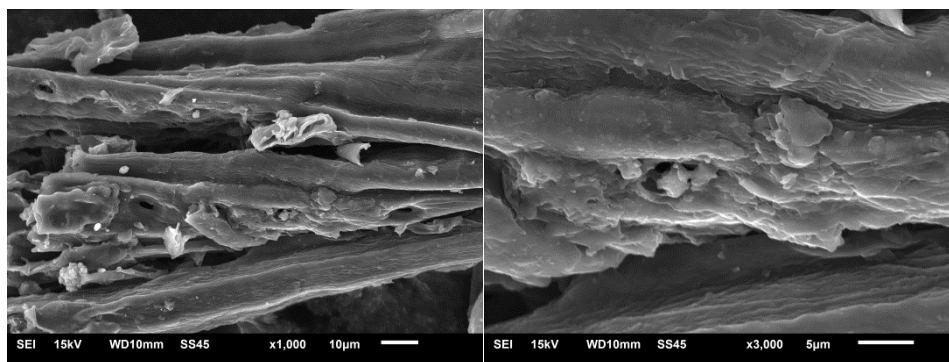
The biochar SEM images are shown in Figure 1. The biochar has an irregular surface, with several cavities and cracks. Also, it can be observed the fibrous character, typical of the MDF. Ferreira et al. (2018) observed similar characteristics in the products of MDF pyrolysis, i.e., a broken fiber structure, with pores on the external surface. These features are favorable for accommodating dye molecules, giving properties suitable for application as an adsorbent (ZAZYCKI et al., 2018).

Figure 1– SEM images of the MDF biochar showing (a) and (b) the particle and (c) and (d) the cavities of the material.



a)

b)



c)

d)

The FTIR spectra of MDF residues and its biochar are shown in Figure 2. The main bands of MDF waste are in 3396 cm^{-1} , 2916 cm^{-1} , 1728 cm^{-1} , 1658 cm^{-1} , 1259 cm^{-1} and 1032 cm^{-1} . The band 3396 cm^{-1} is assigned to the stretching O–H, corresponding to the adsorbed moisture to cellulose and also to the urea–formaldehyde resin which is one of the constituents of MDF. In 2916 cm^{-1} it is observed the stretching C–H, 1728 cm^{-1} the vibration corresponding to the carbonyl group (C=O), belonging to carboxylic acid or ester group bonds. The band 1658 cm^{-1} is related to the absorption of O–H and C–O conjugate (ether). During the pressing process, the MDF surface can reach up to $200\text{ }^{\circ}\text{C}$, which can lead to the opening of the furfural ring present in the MDF, resulting in polyioses residues (MULLER, 2009). The band 1259 cm^{-1} shows the C–O stretching of the acetyl group present in lignin, hemicellulose and the methoxy groups of the guaiacil aromatic ring. Softwood lignins are mainly composed of guaiacil lignin. In contrast, hardwood–derived lignins are composed of guaiacil and syringyl units (1235 cm^{-1}). This result confirms the presence of softwood pine in the composition of the analyzed MDF (OBST, 1982). Finally, at 1035 cm^{-1} , the vibrations of C–O and O–H relative to polysaccharides present in cellulose (FERREIRA et al., 2015) are observed. In the black spectrum (after pyrolysis), only the bands at 3396 and 1032 cm^{-1} remained, but with lower intensity. This confirms that the volatile matter was removed from the MDF residues.

Figure 2– FTIR vibrational spectra of MDF residues and MDF biochar.

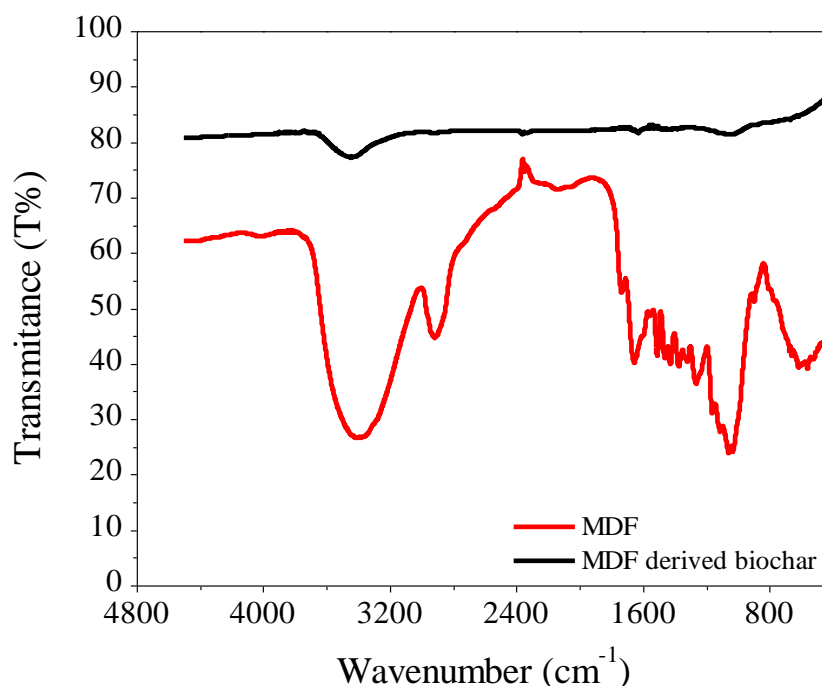
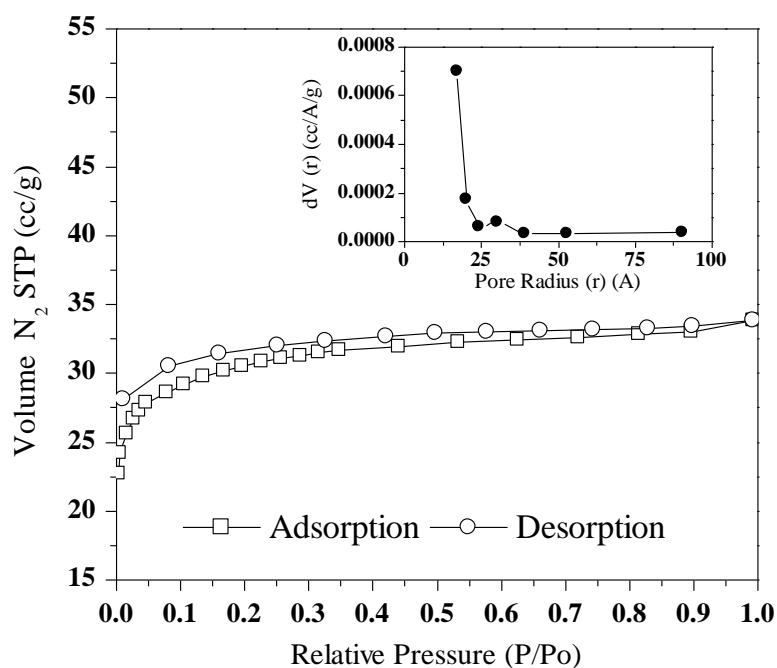


Figure 3 shows the N_2 adsorption–desorption isotherms and the pore size distribution (inside) curves of the MDF derived biochar. The adsorption isotherm were of Type IV (a) (Figure 3) (THOMMES et al., 2015), with hysteresis loop H4. This is relative to capillary condensation in mesopores (Ferreira et al., 2015). According to Thommes et al. (2015), the H4 loops are found in some mesoporous zeolites, and micro–mesoporous carbons. This is confirmed by the pore size distribution, which showed the presence of micro and mesopores. The biochar presented BET surface area of $218.8 \text{ m}^2 \text{ g}^{-1}$, total pore volume of $0.122 \text{ cm}^3 \text{ g}^{-1}$ and a mean pore size of 11.16 \AA . For comparison, in our recent papers (ZAZYCKI et al. 2018, 2019), biochars were developed from pecan nutshells and chitin, presenting surface areas of $93 \text{ m}^2 \text{ g}^{-1}$ and $275 \text{ m}^2 \text{ g}^{-1}$, respectively. These biochars were efficient to remove textile dyes from effluents. Chen et al. (2019) prepared a biochar from sludge–rice husk and found surface area around $30 \text{ m}^2 \text{ g}^{-1}$. The biochar was efficient to adsorb four different dyes. Considering the results presented in this work, in comparison with other published papers, it can be stated that the MDF biochar has interesting characteristics for dye adsorption.

Figure 3– Nitrogen adsorption–desorption isotherms and the Barrett–Joyner–Halenda desorption pore size distribution (inside).



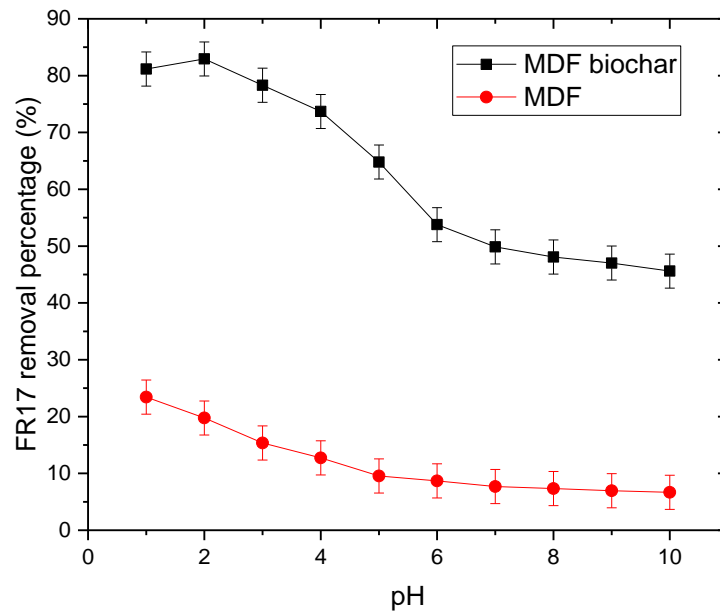
Concerning the point of zero charge (pH_{ZPC}), MDF presented pH_{ZPC} of 5.5 while MDF biochar presented pH_{ZPC} equal to 7.0. This shows that the MDF precursor has positive charge in a narrow pH range (from 1 to 5.4) and has a negative charged surface at pH values higher than 5.5. This facility to be negatively charged can be attributed to the surface oxygenated groups present in the surface, as presented in FTIR spectrum (Figure 2). In the case of MDF biochar, the surface is positively charged in a larger range of pH (until 6.9), while is negatively charged at pH values higher than 7.0. This can be explained by the volatilization of the functional groups present in the MDF surface, generating a biochar with better textural characteristics. These findings indicate that the MDF biochar is attractive to adsorb FR17, an anionic dye (Figure 1S), than its precursor. This supposition will be discussed in the section 3.3 (evaluation of pH and adsorbent dosage on the FR17 adsorption).

3.3 EVALUATION OF PH AND ADSORBENT DOSAGE ON THE FR17 ADSORPTION

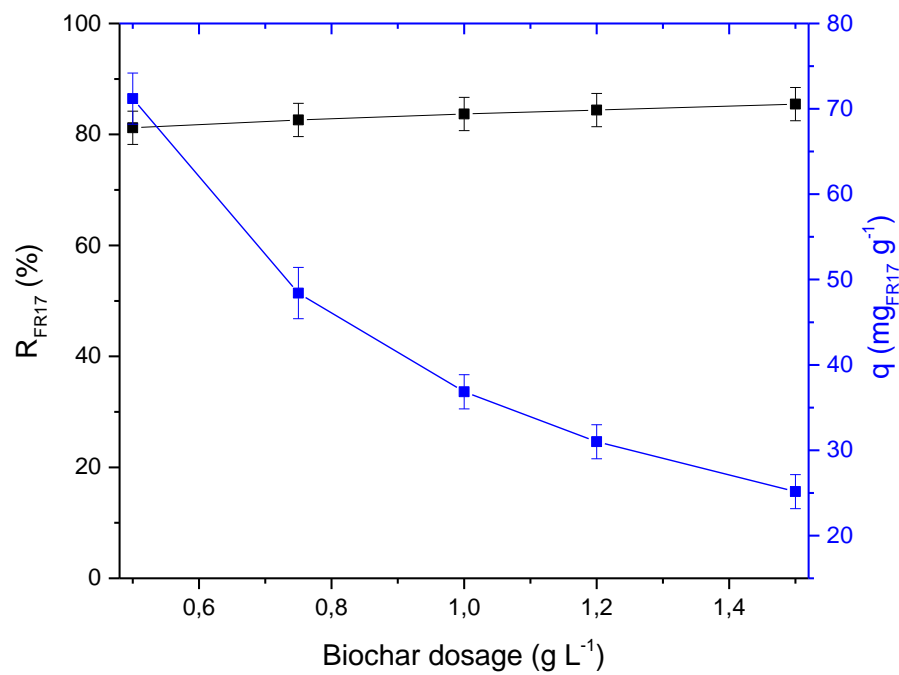
The adsorption of FR17 on MDF and MDF biochar was evaluated at different pH values, from 1 to 10. The results are presented in Figure 4(a). Two important behaviors can be highlighted in Figure 4(a): the first is that MDF biochar presented a far better performance than MDF for FR17 removal. While biochar was able to remove from 45 to 85% of the dye,

the maximum removal attained using MDF was around 25%; the second is that, for both materials, the adsorption was favored by the pH decrease.

Figure 4– Effects of pH (a) and adsorbent dosage (b) on the adsorption of FR17 dye by MDF and MDF biochar.



a)



b)

The first trend (Figure 4(a)) can be attributed to the better textural characteristics of the biochar, which were obtained by the thermochemical conversion. MDF biochar has surface area higher than $200 \text{ m}^2 \text{ g}^{-1}$ while the precursor has surface area in the order of units (FERREIRA et al., 2015). In addition, the oxygenated groups of the precursor, which can repeal the anionic dye, were removed during the pyrolysis process. Concerning the second trend, at high pH values (higher than 7), for both materials, the adsorption was poor and independent of pH. This is result of an electrostatic repulsion between FR17 anionic dye and the negatively charged surface of the adsorbent materials. On the contrary, higher removal percentages were found at lower pH, due to the electrostatic attraction between FR17 and the MDF biochar. These results are in accordance with the literature, where, FR17 is normally better adsorbed under acid conditions (PICCIN et al., 2011; SCHIO et al., 2019). Based in Figure 4(a), the subsequent tests were carried out at pH of 2.0 using MDF biochar.

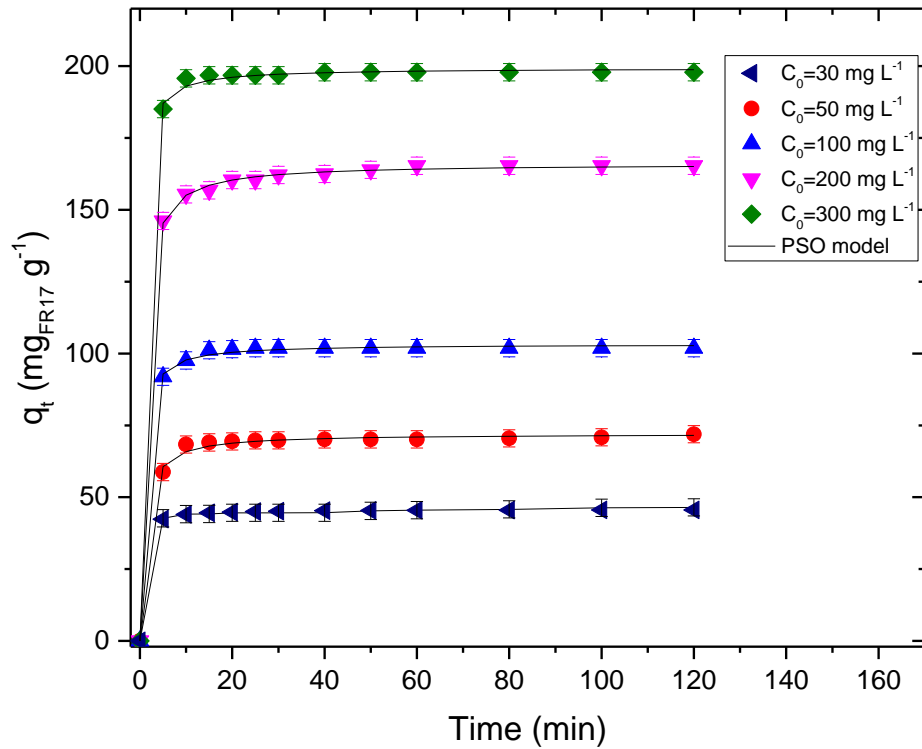
Figure 4(b) depicts the effect of biochar dosage on the FR17 removal percentage and adsorption capacity. It can be verified in Figure 4(b) that the increase in biochar dosage presented no effect on the FR17 removal, being the values around 80 to 85%. On the other hand, adsorption capacity was strongly affected by the MDF biochar dosage. Adsorption capacity increased from 25 to 73 mg g^{-1} when the dosage decreased from 1.5 g L^{-1} to 0.50 g L^{-1} . This trend is normally related with the superposition of adsorption sites (TRAN et al., 2019). Based on Figure 6, it was selected 0.50 g L^{-1} as the best biochar dosage, to find higher values of adsorption capacity and satisfactory values of removal percentage.

3.4 ADSORPTION KINETIC PROFILES

Five kinetic curves, at different initial dye concentrations, were obtained for the system MDF biochar/FR17. The profiles are shown in Figure 5.

The profiles indicate fast adsorption kinetics regardless the initial dye concentration. The curves were characterized by an initial step, from 0 to 5 min, where a greater increase in adsorption capacity occurred, indicating a fast adsorption rate. From 5 to 20 min, the adsorption rate decreased. The equilibrium was achieved within 20 min for all studied concentrations. This is extremely useful for effluents treatment plants, since the total operation time is considerably reduced. As expected, adsorption capacity increased with initial dye concentration. This trend is attributed to the better occupation of the adsorption sites.

Figure 5– Adsorption kinetic profiles for the system MDF biochar/FR17.

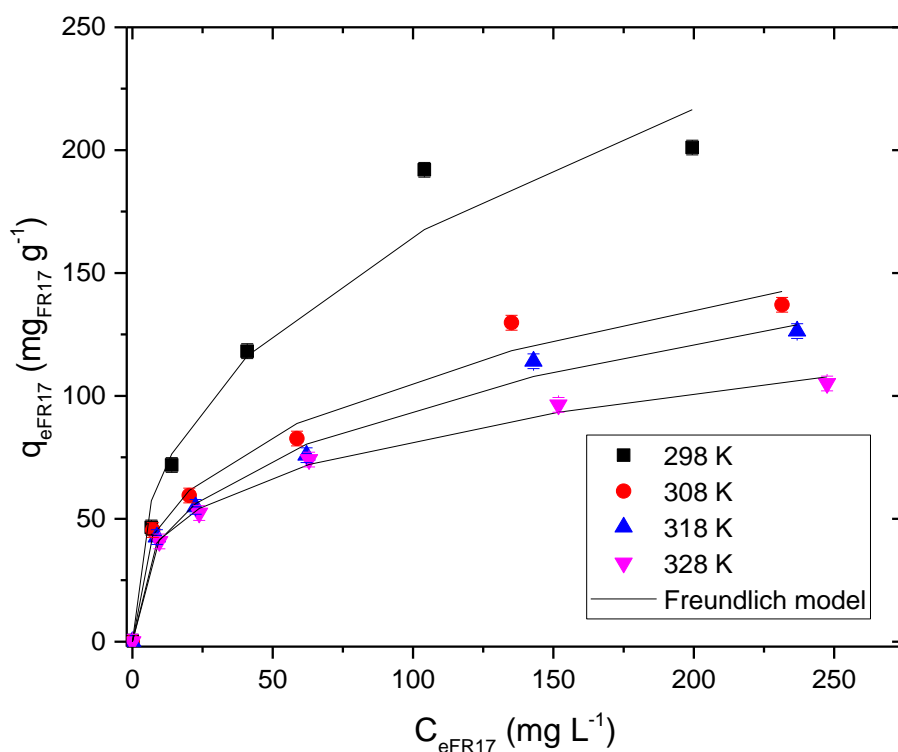


The profiles of Figure 5 were represented by the adsorption reaction models (Pseudo–first order, PFO and pseudo–second order, PSO). The results are in Table 1S. It can be seen that both models presented excellent statistical indicators, i.e. R^2_{adj} and R^2 were higher than 0.99 for all cases. In addition, the average relative error (ARE) was lower than 1.5% independent of the model or experimental condition. Thus PFO and PSO models can be used to represent the kinetic profile of FR17 adsorption on MDF biochar. Comparing the values of q_1 and q_2 with the experimental value, q_e , it can be stated that the parameter q_2 (PSO) is closer with the experimental value than the parameter q_1 (PFO). In this sense, PSO model was slightly better to predict the adsorption system. Concerning now the initial adsorption rate (represented by the parameter h_0 , $h_0 = k_2 q_2^2$), it was found that, in general, h_0 increased with the initial concentration. This indicates a faster adsorption in the initial stages, when higher FR17 concentrations are used.

3.5 ADSORPTION ISOTHERM CURVES

Four isotherm curves, at different temperatures, were obtained for the system MDF biochar/FR17. The profiles are shown in Figure 6. The equilibrium curves of Figure 6 presented a convex shape in relation to the Y axis, with a progressive increase in adsorption capacity. The values of adsorption capacity not attained a constant value (plateau). This is a typical behavior of an L1 type isotherm (GILES et al., 1974). Based on this, it is possible infer that FR17 molecules progressively occupied the adsorption sites on the biochar surface, but, some sites remained empty. In relation to the temperature effect, it was verified an exothermic behavior, since an inversely proportional behavior was verified between the temperature and adsorption capacity. According to Ruthven (1984) this is typical of physical adsorption processes.

Figure 6– Adsorption isotherm profiles for the system MDF biochar/FR17.



The isotherm curves were represented by the Freundlich, Langmuir and Sips models. The fitting results are depicted in Table 2S. The statistical indicators were better for the Freundlich and Sips models than the Langmuir model (ARE values were lower and R^2_{adj} and R^2 were higher). In spite of the Sips model presents better fit than the Freundlich model in

some cases, its parameters (q_m , k_s and m) presented no physical trend in relation to the temperature. In addition, this model has 3 parameters. On the other hand, the Freundlich parameters presented a physical behavior in relation to the temperature. Because this, the Freundlich model was selected to represent the FR17 adsorption onto the MDF biochar. The parameter k_F (Table 2S) increased with the temperature decrease. The same was observed for the $1/n_F$. These findings corroborate that the adsorption capacity and the affinity between MDF biochar and FR17 are higher at 298 K.

The quality of an adsorbent is normally measured by its maximum adsorption capacity. Table 1 shows the maximum adsorption capacities attained for FR17 of different adsorbents. Among the adsorbents, it can be seen that MDF biochar has a competitive adsorption capacity. In addition to this, MDF biochar is derived from a residual material, and presented fast kinetics. Because this, MDF biochar can be considered an alternative adsorbent to treat colored effluents containing FR17 dye.

Table 1– Maximum adsorption capacities of different adsorbents for FR17 dye.

| Adsorbent | T (K), pH | q_m (mg g ⁻¹) | Reference |
|---------------------------------|---------------|-----------------------------|----------------------------|
| Vine-trimming waste | 298, 6 | 135.1 | SÜTCÜ, 2014 |
| Sludge derived activated carbon | 328, 2 | 287 | STREIT et al., 2019 |
| Activated carbon | 303, 6 | 137 | DURÁN-JIMÉNEZ et al., 2014 |
| Chitosan/AC hydrogel | 298, 3 | 133.9 | GONÇALVES et al., 2017 |
| Chitosan hydrogel | 298, 3 | 92.9 | GONÇALVES et al., 2017 |
| Polyurethane/chitosan foam | 328, 2 | 267.2 | SCHIO et al., 2019 |
| MDF biochar | 298, 2 | 210.0 | This study |

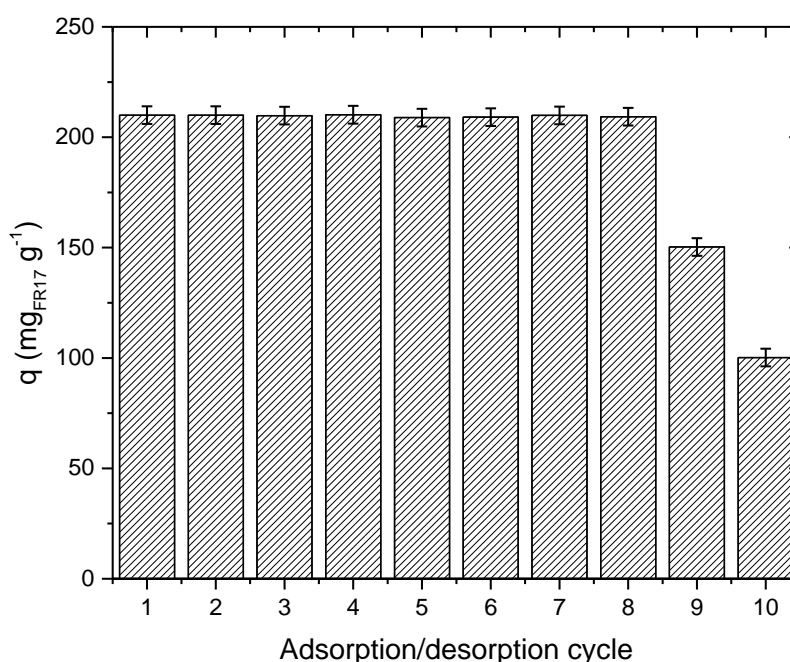
3.6 THERMODYNAMIC RESULTS

Thermodynamic information's regarding the FR17 adsorption on the MDF biochar were assessed according to the values of ΔG^0 , ΔH^0 and ΔS^0 . These values are presented in Table 3S. At first, it was confirmed the spontaneity of the FR17 adsorption onto the MDF biochar, due to the negative values of ΔG^0 . Also, it was found that the disorder in the solid/liquid interface has increased after FR17 adsorption onto the MDF biochar, since the ΔS^0 value was positive. The negative ΔH^0 value confirms the exothermic nature of this adsorption process. Its magnitude is in agreement with physical adsorption (LIMA et al., 2019; TRAN et al., 2019).

3.7 RECYCLABILITY OF MDF BIOCHAR

The recyclability of the MDF biochar was tested performing ten adsorption–desorption cycles. NaOH at different concentrations (0.1, 0.3, 0.5, 0.7 or 1.0 mol L⁻¹) was evaluated as eluent. It was verified that 0.5 mol L⁻¹ NaOH was the best eluent. Using this eluent, all the FR17 dye was transferred from the MDF biochar to the solution within 15 min. The results of adsorption capacity found in all adsorption–desorption cycles are depicted in Figure 7. It is possible to verify that the MDF biochar maintained its maximum adsorption capacity even after 8 adsorption–desorption cycles. The adsorption capacity was reduced in the reuses 9 and 10, probably, because the sites were damaged by the alkali used in desorption. The possibility to use MDF biochar for eight times is excellent for practical applications, reducing the operational costs.

Figure 7– Adsorption capacities found in the consecutive adsorption–desorption cycles for the system MDF biochar/FR17.



4 CONCLUSION

Medium density fiberboard (MDF) wastes, a typical residue generated in large amounts for the furniture industry, was successfully converted in an efficient biochar, which in turn, was able to treat colored effluents containing FR17 dye. The pyrolysis process used for this conversion presented 29% of biochar yield. This biochar was a mesoporous material,

with surface area of $218.8 \text{ m}^2 \text{ g}^{-1}$ and total pore volume of $0.122 \text{ cm}^3 \text{ g}^{-1}$. Concerning the FR17 adsorption onto the biochar, the process was favored at pH of 2.0. The adsorption of FR17 on the MDF biochar was a fast process, reaching the equilibrium within 20 min. PSO and Freundlich models were the best models to represent, respectively, the adsorption kinetics and isotherms. The process was exothermic and physical in nature. The maximum adsorption capacity was 210 mg g^{-1} , and, this capacity was maintained for eight adsorption–desorption cycles. In summary, it was demonstrated that MDF wastes can be converted in an effective and reusable adsorbent with potential to treat colored effluents containing the FR17 dye.

REFERENCES

- Aslan, D.I., Özoğul, B., Ceylan, S., Geyikçi, F. 2018. Thermokinetic analysis and product characterization of Medium Density Fiberboard pyrolysis. *Bioresour. Technol.* 258, 105–110.
- Chen, S., Qin, C., Wang, T., Chen, F., Li, X., Hou, H., Zhou, M., 2019. Study on the adsorption of dyestuffs with different properties by sludge–rice husk biochar: Adsorption capacity, isotherm, kinetic, thermodynamics and mechanism. *J. Mol. Liq.* 285, 62–74.
- Dotto, G.L., Costa, J.A.V, Pinto, L.A.A., 2013. Kinetic studies on the biosorption of phenol by nanoparticles from *Spirulina* sp. *LEB 18. J. Environ. Chem. Eng.* 1, 1137–1143.
- Drumm, F.C., Grassi, P., Georgin, J., Tonato, D., Franco, D.S.P., Chaves Neto, J.R., Mazutti, M.A., Jahn, S.L., Dotto, G.L. 2019. Potentiality of the *Phoma* sp. inactive fungal biomass, a waste from the bioherbicide production, for the treatment of colored effluents. *Chemosphere* 235, 596–605.
- Durán–Jiménez, G., Hernández–Montoya, V., Montes–Morán, M.A., Bonilla–Petriciolet, A., Rangel–Vázquez, N.A. 2014. Adsorption of dyes with different molecular properties on activated carbons prepared from lignocellulosic wastes by Taguchi method. *Micro. Meso. Mater.* 199, 99–107.
- FAOSTAT – Food and Agriculture Organisation of the United Nations. 2017. Forestry Database, Forestry Production and Trade. Available at: <<http://www.fao.org/faostat/en/>> (accessed August 30, 2019).
- Ferreira, S.D., Altafini, C.R., Perondi, D., Godinho, M., 2015. Pyrolysis of Medium Density Fiberboard (MDF) wastes in a screw reactor. *Energ. Conver. Manage.* 92, 223–233.
- Franciski, M.A., Peres, E.C., Godinho, M., Perondi, D., Foletto, E.L., Collazzo, G.C., Dotto, G.L., 2018. Development of CO₂ activated biochar from solid wastes of a beer industry and its application for methylene blue adsorption. *Waste Manage.* 78, 630–638.
- Freundlich, H.M., 1906. Over the adsorption in solution. *J. Phys. Chem.* 57, 385–470.

- Garcia, R., Freire, F., 2014. Carbon footprint of particleboard: a comparison between. *J. Clean. Prod.* 66, 199–209.
- ISO/TS 14067, GHG Protocol, PAS 2050 and Climate Declaration. *J. Clean. Prod.* 66, 199–209.
- Giles, C.H., Smith, D., Huitson, A., 1974. A general treatment and classification of the solute adsorption isotherm. I. Theoretical. *J. Colloid Interface Sci.* 47, 755–765.
- Gonçalves, J.O., Santos, J.P., Rios, E.C., Crispim, M.M., Dotto, G.L., Pinto, L.A.A., 2017. Development of chitosan based hybrid hydrogels for dyes removal from aqueous binary system. *J. Mol. Liq.* 225, 265–270.
- Haeldermans, T., Claesen, J., Maggen, J., Carleer, R., Ypermana, J., Adriaensens, P., Samyna, P., Vandamme, D., Cuypers, A., Vanreppelen, K., Schreurs, S., 2019. Microwave assisted and conventional pyrolysis of MDF – Characterization of the produced biochars. *J. Anal. Appl. Pyrol.* 138, 218–230.
- Han, T.U., Kim, Y.M., Watanabe, C., Teramae, N., Park, Y.K., Kim, S., Lee, Y., 2015. Analytical pyrolysis properties of waste medium-density fiberboard and particle board. *J. Ind. Eng. Chem.* 32, 345–352.
- Hassan, M.M., Carr, C.M., 2018. A critical review on recent advancements of the removal of reactive dyes from dyehouse effluent by ion-exchange adsorbents. *Chemosphere* 209, 201–219.
- Ho, Y.S., McKay, G., 1998. Kinetic models for the sorption of dye from aqueous solution by wood. *Process Saf. Environ. Prot.* 76, 183–191.
- Isahak, W., Hisham, M., Yarmo, M., Yun Hin, T.A., 2012. Review on bio-oil production from biomass by using pyrolysis method. *Renew. Sust. Energ. Rev.* 16, 5910–5923.
- Katheresan, V., Kansedo, J., Lau, S.Y., 2018. Efficiency of various recent wastewater dye removal methods: A review. *J. Environ. Chem. Eng.* 6, 4676–4697.
- Langmuir, I., 1918. The adsorption of gases on plane surfaces of glass, mica and platinum. *J. Am. Chem. Soc.* 40, 1361–1403.
- Lima, E.C., Hosseini-Bandegharai, A., Moreno-Piraján, J.C., Anastopoulos, I., 2019. A critical review of the estimation of the thermodynamic parameters on adsorption equilibria. Wrong use of equilibrium constant in the Van't Hoof equation for calculation of thermodynamic parameters of adsorption. *J. Mol. Liq.* 273, 425–434.
- Lagergren, S., 1898. About the theory of so-called adsorption of soluble substances. *K. Sven. Vetenskapsakademiens Handl.* 24, 1–39.

Mayer, F.M., Teixeira, C.M., Pacheco, J.G.A., Souza, C.T., Bauer, D.V., Caramão, E.B., Espíndola, J.S., Trierweiler, J.O., Lopez, O.W.P., Zini, C.A., 2018. Characterization of analytical fast pyrolysis vapors of medium-density fiberboard (mdf) using metal-modified HZSM-5. *J. Anal. Appl. Pyrol.* 136, 87–95.

Muller, G., Schopper, C., Vos, H., Kharazipour, A., Polle, A., 2009. FTIR-ATR Spectroscopic analyses of changes in wood properties during particle- and fiberboard production of hard- and softwood trees. *BioResources* 4, 49–71.

Obst, J.R., 1982. Guaiacyl and Syringyl Lignin Composition in Hardwood Cell Components. *Holzforschung* 36, 143–152.

Piccin, J.S., Dotto, G.L., Vieira, M.L.G., Pinto, L.A.A., 2011. Kinetics and mechanism of the food dye FD&C Red 40 adsorption onto chitosan. *J. Chem. Eng. Data* 56, 3759–3765.

Ruthven, D.M., 1984. Principles of adsorption and adsorption processes. John Wiley & Sons, Hoboken, 433 p.

Schio, R.R., Rosa, B.C., Gonçalves, J.O., Pinto, L.A.A., Mallmann, E.S., Dotto, G.L., 2019. Synthesis of a bio-based polyurethane/chitosan composite foam using ricinoleic acid for the adsorption of Food Red 17 dye. *Int. J. Biol. Macromol.* 121, 373–380.

Sips, R., 1948. Combined form of Langmuir and Freundlich equations. *J. Chem. Phys.* 16, 490–495.

Streit, A.F.M., Côrtes, L.N., Druzian, S.P., Godinho, M., Collazzo, G.C., Perondi, D., Dotto, G.L., 2019. Development of high quality activated carbon from biological sludge and its application for dyes removal from aqueous solutions. *Sci. Total Environ.* 660, 277–287.

Sütcü, H., 2014. Removal of FD&C red no.40 food dye from an aqueous solution by vine-trimming waste. *Int. J. Chem. Eng. Appl.* 5, 420–423.

Tan, X., Liu, Y., Gu, Y., Xu, Y., Zeng, G., Hu, X., Liu, S., Wang, X., Liu, S., Li, J., 2016. Biochar-based nano-composites for the decontamination of wastewater: a review. *Bioresour. Technol.* 212, 318–333.

Thommes, M., Kaneko, K., Neimark, A.V., Olivier, J.P., Rodriguez-Reinoso, F., Rouquerol, J., Sing, K.S.W., 2015. Physisorption of gases, with special reference to the evaluation of surface area and pore size distribution (IUPAC Technical Report). *Pure Appl. Chem.* 87, 1051–1069.

Tran, H.N., Nguyen, H.C., Woo, S.H., Nguyen, T.V., Vigneswaran, S., Hosseini-Bandegharai, A., Rinklebe, J., Sarmah, A.K., Ivanets, A., Dotto, G.L., Bui, T.T., Juang, R.S., Chao, H.P., 2019. Removal of various contaminants from water by renewable lignocellulose-derived biosorbents: a comprehensive and critical review. *Critical Reviews Environ. Sci.*

Technol. 49, 2155–2219.

Woo, S.H., Enders, A., Lehmann, J., 2016. Microbial mineralization of pyrogenic organic matter in different mineral systems. *Organ. Geochem.* 98, 18–26.

Zazycki, M.A., Godinho, M., Perondi, D., Foletto, E.L., Collazzo, G.C., Dotto, G.L., 2018. New biochar from pecan nutshells as an alternative adsorbent for removing reactive red 141 from aqueous solutions. *J. Clean. Prod.* 17, 57–65.

Zazycki, M.A., Borba, P.A., Silva, R.N.F., Peres, E.C., Perondi, D., Collazzo, G.C., Dotto, G.L., 2019. Chitin derived biochar as an alternative adsorbent to treat colored effluents containing methyl violet dye. *Adv. Powder Technol.* 30, 1494–1503.

Zhou, Y., Lu, J., Zhou, Y., Liu, Y., 2019. Recent advances for dyes removal using novel adsorbents: A review. *Environ. Pollut.* 252, 352–365.

SUPPLEMENTARY MATERIAL

S.1. KINETICS, ISOTHERMS AND THERMODYNAMICS

Kinetic behavior was verified through the Pseudo–first order (PFO) (Equation (1S)) (Lagergren, 1898) and Pseudo–second order (PSO) (Equation (2S)) (Ho and McKay, 1998) models. The models are mathematically simple and allow the comparison of the adsorption capacities, although they consider adsorption as a chemical reaction.

$$q_t = q_1(1 - \exp(-k_1 t)) \quad (1S)$$

$$q_t = \frac{1}{(1/k_2 q_2^2) + (t/q_2)} \quad (2S)$$

where, k_1 (min^{-1}) and k_2 ($\text{g mg}^{-1} \text{min}^{-1}$) are the rate constants of the models and q_1 and q_2 (mg g^{-1}) are the predicted adsorption capacities.

To represent the FR17 adsorption on the biochar, the models of Freundlich (Equation (3S)) (Freundlich, 1906), Langmuir (Equation (4S)) (Langmuir, 1918) and Sips (Equation (5S)) (Sips, 1948) were adjusted to the experimental data. The models, chosen according to the shape of the isotherm, provide mathematical relation between the amount of FR17 in the solid phase (q_e) and the amount of FR17 in liquid phase (C_e) at equilibrium.

$$q_e = k_F C_e^{1/n_F} \quad (3S)$$

$$q_e = \frac{q_m k_L C_e}{1 + k_L C_e} \quad (4S)$$

$$q_e = \frac{q_m (k_S C_e)^m}{1 + (k_S C_e)^m} \quad (5S)$$

being, k_F the Freundlich constant ($\text{mg g}^{-1})(\text{mg L}^{-1})^{-1/n_F}$, $1/n_F$ the heterogeneity factor, q_m the maximum adsorption capacity (mg g^{-1}), k_L the Langmuir constant (L mg^{-1}), k_S the Sips constant (L mg^{-1}) and m , the Sips exponent.

S.2. ADSORPTION THERMODYNAMICS

The FR17 adsorption on the biochar was also analyzed from the thermodynamic parameters. The values of ΔG° (kJ mol^{-1}), ΔH° (kJ mol^{-1}) and ΔS° ($\text{kJ mol}^{-1} \text{K}^{-1}$), which represent, respectively, the variations of Gibbs free energy, enthalpy and entropy were calculated using Equations (6S–7S) (Lima et al., 2019).

$$\Delta G^\circ = -RT \ln(K^\circ) \quad (6S)$$

$$\ln(K^\circ) = \frac{\Delta S^\circ}{R} - \frac{\Delta H^\circ}{RT} \quad (7S)$$

where K° is the thermodynamic constant (dimensionless), R is the gases constant ($\text{kJ mol}^{-1} \text{K}^{-1}$) and T is temperature (K). K° was estimated as described by Lima et al. (2019) (Lima et al., 2019).

S.3. PARAMETERS ESTIMATION

The kinetic and isotherm parameters were estimated using the Statistic 9.1 software (Statsoft, USA) by nonlinear regression with the original form of the models. The minimization of the least squares function based on the Quasi–Newton method was used to estimate the parameters. The quality of the adjust was measured through determination coefficient (R^2), adjusted determination coefficient (R^2_{adj}) and average relative error (ARE) (Dotto et al., 2013).

S.4. SUPPLEMENTARY FIGURES AND TABLES

Figure 1S– Chemical structure of Food Red 17 dye.

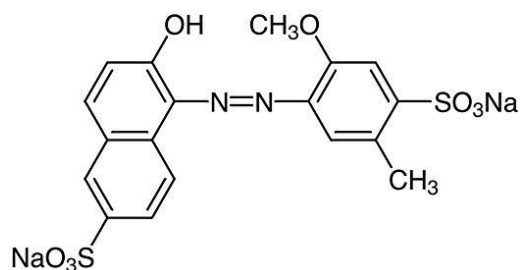


Table 1S– Kinetic parameters for FR17 adsorption onto the MDF biochar.

| Kinetic model | Initial FR17 concentration (mg L ⁻¹) | | | | |
|--|--|--------|--------|--------|--------|
| | 30 | 50 | 100 | 200 | 300 |
| Pseudo–first order | | | | | |
| q ₁ (mg g ⁻¹) | 45.11 | 70.22 | 101.54 | 162.37 | 197.37 |
| k ₁ (min ⁻¹) | 0.5762 | 0.3612 | 0.4592 | 0.4450 | 0.5531 |
| ARE (%) | 1.32 | 0.59 | 0.50 | 1.42 | 0.24 |
| R ² | 0.9964 | 0.9988 | 0.9989 | 0.9957 | 0.9999 |
| R ² _{adj} | 0.9961 | 0.9987 | 0.9988 | 0.9953 | 0.9999 |
| Pseudo–second order | | | | | |
| q ₂ (mg g ⁻¹) | 45.74 | 72.07 | 102.05 | 166.08 | 199.03 |
| k ₂ × 10 ³ (g mg ⁻¹ min ⁻¹) | 0.0545 | 0.0147 | 0.0173 | 0.0084 | 0.0153 |
| h ₀ (mg g ⁻¹ min ⁻¹) | 114.03 | 76.35 | 184.42 | 231.69 | 607.88 |
| ARE (%) | 0.84 | 1.15 | 0.63 | 0.36 | 0.42 |
| R ² | 0.9985 | 0.9969 | 0.9991 | 0.9996 | 0.9995 |
| R ² _{adj} | 0.9984 | 0.9966 | 0.9990 | 0.9996 | 0.9995 |
| q _e (mg g ⁻¹) | 46.47 | 71.91 | 101.86 | 165.33 | 197.86 |

Table 2S– Equilibrium parameters for the adsorption of FR17 onto the MDF biochar.

| Isotherm model | Temperature (K) | | | |
|---|-----------------|--------|--------|--------|
| | 298 | 308 | 318 | 328 |
| Freundlich model | | | | |
| $k_F (\text{mg g}^{-1})(\text{mg L}^{-1})^{-1/n_F}$ | 27.08 | 21.80 | 18.69 | 21.38 |
| $1/n_F$ | 0.3925 | 0.3548 | 0.3533 | 0.2934 |
| R^2 | 0.9700 | 0.9848 | 0.9933 | 0.9967 |
| R^2_{adj} | 0.9625 | 0.9810 | 0.9916 | 0.9959 |
| ARE (%) | 8.62 | 4.74 | 3.59 | 2.29 |
| Langmuir model | | | | |
| $q_m (\text{mg g}^{-1})$ | 241.08 | 152.14 | 139.05 | 110.75 |
| $k_L (\text{L mg}^{-1})$ | 0.0288 | 0.0319 | 0.0291 | 0.0425 |
| R^2 | 0.9892 | 0.9560 | 0.9617 | 0.9808 |
| R^2_{adj} | 0.9865 | 0.9450 | 0.9521 | 0.9760 |
| ARE (%) | 6.17 | 10.72 | 9.68 | 6.79 |
| Sips model | | | | |
| $q_m (\text{mg g}^{-1})$ | 261.21 | 381.63 | 382.07 | 210.62 |
| $k_s (\text{L mg}^{-1})$ | 0.0232 | 0.0013 | 0.0009 | 0.0041 |
| m | 0.8781 | 0.4584 | 0.4550 | 0.4576 |
| R^2 | 0.9903 | 0.9849 | 0.9924 | 0.9985 |
| R^2_{adj} | 0.9879 | 0.9811 | 0.9905 | 0.9981 |
| ARE (%) | 4.40 | 5.58 | 4.24 | 1.76 |

Table 3S– Thermodynamic parameters for the FR17 adsorption onto the MDF biochar.

| Temperature (K) | $\Delta G^0 (\text{kJ mol}^{-1})^*$ | $\Delta H^0 (\text{kJ mol}^{-1})^*$ | $\Delta S^0 (\text{kJ mol}^{-1} \text{K}^{-1})^*$ |
|-----------------|-------------------------------------|-------------------------------------|---|
| 298 | -21.90±0.03 | | |
| 308 | -21.71±0.10 | | |
| 318 | -21.92±0.02 | -11.52±0.12 | 0.03±0.01 |
| 328 | -23.01±0.04 | | |

*mean ± standard error.

5 DISCUSSÃO DOS RESULTADOS

Os três artigos apresentados na seção 4 têm como foco a preparação de *biochars* a partir de resíduos sem valor econômico e, abundantes no Rio Grande do Sul, e a aplicação como adsorventes alternativos na remoção de corantes de soluções aquosas. No artigo 1, o *biochar* derivado de resíduos de cascas de noz-pecan, foi utilizado para remover o corante RR141. No artigo 2, o *biochar* derivado da quitina foi empregado na remoção do corante MV. E, no artigo 3, foi preparado um *biochar* derivado de resíduos de chapas de MDF para aplicação na remoção do corante FR17.

Os três materiais comprovaram que são promissores para o processo de pirólise e conseqüentemente para a produção de *biochar*. As condições de pirólise utilizadas neste estudo, temperatura de operação, taxa de aquecimento e tempo de isoterma, mostraram-se eficazes uma vez que as amostras estudadas compreendiam: cascas de noz-pecan, quitina e lascas de MDF. A temperatura de 800°C com baixa taxa de aquecimento e tempo de isoterma elevada garantiram a eliminação de toda matéria volátil presentes nas amostras, comprovadas nas análises de FTIR antes e depois do processo de pirólise. Após o processo pirolítico, os rendimentos dos três *biochars* foram cerca de 30%, o que pode-se considerar um bom rendimento uma vez que a quantidade de material volátil presentes nestas amostras é alta. Por fim, pode-se concluir que os *biochars* produzidos são formados de uma estrutura carbonosa, com alta área de superfície e estruturas microporosas e mesoporosas evidenciados nas técnicas de caracterização.

Em relação ao desempenho como adsorventes, cada um dos *biochars* foi utilizado para remover moléculas diferentes, e os resultados foram satisfatórios. O *biochar* derivado dos resíduos de cascas de noz-pecan teve uma porcentagem de remoção do corante RR141 de 85% e uma máxima capacidade de adsorção de cerca de 130 mg g⁻¹, o *biochar* derivado da quitina removeu 95% do corante MV e capacidade máxima de adsorção de 1120,8 mg g⁻¹ e para o *biochar* derivado de resíduos de chapas de MDF uma remoção em torno de 70% do FR17 com uma capacidade máxima de adsorção de de 210 mg g⁻¹.

Do ponto de vista ambiental, o tratamento térmico por pirólise, tem recebido grande destaque, por reduzir os resíduos em até 90%, além de gerar três produtos (*biochar*, bio-óleo e biogás), todos com potencial valor econômico. Neste trabalho, o foco foi o desenvolvimento e aplicação da fração sólida da pirólise como adsorvente no tratamento de efluentes coloridos. O desenvolvimento de *biochars* a partir de matérias primas alternativas e abundantes e sua aplicação como adsorventes reduz os custos dos processos de tratamento de efluentes,

tornando-os economicamente viáveis, e, além disso, contribui para o gerenciamento dos resíduos sólidos. A valorização das outras frações obtidas na pirólise, para a geração simultânea de mais produtos com valor agregado, é uma boa alternativa para trabalhos futuros.

6 CONCLUSÕES

Neste trabalho, *biochars* foram preparados a partir de resíduos sólidos problemáticos encontrados no Rio Grande do Sul (cascas de noz-pecan, quitina e chapas de MDF) e aplicados como adsorventes alternativos para a remoção dos corantes RR141, MV e FR17 de soluções aquosas. Os resultados demonstraram que os *biochars* podem ser preparados a partir de resíduos, usando um processo simples na sua preparação, sendo uma alternativa viável para adsorção de corantes em soluções aquosas.

Com base nas técnicas de caracterização, verificou-se que os três *biochars* apresentaram características adequadas para adsorção, incluindo porosidade desenvolvida e alta área de superfície. Os *biochars* apresentaram estruturas microporosas e mesoporosas. Também foram observadas cavidades e protuberâncias na superfície dos *biochars*. O *biochar* derivado de resíduos de cascas de noz-pecan apresentou uma área de superfície de $93 \text{ m}^2 \text{ g}^{-1}$, volume total de poros de $0,055 \text{ cm}^3 \text{ g}^{-1}$ e tamanho médio de poros de 12 \AA . O *biochar* derivado da quitina apresentou uma área de superfície de $275 \text{ m}^2 \text{ g}^{-1}$, volume total de poros de $0,178 \text{ cm}^3 \text{ g}^{-1}$ e tamanho médio de poros de 13 \AA . O *biochar* derivado de resíduos de chapas de MDF apresentou área de superfície de $218,8 \text{ m}^2 \text{ g}^{-1}$, volume total de poros de $0,122 \text{ cm}^3 \text{ g}^{-1}$ e tamanho médio de poros de 11 \AA .

O *biochar* derivado de cascas de noz-pecan foi um excelente adsorvente para remover o corante RR141 de soluções aquosas quando comparado com seu precursor. A remoção do corante foi de 85% usando o *biochar* e apenas 23% usando o material precursor. A adsorção foi favorecida no pH de 3,0. A cinética de adsorção seguiu o modelo de PSO e 80% da saturação foi atingida em 10 min. A capacidade máxima de adsorção foi de 130 mg g^{-1} a 298 K. Por fim a adsorção foi um processo espontâneo, favorável e exotérmico.

No *biochar* derivado da quitina, o pH ideal foi de 6,8 e dosagem de adsorvente de $0,5 \text{ g L}^{-1}$. A cinética teve uma alta taxa de adsorção, sendo o equilíbrio atingido em torno de 10 min e as curvas foram bem representadas pelo modelo PSO. A capacidade máxima de adsorção, estimada pelo modelo de Liu, foi de $1120,8 \text{ mg g}^{-1}$, a 298 K. O *biochar* apresentou excelente potencial de reutilização, sendo possíveis 7 ciclos consecutivos de adsorção/dessorção, mantendo a mesma capacidade de adsorção.

Em relação à adsorção do corante FR17 no *biochar*, o processo foi favorecido em pH de 2,0. A cinética de adsorção foi rápida, sendo o equilíbrio alcançado em 20 min. Os modelos PSO e Freundlich foram os melhores modelos para representar, respectivamente, a

cinética e as isothermas de adsorção. A capacidade máxima de adsorção foi de 210 mg g^{-1} e essa capacidade foi mantida por oito ciclos de adsorção–dessorção.

REFERÊNCIAS

ABBASIAN, M. et al. Grafting of aniline derivatives onto chitosan and their applications for removal of reactive dyes from industrial effluents. **International Journal of Biological Macromolecules**, v. 95, p. 393–403, 2017.

AFTAB, U. et al. Decolourization and degradation of textile azo dyes by corynebacterium sp. Isolated from industrial effluent. **Pakistan Journal of Zoology**, v. 43, p. 1–8, 2011.

AHMED, M. J. Application of agricultural based activated carbons by microwave and conventional activations for basic dye adsorption: Review. **Journal of Environmental Chemical Engineering**, v. 4, p. 89–99, 2016.

ALENCAR, W. S. et al. Application of *Mangifera indica* (mango) seeds as a biosorbent for removal of Victazol Orange 3R dye from aqueous solution and study of the biosorption mechanism. **Chemical Engineering Journal**, v. 209, p. 577–588, 2012.

ALI, I. et al. Low cost adsorbents for the removal of organic pollutants from wastewater. **Journal of Environmental Management**, v. 113, p. 170–183, 2012.

AL-QODAH, Z. Adsorption of dyes using shale oil ash. **Water Research**, v. 34, p. 4295–4303, 2000.

ALTENOR, S. et al. Adsorption studies of methylene blue and phenol onto vetiver roots activated carbon prepared by chemical activation. **Journal of Hazardous Material**, v. 165, p. 1029–1039, 2009.

Associação Brasileira das Indústrias do Mobiliário – **ABIMÓVEL**, 2012. Disponível em: <http://www.abimovel.com/dados-do-setor/moveleiro>.

Associação das Indústrias de Móveis do Estado do Rio Grande do Sul – **MOVERGS**, 2015. Disponível em: <http://www.movergs.com.br/dados-setor-moveleiro>.

BANSODE, R. R. et al. Adsorption of metal ions by pecan shell-based granular activated carbons. **Bioresource Technology**, v. 89, p. 115–119, 2003.

BORTOLUZZI, B. M. A. Remoção dos corantes azul de metileno e cristal violeta de solução aquosa utilizando epicarpo (casca) de uva niágara rosada (*vitis labrusca*) como adsorvente. 2015. **Dissertação** (Mestrado em Engenharia) - Universidade Federal do Pampa, Bagé, 2015.

BRIDGWATER, A.V. Review of fast pyrolysis of biomass and product upgrading. **Biomass and Energy**, v. 38, p. 68–94, 2012.

CHEN, D. et al. Pyrolysis technologies for municipal solid waste: a review. **Waste Management**, v. 34, p. 2466–2486, 2014.

CHEN, B. et al. A novel magnetic *biochar* efficiently sorbs organic pollutants and phosphate. **Bioresource Technology**, v. 102, p. 716–723, 2011.

COLLAZZO, G. C. et al. Evaluation of niobium oxide doped with metals in photocatalytic degradation of leather dye. **Latin American Applied Research**, v. 42, p. 51–54, 2012.

CONSELHO NACIONAL DO MEIO AMBIENTE – CONAMA. **Resolução nº 357, de 17 de março de 2005**. Dispõe sobre a classificação dos corpos de água e diretrizes ambientais para o seu enquadramento, bem como estabelece as condições e padrões de lançamento de efluentes, e dá outras providências. Alterado pela Resolução CONAMA 397/2008. Disponível em: <http://www.mma.gov.br/conama>.

DÁVILA, I. V. J. Remoção de Vermelho Reativo 120 em solução aquosa usando hidroxicarbonatos de Mg-Al, Mg-Fe e Mg como sólidos sorventes. 2016. **Dissertação** (Mestrado em Engenharia Química) – Departamento de Engenharia Química, Universidade Federal do Rio Grande do Sul, Porto Alegre, 2016.

DING, G. et al. Simultaneous adsorption of methyl red and methylene blue onto *biochar* and an equilibrium modeling at high concentration. **Chemosphere**, v. 163, p. 283–289, 2016.

DOTTO, G. L. et al. A. Treatment of chitin effluents by coagulation–flocculation with chitin and aluminum sulfate. **Journal of Environmental Chemical Engineering**, v. 1, p. 50–55. 2013.

DOTTO, G. L. et al. Adsorption of methylene blue by ultrasonic surface modified chitin. **Journal Colloid Interface Science**, v. 446, p. 133–140, 2015.

DOTTO, G. L.; PINTO, L. A. A. Adsorption of food dyes acid blue 9 and food yellow 3 onto chitosan: Stirring rate effect in kinetics and mechanism. **Journal of Hazardous Materials**, v. 187, p. 164–170, 2011.

FAOSTAT–Food and Agriculture Organization of the United Nations, 2014i. **Forestry Database**, Forestry Production and Trade.

FERNANDES, A. C. P. et al. Adsorção de efluentes têxteis: tratamento de efluentes da indústria têxtil por adsorção em materiais de baixo custo. **Relatório de projeto**. Faculdade de Engenharia da Universidade do Porto, 2010.

FIGUEIREDO, C. C. et al. Short-term effects of a sewage sludge biochar amendment on total and available heavy metal content of a tropical soil. **Geoderma**, v. 344, p. 31–39, 2019.

FREUNDLICH, H. Over the adsorption in solution. **Journal of Physical Chemistry**, v. 57, p. 385–470, 1906.

GAUTAM, R. K. et al. Biomass-derived biosorbents for metal ions sequestration: Adsorbent modification and activation methods and adsorbent regeneration. **Journal of Environmental Chemical Engineering**, v. 2, n. 1, p. 239–259, 2014.

GEANKOPLIS, C. J. **Transport Process and Unit Operations**. 3 ed. New Jersey: Prentice ± Hall International, 1993.

GOMIDE, R. **Operações Unitárias**, São Paulo: Edição do Autor, 1980.

GUPTA, V. K.; SUHAS. Application of low-cost adsorbents for dye removal- A review. **Journal of Environmental Management**, v. 90, p. 2313-2342, 2009.

HAGHSERESHT, F. et al. Effects of surfaces chemistry on aromatic compound adsorption from dilute aqueous solutions by activated carbon. **Journal of Physical Chemistry**, v. 106, p. 10935–10943, 2002.

KAJEKAR, A. J. et al. Preparation and characterization of novel PSf/PVP/PANI–nanofiber nanocomposite hollow fiber ultra filtration membranes and their possible applications for hazardous dye rejection. **Desalination**, v. 365, p. 117–125, 2015.

KHAN, R. et al. Microbial decolorization and degradation of synthetic dyes: a review. **Reviews in Environmental Science and Bio/Technology**, v. 12, p. 75–97, 2013.

KHOR, E. Chitin: a biomaterial in waiting. **Current Opinion in Solid State and Materials Science**, v. 6, p. 313–317, 2002.

KIM, K. H. et al. Influence of pyrolysis temperature on physicochemical properties of *biochar* obtained from the fast pyrolysis of pitch pine (*Pinus rigida*). **Bioresource Technology**, v. 118, p. 158–162, 2012.

KUMAR, R.; AHMAD, R. Biosorption of hazardous crystal violet dye from aqueous solution onto treated ginger waste (TGW), **Desalination**, p. 265, v. 112, 2011.

LAHKIMI, A. et al. Removal of textile dyes from water by the electro–Fenton process. **Environmental Chemistry Letters**, v. 5, p. 35–39, 2007.

LANGMUIR, I. The adsorption of gases on plane surfaces of glass, mica and platinum. **Journal of the American Chemical Society**, v. 40, p. 1361–1403, 1918.

LI, H. et al. Effect of pyrolysis temperature on characteristics and aromatic contaminants adsorption behavior of magnetic *biochar* derived from pyrolysis oil distillation residue. **Bioresource Technology**, v. 223, p. 20–26, 2017.

LIANG, C. et al. Biochar from pruning residues as a soil amendment: effects of pyrolysis temperature and particle size. **Soil & Tillage Research**, v. 164, p. 3–10, 2016.

LIU, N. et al. Adsorption characteristics of Direct Red 23 from aqueous solution by *biochar*. **Journal of Molecular Liquids**, v. 223, p. 335–342, 2016.

LIU, Y. Is the Free Energy Change of Adsorption Correctly Calculated. **Journal of Chemical Engineering and Data**, v. 54, p. 1981–1985, 2009.

LONAPPAN, L. et al. Adsorption of methylene blue on *biochar* microparticles derived from different waste materials. **Waste Management**, v. 49, p. 537–544, 2016.

LU, H. et al. Effect of biochar in cadmium availability and soil biological activity in an anthrosol following acid rain deposition and aging. **Water, Air & Soil Pollution**, v. 226, n. 5, p. 1–11, 2015.

McCABE, Warren L. et al. **Unit Operations of Chemical Engineering**. 7. ed. Nova Iorque: McGraw–Hill, 2005.

MENDONÇA, J. N. Identificação e isolamento de corantes naturais produzidos por actinobactérias. 2011. **Dissertação** (Mestrado em Ciências) – Faculdade de Filosofia, Ciências e Letras, Universidade de São Paulo, Ribeirão Preto, 2011.

MILONJIC, S. K. et al. The influence of cationic impurities in silica on its crystallization and point of zero charge. **Journal of Colloid and Interface Science**, v. 309, p. 155–159, 2007.

MOHAN, D. et al. Organic and inorganic contaminants removal from water with biochar, a renewable, low cost and sustainable adsorbent—a critical review. **Bioresource Technology**, v. 160, p. 191–202, 2014.

MOREIRA, R. Estudo da pirólise lenta da casca da castanha de caju. 2015. 66 p. **Dissertação** (Mestrado em Ciências na Área de Tecnologia Nuclear – Materiais) – Instituto de Pesquisas Energéticas e Nucleares, Autarquia associada à Universidade de São Paulo, São Paulo, 2015.

NAUTIYAL, P. et al. Adsorptive removal of dye using biochar derived from residual algae after in–situ transesterification: Alternate use of waste of biodiesel industry. **Journal of Environmental Management**, v. 182, p. 187–197, 2016.

ORTIZ, E. R. N. 2000. Propriedades nutritivas e nutracêuticas das nozes. **Monografia**, Especialização em Tecnologia de Alimentos, Universidade de Santa Cruz do Sul, Santa Cruz do Sul, 2000.

PANKAJ, T., PATTAYIL, A. J. Superparamagnetic nanocomposite of magnetite and activated carbon for removal of dyes from waste water. **Nanoscience and Nanotechnology Letters**, v. 1, p. 171–175, 2009.

PARADELA, F. M. R. Estudo da pirólise de misturas de resíduos de plásticos, pneus e biomassa. 2012. 322f. **Tese** (Doutorado em Engenharia Química e Bioquímica) – Faculdade de Ciências e Tecnologia, Universidade Nova de Lisboa, Lisboa, 2012.

PIEKARSKI, C. M. Life cycle assessment of medium–density fiberboard (MDF) manufacturing process in Brazil. **Science of the Total Environment**, v. 575, p. 103–111, 2017.

POLAERT, I. et al. Phenol wastewater treatment by a two–step adsorption–oxidation process on activated carbon. **Chemical Engineering Science**, v. 57, p. 1585–1590, 2002.

QIU, M. et al. Studies on the adsorption of dyes into clinoptilolite. **Desalination**, v. 243, p. 286–292, 2009.

RIUL, M.; RIBEIRO, E. L. Diagnóstico e Diretrizes para a Gestão de Resíduos no APL de Móveis de João Pessoa–PB. UNOPAR **Científica Ciências Exatas e Tecnológicas**, Londrina, v. 11, n. 1, p.15–24, nov. 2012.

RODRIGUES, C. S. D. et al. Synthetic textile dyeing wastewater treatment by integration of advanced oxidation and biological processes – Performance analysis with costs reduction. **Journal of Environmental Chemical Engineering**, v. 2, p. 1027–1039, 2014.

RUTHVEN, D. M. **Principles of Adsorption and Adsorption Processes**. John Wiley & Sons: New York, 1997.

SAFA, Y.; BHATTI, H. N. Adsorptive removal of direct textile dyes by lowcost agricultural waste: Application of factorial design analysis. **Chemical Engineering Journal**, v. 167, p. 35–41, 2011.

SAITOH, T. et al. Rapid removal of cationic dyes from water by co precipitation with aluminum hydroxide and sodium dodecyl sulfate. **Journal of Environmental Chemical Engineering**, v. 2, p. 752–758, 2014.

SALLEH, M. A. M. et al. Cationic and anionic dye adsorption by agricultural solid wastes: A comprehensive review. **Desalination**, v. 280, p. 1–13, 2011.

SANTOS, K. G. Aspectos fundamentais da pirólise de biomassa em leito de jorro: fluidodinâmica e cinética do processo. 2011. 261 p. **Tese** (Doutorado em Engenharia Química) – Universidade Federal de Uberlândia, MG, 2011.

SCHIMMEL, D. Adsorção dos corantes reativos azul 5g e azul turquesa qg em carvão ativado comercial. 2008. 83 p. **Dissertação** (Mestrado em Engenharia Química) – Universidade Estadual do Oeste do Paraná, Toledo, 2008.

SEWU, D. D. et al. Highly efficient adsorption of cationic dye by *biochar* produced with Korean cabbage waste. **Bioresource Technology**, v. 224, p. 206–213, 2017.

SHARUDDIN, S. D. A. et al. A review on pyrolysis of plastic wastes. **Energy Conversion and Management**, v. 115, p. 308–326, 2016

SIPS, R. On the structure of a catalyst surface. **Journal of Chemical Physics**, v. 16, p. 490–495, 1948.

SKODRAS, G. et al. Kinetic studies of elemental mercury adsorption in activated carbon fixed bed reactor. **Journal of Hazardous Materials**, v. 158, p. 1–13, 2008.

TAN, I. A. W. et al. Equilibrium and kinetic studies on basic dye adsorption by oil palm fibre activated carbon. **Chemical Engineering Journal**, v. 127, p. 111–119, 2007.

TAN, X. et al. Application of *biochar* for the removal of pollutants from aqueous solutions. **Chemosphere**, v.125, p.70–85, 2015.

TAN, X. F. et al. *Biochar*–based nano–composites for the decontamination of wastewater: a review. **Bioresource Technology**, v. 212, p. 318–333, 2016.

TANG, J. et al. Characteristic of *biochar* and its application in remediation of contaminated soil. **Journal of Bioscience and Bioengineering**, p. 1–7, 2013.

TITIRICI, M. M. et al. Sustainable carbon materials. **Journal Chemical Society Reviews**, v. 44, n. 1, p. 250–290, 2015.

UCHIMIYA, M. et al. Dissolved phosphorus speciation of flash carbonization, slow pyrolysis, and fast pyrolysis biochars. **ACS Sustainable Chemistry & Engineering**, v. 3, n. 7, p. 1642–1649, 2015.

VAGHETTI, J. C. P. Pecan nutshell as biosorbent to remove Cu(II), Mn(II) and Pb(II) from aqueous solutions. **Journal of Hazardous Materials**, v. 162, p. 270–280, 2009.

VAIANO, V. et al. Nanostructured N-doped TiO₂ coated on glass spheres for the photocatalytic removal of organic dyes under UV or visible light irradiation. **Applied Catalysis B: Environmental**, v. 170–171, p. 153–161, 2015.

VANAAMUDAN, A.; SUDHAKAR, P. P. Equilibrium, kinetics and thermodynamic study on adsorption of reactive blue–21 and reactive red–141 by chitosan–organically modified nanoclay (Cloisite 30B) nano–bio composite. **Journal of the Taiwan Institute of Chemical Engineers**, v. 55, p. 145–151, 2015.

VIANNA, V. B.; TORRES, A. R.; AZEVEDO, E. B. Degradação de corantes ácidos por processos oxidativos avançados usando um reator com disco rotatório de baixa velocidade. **Química Nova**, v. 31, p. 1353–1358, 2008.

WAN NGAH, W. S.; TEONG, L. C.; HANAFIAH, M. A. K. M. Adsorption of dyes and heavy metal ions by chitosan composites: A review. **Carbohydrate Polymers**, v. 83, p. 1446–1456, 2011.

WEBER, C. T. et al. Removal of hazardous pharmaceutical dyes by adsorption onto papaya seeds. **Water Science and Technology**, v. 70, p. 102–107, 2014.

WON, S. W.; KWAY, I. S.; YUN, Y. S. The role of biomass in polyethylenimine–coated chitosan/bacterial biomass composite biosorbent fiber for removal of Ru from acetic acid waste solution. **Bioresource Technology**, v. 160, p. 93–97, 2014.

WOO, S. H. et al. Microbial mineralization of pyrogenic organic matter in different mineral systems. **Organic Geochemistry**, v. 98, p. 18–26, 2016.

WU, F. C. et al. Characteristics of Elovich equation used for the analysis of adsorption kinetics in dye chitosan systems. **Chemical Engineering Journal**, v. 150, p. 366–373, 2009.

WU, J. S. et al. Removal of cationic dye methyl violet 2B from water by cation exchange membranes. **Journal of Membrane Science**, v. 309, p. 239–245, 2008.

YAHYA et al. Agricultural bio–waste materials as potential sustainable precursors used for activated carbon production: a review. **Renewable and Sustainable Energy Reviews**, v. 46, p. 218–235, 2015.

YANG, J.; QIU, K. Development of high surface area mesoporous activated carbons from herb residues. **Chemical Engineering Journal**, v. 167, p. 148–154, 2011.

ZHANG, L. et al. Adsorption isotherms and kinetics studies of malachite green on chitin hydrogels. **Journal of Hazardous Materials**, v. 209–210, p. 218–225, 2012.

ZHAO, B. et al. Effect of pyrolysis temperature, heating rate, and residence time on rapeseed stem derived biochar. **Journal of Cleaner Production**, v. 174, p. 977–987, 2018.